Experimental Evaluation of the Effect of Inlet Gas Humidification on Fuel Cell Performance

John P. Evans

Thesis submitted to the faculty of the Virginia Polytechnic and State University in the partial fulfillment of the requirements for the degree

Master of Science
in
Mechanical Engineering

Graduate Committee Members:

Dr. Michael W. Ellis, Chair
Dr. Michael R. Von Spakovsky
Dr. Douglas J. Nelson

September 17, 2003
Blacksburg, Virginia

Keywords: fuel cell, PEMFC, humidification, hydrogen, steam injection, flash evaporation

Experimental Evaluation of the Effect of Inlet Gas Humidification on Fuel Cell Performance

John P. Evans
Mechanical Engineering Department
Virginia Tech

(ABSTRACT)

The development and evaluation of a fuel cell test stand incorporating various methods for controlling the temperature and humidity of fuel cell reactants is described. The test stand is capable of accurately metering gas flows, controlling the temperature and humidity of the gases, and delivering the gases to the fuel cell in a safe manner. Additionally, the test stand can measure the voltage and current produced by the fuel cell during operation. Two test stands were constructed and evaluated, one using steam injection for fuel cell stacks and the other using flash evaporation for individual fuel cells. Both test stands were shown to provide adequate control at the upper end of the design range. The flash evaporation test apparatus was used to investigate the effect of inlet gas humidity on fuel cell performance. The results from this investigation showed that, for a fuel cell and reactant temperature of 75^{o}C, the best performance was achieved with a high relative humidity (90%RH) for the hydrogen and a comparatively low relative humidity (60%) for the air.

Acknowledgments

I would like to thank my adviser, Dr. Michael Ellis, for his guidance and assistance in the construction of the test stands. In addition, I would like to thank Jerry Lucas for the use of the WARE LAB facility and the fuel cell senior design teams of 2001 and 2002 from the Virginia Tech Mechanical Engineering Department. Financial support was provided by the Gate Program at Virginia Tech. Additionally, I would like to thank Dr. W.C. Thomas, Dr. Doug Nelson, and Dr. Michael von Spakovsky for their expertise in solving many of the technical problems encountered during the construction and evaluation of the test stand.

Finally, I am dedicating this to my wife, Shannon. Her love and reassurance helped me finish my thesis after a very unconventional graduate school experience.

Table of Contents

Acknowledgements ..... **iii**

List of Figures ..... **vi**

List of Tables ..... **viii**

Nomenclature ..... **ix**

Chapter 1: Introduction **1**
1.1 Historical Perspective 2
1.2 Proton Exchange Membrane Fuel Cells 3
1.3 Motivation and Scope 5
1.4 Approach 6
1.5 Document Outline 9

Chapter 2: Literature Review **11**
2.1 Mechanisms of Water Transport 11
2.2 Methods of Humidification 15
2.3 Effect of Reactant Gas Humidification 20
2.4 Summary 24

Chapter 3: Test Apparatus **26**
3.1 Phase I Test Stand Design 26
3.2 Objectives for Phase II Design 27
3.3 Phase II Design 28
3.3.1 Fuel Flow Control Subsystem *30*
3.3.2 Oxidant Flow Control Subsystem *33*
3.3.3 Humidification and Air System *36*
3.3.3.1 Bubbling and Packed Tower Humidification 38
3.3.3.2 Liquid Injection *38*
3.3.3.3 Vapor Injection *39*
3.3.3.4 Flash Evaporation System *48*
3.3.4 Measurement and Control Subsystem *49*
3.3.4.1 Data Acquisition and Control *49*
3.3.4.2 Measurement Devices *50*
3.3.4.3 Control Devices *52*
3.3.5 Safety Subsystem *54*
3.3.5.1 Hydrogen Leak Detection 54
3.3.5.2 Exhaust Hood 55
3.3.5.3 Emergency Shutdown Switch 55
3.3.5.4 Nitrogen Purge 56
3.3.5.5 Flame Arrestor 56
3.3.5.6 High Temperature Safety Precautions 57

3.4 Validation of Test Apparatus ……..... 57
3.4.1 Fuel Flow Control Subsystem …… *58*
3.4.2 Oxidant Flow Control Subsystem …. ……... *58*
3.4.3 Hydrogen/Air Humidification System …… *58*
3.4.3.1 Relative Humidity Control ……..…….. *59*
3.4.3.2 Water Droplet Removal ……..…….. *59*
3.4.4 Measurement and Control Subsystems ……... *61*
3.4.4.1 Pressure Transducer …… *61*
3.4.4.2 Relative Humidity Transmitter …… *61*
3.4.4.3 Mass Flow Controllers …… *62*
3.4.4.4 Thermocouples…….. *62*
3.4.5 Safety System …….. *63*
3.4.6 Summary……..……*63*

Chapter 4: Results of Humidification System Evaluations ……..... 64
4.1 Evaluation of Humidification System Performance 64
4.1.1 Water Evaporation …… *64*
4.1.2 Steam Injection ……..…….. *65*
4.1.3 Flash Evaporation …… *67*
4.2 Effects of Humidity on Fuel Cell Performance..... 68
4.3 Analysis of Uncertainty ……..... 72
4.3.1 Uncertainty of Controlled Parameters *72*
4.3.2 Uncertainty of Measured Parameters ……..... *73*
4.3.3 Uncertainty from Additional Sources *75*
4.3.4 Summary of Uncertainties ……..... *75*

Chapter 5: Conclusion ……..... 76

References ……... 79

Appendix A: Humidification Subsystem Calculations..... 82
A.1 Steam Injection Humidifier Calculations …….. 82
A.2 Hydrogen Cooler Calculations …….. 88
A.3 Air Cooler Calculations …… 94
A.4 Energy Balance for the Coolant System ……..…….. 95

Appendix B: Calculations for Design of Fuel Subsystem 98

Appendix C: Properties of Tube-in-Tube Heat Exchanger 100

Vita ……..…….. 101

List of Figures

Figure 1-1: Conversion of fuel (hydrogen) and oxidant (oxygen in air) into electrical current and water in a PEMFC [www.fuelcells.org, 2001] 1

Figure 1-2: Diagram showing the membrane electrode assembly of a proton exchange membrane fuel cell, as well as a close up of the membrane-electrode interface [Energy Partners, 2001] ……..……. 4

Figure 1-3: Diagram of humidification system using steam injection ……...……...……... 8

Figure 2-1: Diagram showing three transport mechanisms of water vapor within the fuel cell membrane: pressure driven flow, electro-osmotic drag, and back diffusion ...…... 12

Figure 2-2: Six diagrams showing conventional fuel cell humidification methods used in research ……... 16

Figure 3-1: Overall systems layout for 5kW fuel cell test stand. Elements of the six subsystems are included and indicated ……..... 29

Figure 3-2: Flow controller layout for fuel subsystem. Flow to each combination mass flow meter/mass flow controller is controlled by a ball valve …….. 31

Figure 3-3: Outlet piping for fuel subsystem ……...…… 32

Figure 3-4: Flow controller layout for the air subsystem ……...……. 34

Figure 3-5: Outlet piping of the air subsystem …… 35

Figure 3-6: Plot of mass flow rate of water required to fully saturate hydrogen as a function of temperature ……..…. 37

Figure 3-7: Diagram showing the arrangement of components within the humidification subsystem ……...…….. 40

Figure 3-8: Diagram of hydrogen humidification enclosure piping ……...……. 42

Figure 3-9: Humidification enclosure for the air system ……...…….. 44

Figure 3-10: Front view and top view of boiler system and piping ……...…….. 46

Figure 3-11: Piping scheme for the water supply module ……...…… 47

Figure 3-12: Diagram for the coolant system piping ……...…… 47

Figure 3-13: Diagram of data acquisition system ……...……. 49

Figure 4-1: Polarization curves for low relative humidity of air ……...….. 69

Figure 4-2: Polarization curves for medium relative humidity levels of air ……...…. 70

Figure 4-3: Polarization curves for high relative humidity levels of air ……...….... 70

Figure 4-4: Maximum power showing that the maximum power was achieved at low relative humidity of air and high relative humidity of hydrogen …….. 72

Figure A-1: Block diagram of energy balance on the current system ……...…….. 82

Figure A-2: Humidity ratio as a function of desired temperature for relative humidity levels of 50%, 75%, 90%, and 100% and a total pressure of 2 atm ……..….. 84

Figure A-3: Humidity ratio of the air as a function of desired temperature for relative humidity levels of 50%, 75%, 90%, and 100% at a pressure of 2 atm ……...…. 85

Figure A-4: Temperature of the hydrogen vapor mixture following steam injection as a function of the humidity ratio …….…… 87

Figure A-5: Temperature of the air vapor mixture following steam injection as a function of the humidity ratio …….…….. 88

List of Tables

Table 2-1: Summary of research reviewed for this document ……...….. 25

Table 3-1: Flow rate and error values for Sierra Side-Trak model 840 flow meters ……...… 51

Table 3-2: Range of operation for Dynaload RBL-100-600-4000 …….. 54

Table 4-1: Actual humidity levels achieved during testing of the fuel cell membrane ……...… 68

Table 4-2: Maximum power points obtained from each cell of the test matrix ……..…… 71

Table A-1: Values resulting from the hydrogen cooler calculations using equations A-1 to A-16 ……..…… 89

Table A-2: Design conditions used for heat exchanger ……..... 90

Table A-3: Values resulting from the air side calculations with equations A.1 to A.16 ……..... 94

Table C-1: Properties of tube-in-tube heat exchangers used in the humidification subsystem.. 100

Nomenclature

ω = the humidity ratio of the gas, $\frac{kg_{H_2O}}{kg_{gas}}$

R_g = gas constant for the gas (air or hydrogen), $\frac{kJ}{kg \cdot K}$

ϕ = the relative humidity of the gas

$P_s(T)$ = the saturation pressure of water at temperature, T, kPa

$P_m(T)$ = the mixture pressure, kPa

R_w = gas constant for water vapor, $\frac{kJ}{kg \cdot K}$

V = the calculated cell voltage

E = the open circuit voltage

i = the actual current density found during testing

i_o = the exchange current density

i_l = the limiting current density

Chapter 1: Introduction

Over the past four decades, the science and engineering community has explored numerous alternative methods of power generation in the search for a replacement to traditional generation systems, particularly those that rely on combustion of fossil fuels. Any potential replacement must be comparable in cost to existing systems, be more efficient than traditional power generation, and be able to produce significantly lower levels of greenhouse gas emissions. Fuel cells have recently moved to the forefront in this search, primarily because of the method in which they convert energy. Using electrochemical reactions, fuel cells directly convert the chemical energy of a fuel into electrical energy. A simple diagram of this conversion in a proton exchange membrane fuel cell (also called a polymer electrolyte membrane fuel cell or PEMFC) is shown in Figure 1-1.

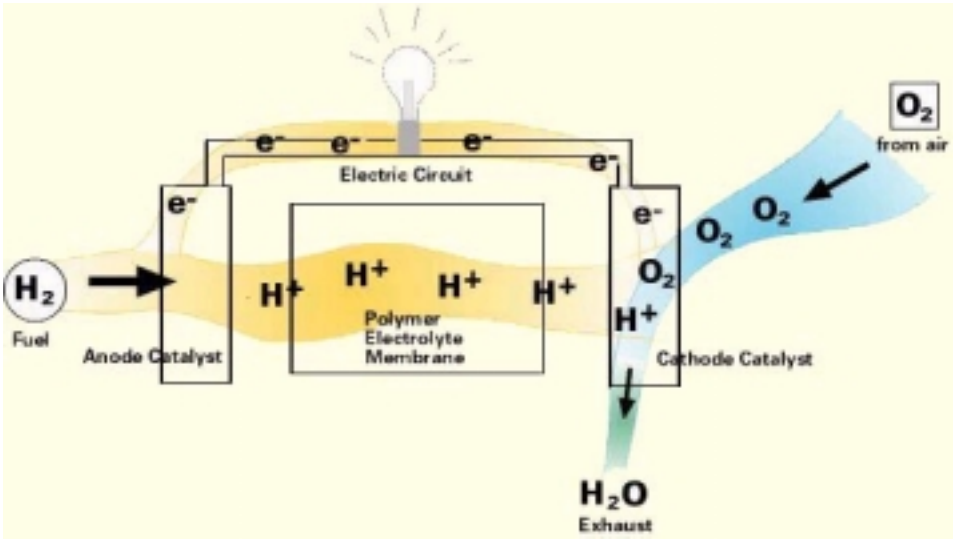

Figure 1-1. Conversion of fuel (hydrogen) and oxidant (oxygen in air) into electrical current and water in a PEMFC [www.fuelcells.org, 2001].

The energy conversion used in fuel cell technology provides several advantages over the combustion of fossil fuels. First, the only emission that arises directly from the fuel cell is pure water[1]. Second, most fuel cells have higher design and off-design efficiencies than conventional energy conversion processes, which rely on combustion. Finally, the technology can be easily

[1] Additional emissions may arise from the production of hydrogen if the primary energy source is a fossil fuel. However, even with these considerations, fuel cells typically have lower emissions than traditional energy systems.

scaled from an energy source for something as small as a cellular phone to something as large as a power generating utility.

Because of these advantages, the public and private sectors have devoted a significant amount of time and money to fuel cell research and development in the past decade. In the next decade, fuel cells are expected to see many widespread uses, including power systems for personal electronics, power sources for military applications, combined heat and power systems for buildings, large scale power generation for utilities and industrial plants, and alternatives to the internal combustion engine in automobiles. In particular, the PEMFC offers significant promise for widespread use in the aforementioned applications [www.fuelcells.org, 2001]. This section presents a brief historical perspective of fuel cells, a review of the principles at work in the PEMFC, the motivation behind my research, and the approach that this research has taken.

1.1 Historical Perspective

Although recent popular literature portrays fuel cells as a newly emerging science, the technology was actually invented in the 19th century. In 1839, Sir William Grove, a Welsh judge and scientist, assembled the first fuel cell. For the majority of time since then, fuel cells have been used primarily in research settings. NASA selected fuel cells for the space program in the 1960s, rejecting both nuclear power, which had a higher safety risk, and solar power, which had a higher cost. Alkaline fuel cells provided power for the Gemini and Apollo missions and today provide water and electricity to the space shuttle [www.fuelcells.org, 2001]. Despite their high profile use in the space program, the commercialization of fuel cell technology was not explored until the early 1980s.

Several factors have limited the commercial development of fuel cells, including manufacturing cost, fuel generation and distribution, and system complexity. The high manufacturing cost is caused by a number of factors: expensive raw materials used as catalysts, expensive membrane materials, and expensive fabrication processes for the collector plates. In 1980, the amount of platinum catalyst required for a 7 kW PEMFC stack was worth $9,000 [www.fuelcells.org, 2001]. By 2000, new techniques for using platinum catalyst in the electrodes had reduced the cost to $50. Early fuel cells were constructed and assembled by hand in short

runs of "prototype" production, and the cost of manufacturing a PEMFC was still over $10,000 per kilowatt in the mid 1990s [Ellis et al., 2000]. However, International Fuel Cells is currently marketing a stationary power generation unit for approximately $5,000 per kilowatt. [ONSI Corporation, 2001]. Currently, these systems generate electricity for around 13 cents per kWh, which makes them cost effective only to niche market consumers where electricity prices are relatively high. In a report to the Department of Energy, Arthur D. Little, a fuel cell research firm, estimates that market penetration will occur nationwide when fuel cells cost $1,200 per kilowatt [Casten and Zogg, 2000].

In addition to manufacturing cost, fuel generation and distribution have also prevented widespread commercialization. Most fuel cells consume pure hydrogen or hydrogen-rich gas as the primary fuel. However, an infrastructure does not exist for distribution and delivery of hydrogen to customers. One solution for the short term is to reform a common hydrocarbon fuel, such as natural gas or gasoline, to extract pure hydrogen. Currently, these reformers are large, expensive, and operate at high temperatures as high as 870^{o}C (1600^{o}F). General Motors demonstrated a working fuel cell reformer in August 2001 [GM, 2003], but widespread use still requires years of development.

The final obstacle in the commercialization of fuel cells is the complexity of the fuel cell and its support systems. This complexity makes optimal design of fuel cell systems difficult. To improve fuel cell design, researchers are trying to develop a better understanding of fuel cell behavior through computer modeling of the individual fuel cells, computer modeling of system components and integration, and experimental evaluation of fuel cell performance. Specifically, this document will focus on research dedicated to experimental evaluation of PEMFCs.

1.2 Proton Exchange Membrane Fuel Cells

In the most basic form of a fuel cell, two electrodes surround an electrolytic material. The composition of the electrodes and the electrolyte distinguish one fuel cell from another. In a PEMFC, the electrolyte material is a polymer, typically Dupont Nafion, and the electrodes are carbon paper water-proofed with Teflon. The fuel cell reactions occur in the catalyst layer located between the carbon paper and the membrane. The electrode on the hydrogen side is the

anode, and the electrode on the oxygen side is the cathode. Collectively, this assembly is called a Membrane Electrode Assembly (MEA), which is shown in Figure 1-2. A cell is formed when two bipolar collector plates with flow channels are added on either side of an MEA. Finally, if several cells are connected electrically, they are called a stack. The ability to connect several cells together allows fuel cells to be readily scaled from small to large applications.

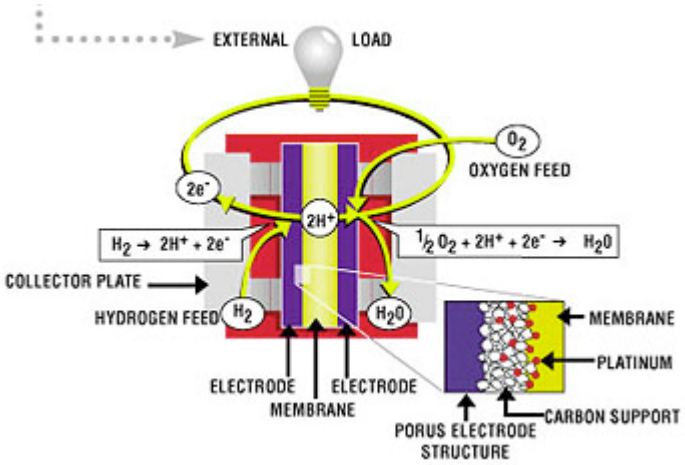

Figure 1-2. Diagram showing the membrane electrode assembly of a proton exchange membrane fuel cell, as well as a close up of the membrane-electrode interface [Energy Partners, 2001].

The unique properties of the membrane itself make PEMFCs possible. Hydrogen ions and water are allowed to pass through the membrane, but hydrogen and oxygen gases are not. As hydrogen gas is introduced, a reaction occurs with the catalyst on the anode, liberating an electron and forming a hydrogen proton. The electron migrates as a current through the collector plates from the anode to the cathode becoming useful electricity in the process. The protons also pass to the cathode side, but they travel through the membrane itself. Water dissolved into the membrane facilitates the passage of positive hydrogen ions through the membrane.

On the cathode side, a platinum catalyst causes oxygen gas to react with the hydrogen protons and the electrons from the anode to form water. In addition to electrical energy and water, the chemical reaction in the fuel cell yields low quality thermal energy (capable of being used in residential heating) and pure water. The electrical conversion efficiency of PEMFCs can be as high as 55% [Ellis et al., 2000]. When thermal energy is also recovered, overall first law efficiencies can reach as high as 80%. In addition to high efficiency, PEMFCs provide more

rapid startup times than most other fuel cells, provide higher power density, have longer life spans, and have lower operating temperatures. For these reasons, PEMFCs are being explored for a variety of uses including personal electronics, military applications, automotive drive systems, and stationary residential power.

1.3 Motivation and Scope

The promise of fuel cell systems as well as the complexity of the physical and electrochemical processes occurring within the fuel cell has prompted many researchers (including the research group at Virginia Tech) to study PEMFCs. As mentioned in the previous section, membrane hydration is required to promote the passage of protons through the membrane. The hydrogen and air entering the flow channels must be humidified to prevent the membrane from drying out. However, if water enters the fuel cell in droplet form, the catalyst sites will become flooded, thus inhibiting electrochemical reactions. Thus, water content of the membrane and the reactant gases directly affects fuel cell performance.

Since water content of the membrane is of such importance, a great deal of research has been performed to understand water transport within the membrane itself. Three mechanisms dominate this phenomenon: convective transport due to pressure gradients in the cell, diffusive transport due to a concentration gradient, and electro-osmotic drag due to protons migrating from the anode to the cathode. In the first instance, pressure gradients in the stack force water to areas of lower pressure. In the second case, water diffuses through the membrane to regions of lower concentration. Finally, as protons move through the membrane, they drag water molecules with them. There have been several efforts to describe the movement of water within the MEA using computer models in one, two, or three dimensions. While these models can provide insight and greater knowledge of the processes occurring within the fuel cell, experimental work is necessary to validate the models and to enhance the understanding of fuel cell phenomena.

The scope of my work is motivated by several experimental results found at temperatures below 60^{o}C and pressures near atmospheric. The work of Jansen and Overvelde [2001], Morner and Klein [2001], and Sridhar et al. [2001] have all dealt indirectly with the effect of inlet gas humidification on fuel cell performance. However, these groups all used either dry or fully

saturated inlet gases and did not evaluate multiple humidity levels both for the hydrogen and oxygen or air streams. In contrast, Chu and Jiang [1999] did evaluate multiple humidity levels for the air stream and were able to quantitatively give an optimum range of operation for their stack. However, they operated the air at ambient pressure, operated at lower temperatures (20^oC to 40^oC), and used only dry or fully saturated cases of hydrogen. In my study, I will evaluate the effect of varying humidity levels of both the hydrogen and air streams on fuel cell performance. These evaluations will occur at pressures higher than ambient and temperatures between 60^oC and 80^oC.

The goal of my research is to develop and/or evaluate various methods for controlling the temperature and humidity of fuel cell reactants and to apply one of these methods to determine the effect of both hydrogen and air humidity on cell performance.

1.4 Approach

The research described here includes the evaluation of a variety of humidification approaches and the application of one of these approaches to gather data showing the influence of reactant gas humidity on the performance of a commercially available 50 cm^2 fuel cell. The humidification approaches that were considered included water spray injection, steam injection, and flash evaporation. A steam injection system was designed to accommodate fuel cell stacks as large as 5 kW. A flash evaporation system was used in conjunction with a 50 cm^2 fuel cell to gather data for evaluating the effect of reactant gas humidity

Many approaches have been tried for precisely humidifying inlet gas steams including bubbling, packed towers, water spray injectors, steam injection, flash evaporation, and combinations of these approaches. Past efforts at Virginia Tech included bubbling the gases through a packed bed of wet beads and injecting water into the gas stream with fog nozzles [Davis, 2000]. The former method was ultimately rejected because water repeatedly flooded the bed and passed downstream to the fuel cell. The latter method of "fogging" the gas stream relied on evaporation to achieve full humidification. Unfortunately, the latent heat required to evaporate the water droplets resulted in a significant drop in inlet gas temperature.

More recently, strip heaters were added to the outside of the injection chamber in an attempt to raise the gas temperature. Although the heated injection system was able to achieve the target of 80^{o}C and 100% humidity, the required injection chamber length made the system quite large [Davis, 2000]. As a result, the humidification system could not be placed in close proximity to the fuel cell. The heat loss caused by this extra distance of pipe resulted in a drop of gas temperatures, which in turn prevented the accurate control of inlet gas conditions. Furthermore water droplets that inevitably were introduced into the system made control of temperature and humidity difficult.

After a review of the previous humidification systems, we selected four criteria for a new design based on the problems encountered with previous efforts. First, to minimize heat loss in the system itself, the new design had to be compact. Second, to reduce heat loss after the system, the distance between the system outlet and the fuel cell inlet had to be as short as possible. Third, the water had to be delivered in the vapor phase at or above the inlet gas temperature of the fuel cell to prevent temperature drops due to evaporative cooling. Finally, to conduct my research, the humidity level of the inlet gas to the fuel cell had to be capable of being controlled at any level between 50% and 100%.

Although several different concepts for new humidifiers were developed, a system using steam injection followed by cooling appeared to be the best choice to meet all four criteria. With this approach, the steam was produced by a boiler and injected into each gas stream. Since the steam was at a temperature considerably higher than the inlet gas (151^{o}C for the steam and 80^{o}C for the gases), the post-injection temperature and humidity were calculated to be 101^{o}C and 100%, respectively. The length required for sufficient mixing was assumed to be ten times the pipe diameter. Since the largest pipe diameter was ¾ inch, the longest length for mixing was 7½ inches. In contrast, the evaporation systems required a mixing chamber of at least 24 inches in length [Davis, 2000]. This reduction in mixing length made the system significantly more compact and amenable to location near the fuel cell.

After the steam was injected, the humidified gas then passed through a tube in tube heat exchanger. A mixture of 90% propylene glycol and 10% water passed through the outer section

of the heat exchanger in a counter-flow configuration. As the water and gas mixture was chilled to 80°C, excess water vapor in the humidified gas condensed out in the form of droplets. The humidified gas stream then passed through a water trap, which collected any excess water droplets entrained in the flow. For that reason, 100%-humidified gas was available at 80°C to the fuel cell, which satisfied the third criterion given above. Mixing the humidified "wet" stream and a dry gas stream, which bypassed the humidification system, to achieve an exact target of temperature and humidity satisfied the fourth design criterion. The humidification system design is shown in Figure 1-3.

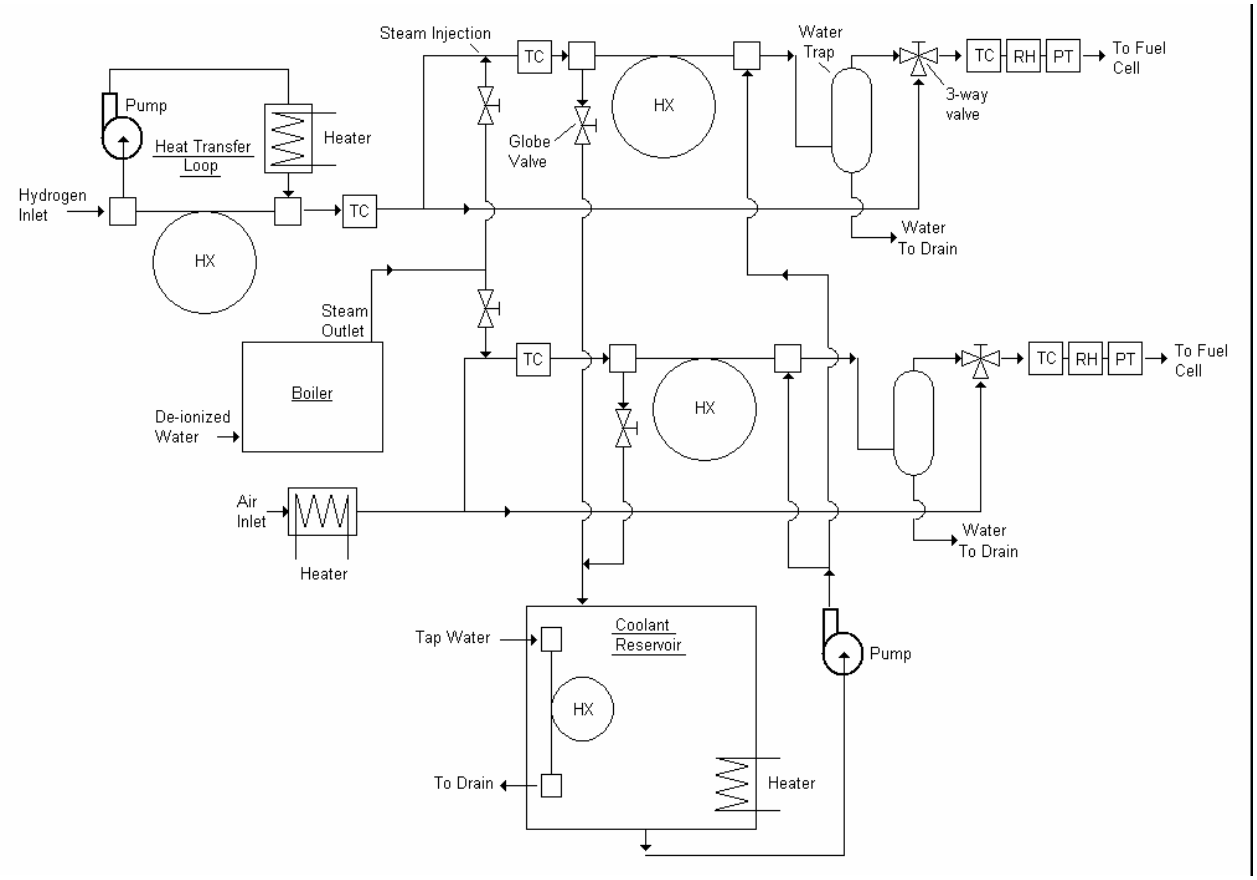

Figure 1-3. Diagram of humidification system using steam injection. Tube-in-tube heat exchangers appear as the abbreviation HX, thermocouples as TC, relative humidity sensors as RH, and pressure transducers as PT.

To achieve the required fuel cell inlet temperatures, both the air and hydrogen streams had to be heated. A simple 100 W resistance heater could be used for the air, but the hydrogen was heated indirectly for safety reasons. A tube-in-tube heat exchanger was selected for this

purpose, with the hydrogen passing through the inner loop. The same propylene glycol-water mixture used in the chillers was also used in the outer loop of the hydrogen heater.

To better quantify the effect of inlet gas humidification on fuel cell performance, single membrane electrode assemblies (MEAs) were used in the evaluation instead of large stacks. Testing of single MEAs avoided the need for the complex water coolant system used for stack testing. However, several modifications had to be made to the electrical and measurements systems to accurately test single MEAs. Previously, only stacks could be effectively tested because the full-scale errors of the flow meters were larger than the flow rates required for single MEAs. To control the flow through the 50 cm^2 MEA that was used during testing, a set of ultra low flow meters was added to the test stand. The addition of these flow meters allowed testing to occur between flow rates of 0.1 and 170 SLPM for hydrogen and 0.6 and 500 SLPM for air. The flow meters were measured and controlled with a National Instruments data acquisition card and the Labview instrumentation control program. Both the hardware and the software were modified to accommodate the two new ultra low flow meters. These changes allowed for a wide variety of fuel cells to be evaluated on Virginia Tech's 5 kW test stand.

1.5 Document Outline

The modified test stand provides a means to study how reactant gas humidification affects fuel cell performance. However, to adequately understand these effects, one must first understand the mechanisms governing water transport within the fuel cell membrane. These mechanisms are discussed extensively in Chapter 2. In addition, previous work on proton exchange membrane fuel cells is also presented in this section, with particular emphasis on work focusing on the experimental evaluation of the humidification of fuel cells. The research discussed in Chapter 2 deals primarily with fuel cells operating at low temperatures (below 60^oC) and atmospheric pressure. The results from this work provide data at a temperature of approximately 75^oC, which is more typical for automotive applications.

Chapter 3 covers the test apparatus constructed to allow evaluation of fuel cell stacks at Virginia Tech. Chapter 3 outlines the design changes to the previous test stand and describes the details of the five subsystems: fuel (hydrogen), oxidant (air), humidification, measurement and

control, and safety. Chapter 3 covers the design methodology of each subsystem, and focuses on the modifications and improvements that were made to the first version of Virginia Tech's test stand. In particular, the previous humidification subsystems are discussed, as well as the design modifications that were implemented to incorporate a steam injection humidification system. While the steam injection system described in Chapter 3 showed promise for fuel cell *stack* testing, difficulties controlling humidification at low flow rates required consideration of another option for testing *individual fuel cells*. Thus, Chapter 3 also describes a commercially available flash evaporation system, which was used in conjunction with the other test stand subsystems to obtain the results discussed in Chapter 4.

Chapter 4 discusses the evaluation of the various humidification systems and presents results obtained using the flash evaporation system that demonstrate the effects of inlet gas humidification on fuel cell performance. Finally, Chapter 5 reviews the conclusions of this research and the recommendations for future work.

Chapter 2: Literature Review

In the past decade, fuel cells have been the subject of a significant amount of research. Due to its potential for both transportation and stationary power applications, the Proton Exchange Membrane Fuel Cell (PEMFC) has been the focus of many of these studies. The performance of a PEMFC is influenced by its operating conditions, including temperature, pressure, and moisture content of the inlet gases. These factors all directly affect membrane water content, which in turn directly affects fuel cell performance. The primary measure of fuel cell performance is the polarization curve, which shows the cell voltage over a range of currents. Fuel cell power output can be determined from polarization curves, and researchers use these curves to quantify the effect of variations in operating conditions. The research presented in this document focuses on the effects of inlet gas humidification on fuel cell performance. This chapter summarizes prior research related to the effects of inlet gas humidification. The chapter is divided into three sections: the mechanisms by which inlet gas humidity affects performance, the methods of delivering humidification to the inlet gas streams, and the effect of reactant gas humidification on fuel cell performance.

2.1 Mechanisms of Water Transport

Hydration of the membrane is a very important determinant of the performance and durability of a PEMFC. If not properly hydrated, the membrane exhibits higher ionic resistance and in extreme cases can be physically damaged. Membrane hydration is affected by the water transport phenomena in the membrane itself, which in turn are affected by the condition of the inlet gases and the operating parameters of the fuel cell. Water is transported through the membrane in three ways: electro-osmotic drag by protons from the anode to the cathode, back diffusion due to concentration gradients from the cathode to the anode (or vice versa in limited cases), and convective transfer due to pressure gradients within the stack. A basic representation of these three transport phenomena is shown in Figure 2-1. In this section, both the mechanisms of this water transport and the factors affecting these mechanisms will be discussed in detail. In addition, the results of experimental and analytical research will be reviewed.

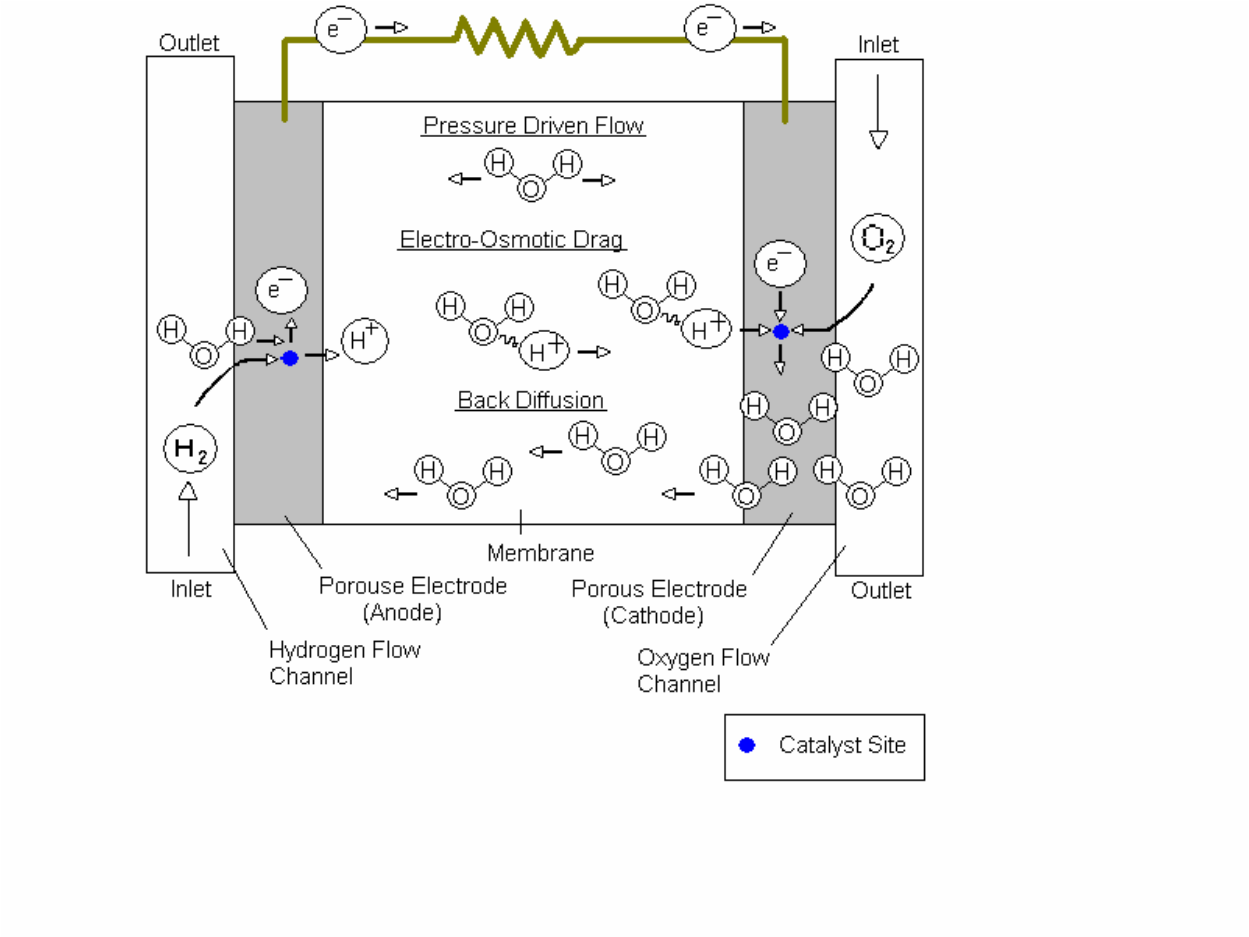

Figure 2-1. Diagram showing three transport mechanisms of water vapor within the fuel cell membrane: pressure driven flow, electro-osmotic drag, and back diffusion. Transport due to pressure driven flow can occur from either electrode, electro-osmotic drag occurs solely from the anode to the cathode, and back-diffusion typically occurs from the cathode to the anode since the water concentration is usually higher at the cathode[2].

Current research has focused on electro-osmotic drag and back diffusion as the dominant mechanisms for water transport within the membrane. Pressure gradients between the two gas flow channels can also be used to drive water either to the cathode or anode. However, maintaining large pressure gradients within a fuel cell stack increases the occurrence of crossover gas leaks. In their research on an air-breathing fuel cell stack, Morner and Klein [2001] used pressurized hydrogen and atmospheric pressure air. During testing, they observed hydrogen crossover leaks within the membrane, which resulted in the hydrogen reacting with the oxygen within the membrane, instead of at the electrodes. The free electron released by the hydrogen

[2] According to Wang et al. [2000], water in the liquid state can also be transported within the membrane via capillary action. Here we consider only electro-osmotic drag, back diffusion, and pressure driven flow.

during the reaction did not travel through the collector plates. For that reason, instead of producing current and heat, the reaction produced only heat. The excess heat created by the reaction caused the stack temperature to rise as much as 8°C when pressurized hydrogen was used. To prevent leaks, most manufacturers specify a maximum pressure gradient allowed between the two flow channels. So, any potential benefits obtained from using pressure gradients to drive water to either electrode are negated by the desire to reduce crossover leaks and to decrease high temperature degradation of the stack.

In contrast to pressure driven flow, water transport via the dominant phenomena of electro-osmotic drag and diffusion is often a function of the fuel cell temperature, current density, and membrane water content. As hydrogen protons move from the anode to the cathode, they drag water molecules with them in a process called electro-osmotic drag. The number of water molecules carried by each proton varies with membrane water content, and is typically assumed to be between 0.5 and 1.5 molecules per proton [Springer, 1991]. This effect causes the moisture content in the hydrogen to decrease along the flow channel. As the current density (defined as current per unit active area of the membrane) increases the flow of protons and water from the anode to cathode increases. At the same time, water is being produced at the cathode by the oxygen reduction reaction. This water begins to diffuse through the membrane from the cathode to the anode. The balance between these two effects, electro-osmotic drag and back diffusion, is key to determining membrane hydration. In their two-dimensional PEMFC model, Nguyen and White [1993] stated that at high current density the transport from the anode by electro-osmotic drag exceeds transport to the anode by back diffusion from the cathode and the membrane will dry out. As the membrane becomes dehydrated, the membrane pores shrink, which further limits the back diffusion of water. For this reason, Nguyen and White concluded that water transport due to back-diffusion is not sufficient to prevent membrane dehydration.

Yi and Nguyen verified these findings in their "Along-the-Channel" fuel cell model [1998]. They found that as the hydrogen moved down the channel, the local anode moisture content decreased. This reduction in moisture content due to water transport from the anode to the cathode eventually caused the membrane to dry out. Yi and Nguyen concluded that the net

water flux from the anode to the cathode was directly proportional to the current density. Sridhar et al. [2001] experimentally confirmed these findings in their study of internal and external humidification methods in a fuel cell stack. At high current densities, the transport from the anode due to electro-osmotic drag is quite large, which causes the anode to dry out and the cathode to flood. Sridhar et al. found that the kinetics of the reduction reaction at the cathode were adversely affected by the increase in water content at the cathode. So, as the cathode floods, the cell voltage drops.

Springer et al. [1991] showed that the cell voltage could also be reduced when membrane water content is low due to anode dehydration. They concluded that maintaining a high water flux from the cathode to the anode lowered the membrane resistance, which increased the cell voltage. To maintain a high water flux through the membrane, inlet gas conditions are often manipulated. By using a small-angle neutron scattering microscope on an operating 4.5 cm^2 fuel cell, Mosdale et al. [1995] were able to determine the water profile within the membrane as inlet conditions changed. When both gases were dry, the water profile appeared as a front moving from the anode to the cathode. In addition, Mosdale et al. noted that dry hydrogen carried away three and a half times more molecules from the anode than the air carried away from the cathode. So, the anode was losing water both due to evaporation into the unused hydrogen and electro-osmotic drag to the cathode side. When hydrogen was supplied in the fully-saturated or "wet" state, the water profile appeared as a parabolic curve between the two electrodes. The low point of the profile was the center of the membrane. When both inlet gases were humidified, a more uniform water profile was observed between the electrodes. Therefore, humidifying the inlet gases helps to balance the effects of the two dominant phenomena of water transport on membrane water content. As a result, the resistance of the membrane remains low, and higher cell voltages can be achieved.

2.2 Methods of Humidification

Since the need for humidification of the inlet gases has been established in the previous section, the next logical step is to review possible methods of humidification. These methods can be organized into either internal or external humidifiers. For this document, internal humidification will be defined as the inlet gases being introduced to the electrochemically active area of the fuel cell at temperatures and humidity levels other than the desired operating conditions of the fuel cell (unconditioned). Internally humidifying fuel cells are typically referred to as self-humidifying fuel cells. In contrast, external humidification will be defined as the inlet gases being heated and humidified (conditioned) before being introduced into the electrochemically active area of the fuel cell. Examples of conventional humidification systems are shown in Figure 2-2.

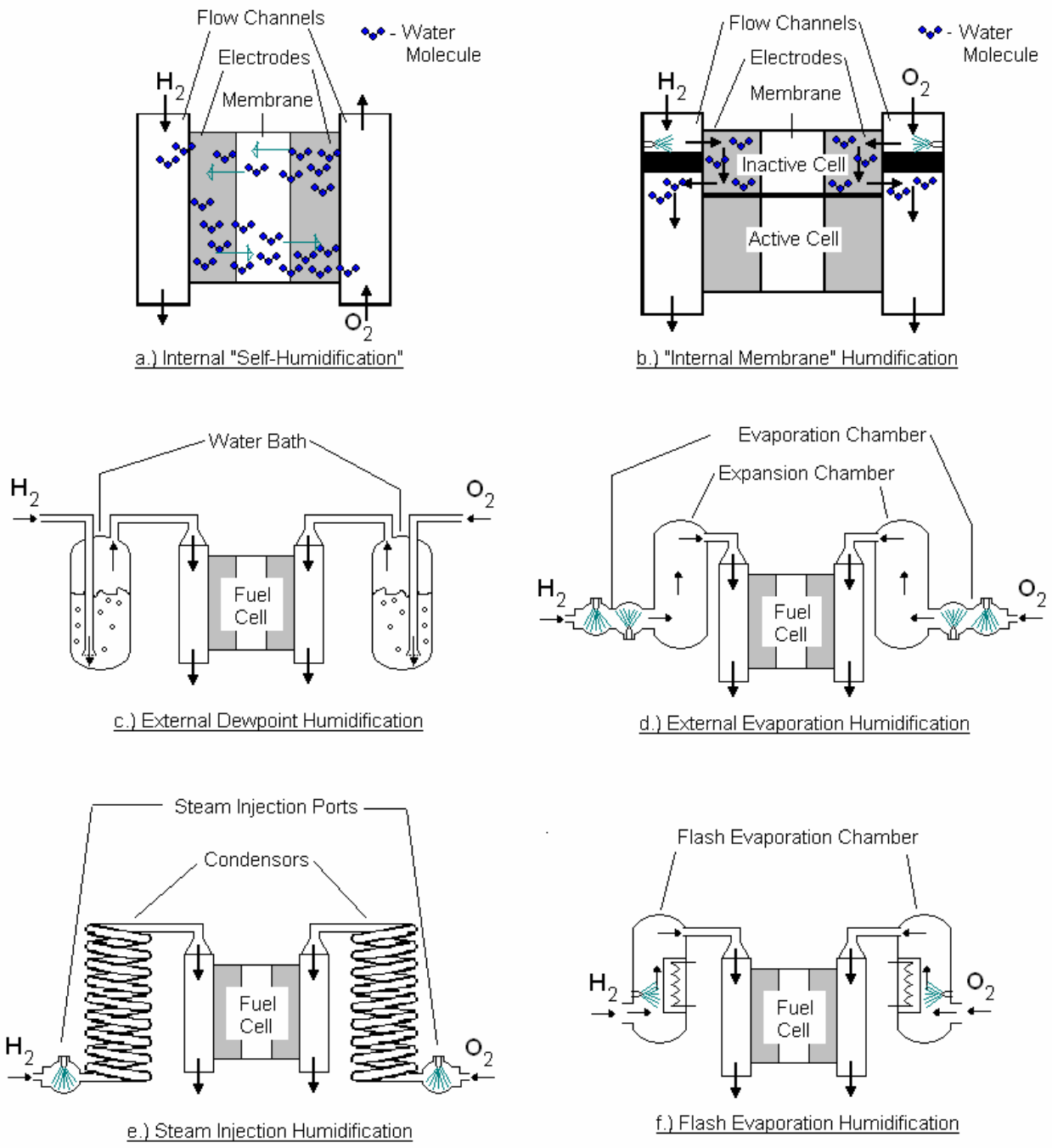

Figure 2-2. Six diagrams showing conventional fuel cell humidification methods used in research: (a) the self-humidifying fuel cell with the water transport phenomena discussed in section 2.1 with no active external humidification of the reactant streams, (b) the setup used by Chow et al. [1995] in their research featuring liquid water injection into an inactive portion of the fuel cell, (c) a typical dew point humidifier that will be discussed in later sections, (d) the evaporation setup employed by Davis [2000] in his work, (e) the steam injection system tested for this research, and (f) the flash evaporation method used to obtain results.

As mentioned in the previous paragraph, self-humidifying fuel cells condition the gases internally. In their "Along-the-Channel" model of a PEMFC, Yi and Nguyen [1998] used direct liquid-injection within the fuel cell to humidify the gases. The water was injected into the flow channels, where it was evaporated into the gas streams. However, Yi and Nguyen concluded that external humidification at a higher temperature was preferable to direct liquid-injection, since the higher temperature allowed for more water to be absorbed by the gas stream and carried into the fuel cell. In contrast to Yi and Nguyen's liquid injection approach, self-humidification concepts involve introducing dry gases into the anode and cathode flow channels, where they absorb water from the porous electrode. In their one-dimensional model of a PEMFC, Bernardi and Verbrugge [1992] theorized that the amount of product water produced by the electrochemical reaction at the cathode would be sufficient to hydrate the membrane for current densities between 0.1 A/cm^2 and 0.6 A/cm^2 (low to medium current densities). However, their conclusions were contingent upon the assumptions that they made regarding parameters such as the electro-osmotic drag coefficient and the back diffusion coefficient. Also, in many applications, the required current density is much higher than the value of 0.6 A/cm^2 that can be supported by self-humidification.

With regards to the previous definitions, internal membrane humidifiers (shown in Figure 2-2b) are somewhat of a misnomer. In internal membrane humidifiers, a portion of the membrane is set aside to humidify the inlet gases and liquid water is injected directly into this inactive portion of the stack. However, this portion is used solely for the purpose of humidification and is not considered to be electrochemically active. Therefore, the gases enter the electrochemically active area of the fuel cell in the conditioned state, and as defined here, internal membrane humidification is actually an *external* humidification method.

In their research, Chow et al. [1995] developed an internal membrane humidification scheme for a PEMFC stack. Dry gas was run through a separate section of the stack to condition the gas before the electrochemically active portion of the cell. In their study, Chow et al. stated both the advantages and disadvantages of such a configuration. Since the gases are conditioned inside the stack, the gas temperatures will be very close to the temperatures of the membrane itself. However, a portion of the electrochemically active section of the stack must be set aside for humidification purposes, which reduces the power density of the stack. In addition, Johnson

et al. [2001] quantified the heat flux required for internal humidification to be 1300 W from the water vapor to produce 2750 W of electric power from a 3 kW stack.

In their comparison of external and internal humidification, Sridhar et al. [2001] showed that self-humidification is limited by the membrane diffusion properties. At higher temperatures (90ºC), the back diffusion rate of water through the membrane becomes a limiting factor. Sridhar et al. showed that as temperature increases, the water uptake by the reactant gases increases and the current density increases, which also increases the water transport due to electro-osmotic drag. Since the membrane limits the back diffusion rate, the electro-osmotic drag becomes the dominant mechanism and water is transported away from the anode. In time, the anode will dry out and the cathode will become flooded. Due to this phenomenon, Sridhar et al. recommend that external humidification be used at higher temperatures. This conclusion was reinforced by the work of Buchi and Srinivasan [1997] on internal humidification of membranes. They concluded that cell performance was better when external humidification was used.

The study by Sridhar et al. [2001] showed that external humidification was preferable to internal humidification at higher temperatures. In their experimental apparatus, Sridhar et al. used bubbling through heated water to humidify both inlet gases, which is a widely used method referred to as dew point humidification. When a gas is bubbled through water, the gas is humidified and for a sufficiently long path the dew point of the gas will approach the water temperature. As noted by Sridhar, the main problem with dewpoint humidification (as well as all methods of external humidification) is that if the gas cools after the humidifier, the excess water condenses out of the gas and enters the fuel cell in droplet form. So, either the experiment must occur at room temperature [Mosdale et al., 1996] or the gas piping after the humidifier must be heated to prevent condensation.

Another widely used method of humidification involves evaporation of liquid water into the gas stream. The latent heat of evaporation required to evaporate the water into the gas will cause the gas temperature to decrease. Davis [2000] documented this phenomenon in the discussion of his humidification method. He used an atomizing nozzle to inject water into the gas flow streams of the hydrogen and air. In both cases, the temperature drop due to evaporation

required the addition of a heater around the injection chamber. In addition, to fully evaporate the liquid water, a long length of pipe was added after the humidifier. The temperature loss in this pipe was also significant for both gases, and additional heaters were added to the sections following the injection chamber. Even after the addition of the heaters, the humidity was difficult to control and the transient response of the system was very slow. One of the recommendations that Davis made was to improve the controllability of the evaporative humidification design.

Several commercial products are available for humidification. The Tenney Environment Chamber was used by Chu and Jiang [1999] in their research on atmospheric fuel cells. The Tenney Environment Chamber is designed to condition gases to specific temperatures and humidity levels. Air is humidified through evaporation at ambient pressures, with chillers used to maintain target humidity levels. The tolerances listed in their product information [2001] are ± 0.3^{o}C and ± 2% RH. However, the system is only applicable for testing at atmospheric pressure, which is not compatible with many current fuel cell system designs. In contrast, the Arbin Instruments Dew Point Humidifier, a part of the Arbin Instruments Fuel Cell Test Stand [2000], is more robust and capable of testing above atmospheric pressure. The humidifier operation is similar to the method of dew point humidification discussed above. However, instead of simply injecting the gas into the water, the gas is premixed with steam and then injected into the water. The steam vapor and gas mixture bubble up through the water bath and the water content in the air equilibrates to the dew point of the water. The result is a 100% humidified gas stream at the temperature of the water bath. The Lynntech humidification system used in this research relied on flash evaporation humidification. This uses the injection of a water stream onto a heated plate to instantly produce water vapor. The water flow rate can be controlled to achieve an exact dew point temperature.

In their research, Ihonen et al. [2001] point out a significant flaw in using dew point humidification in test equipment. They stated that the nominal gas temperatures (temperatures in the center of the gas stream within the pipe) were not the real dew points of the gas. Heat losses between the humidifier and the fuel cell resulted in a drop in gas temperature. To prevent this temperature loss, they recommended that the section between the humidifier and the fuel cell be heated. Unfortunately, this is not possible in most commercial test equipment due to the

proximity of sensitive electronics within the test stand enclosure. Ihonen et al. concluded that a custom-built humidification system would yield more accurate and reproducible results for experimental purposes.

2.3 Effect of Reactant Gas Humidification

A number of analytical, numerical, and empirical models exist which can predict the effect of reactant gas humidification on fuel cell performance. The models of Bernardi and Verbrugge [1992], Nguyen and White [1993], Yi and Nguyen [1998], and Siegel et al. [2003] all are able to draw a conclusion about the effect of gas moisture content on the performance of their fuel cells. Dutta et al. [2001] even went so far as to develop a three-dimensional model to numerically predict the effect of inlet gas humidity level on fuel cell performance. In contrast, a relatively small number of researchers have examined the effect of humidification through experimental means. In this section, both the theoretical and experimental work related to the effect of inlet gas humidification on cell performance will be presented and discussed.

The work of Bernardi and Verbrugge [1992] used a one-dimensional mathematical model to investigate the factors limiting cell performance and the transport phenomena of gas, liquid, and solid phases within the membrane. They assumed that the membrane was fully hydrated, that all temperatures were constant, and that all the gases were fully mixed. Although their study focused on using a pressure differential to drive water from the cathode to the anode, Bernardi and Verbrugge also made some conclusions on how inlet gas humidity affects fuel cell performance. Specifically, they noted that for current densities above 0.4 A/cm^2 enough water was produced by the reaction at the cathode to humidify both gas streams. Also, for current densities below 0.1 A/cm^2, membrane dehydration conditions exist and additional water must be added to prevent dehydration. Bernardi and Verbrugge concluded that relative humidity must exceed 20% to avoid dehydration at low current densities.

Nguyen and White [1993] moved a step forward and developed a two-dimensional model of a proton exchange membrane fuel cell to investigate heat and mass transfer within the fuel cell. They focused on transport both across the membrane and down the flow channels. While they did not focus on specific humidity targets as Bernardi and Verbrugge did, Nguyen and

White were able to draw some general conclusions about the required conditions of the inlet gases. Specifically, they noted that at high current densities the anode side would dry out if the inlet gases were not humidified. Also, they noted that if air were used instead of pure oxygen, then the air stream would have to be externally humidified as well.

In later work, Nguyen worked with Yi [1998] to develop an along-the-channel model of a PEFMC. They used a base case of 80ºC and 1 atm inlet gas conditions and a fuel cell operating level of 1.1 A/cm^2 to evaluate fuel cell performance under several humidification schemes. Without humidification, the transport of water from the anode to the cathode caused the membrane to dry out. They concluded that a small amount of water vapor must be present in the anode stream to prevent the membrane from becoming dehydrated. In addition, they recommended that external anode humidification would significantly improve cell performance. Finally, Yi and Nguyen found that using humidified gases at higher temperature humidified gases was preferable to using internal humidification methods, such as direct-liquid injection.

Similar to Nguyen and Yi [1998], Siegel et al. [2003] used a two-dimensional along-the-channel-model to evaluate fuel cell performance at 80^{o}C. However, they evaluated at higher than atmospheric pressure and assumed fully humidified reactant gases. Siegel et al. [2003] focused on modeling operating regimes where mass transport phenomena were dominant, and included mass transport between vapor, liquid, and dissolved phases of water within the membrane. The model was then solved numerically with a CFD program and the results were evaluated against experimental results. Siegel observed that with fully saturated inlet gases, the loss of performance observed at higher current densities was due to mass transfer limitations associated with the accumulation of water in the cathode gas diffusion layer. Furthermore, the electro-osmotic drag can decrease water content and conductivity at the anode, as well as increase the water saturation of the cathode gas diffusion layer, restricting reactant gas permeability through cathode.

To further test the effect of inlet humidification, Dutta et al. [2001] developed a three-dimensional numerical prediction model to study the flow pattern of water between the electrodes and the membrane. They used inlet gas conditions of 70ºC and 2 atm and choose to

evaluate the cell at 0.6 V, which was in contrast to previous work where current was fixed and voltage was measured. They used four inlet-gas humidity criteria to evaluate water transport: very low humidity (18.5%), low humidity (37.3%), high humidity (72.2%), and very high humidity (193.3%). The humidity levels in excess of 100% indicate the presence of liquid water. For very low humidity levels, the estimated current density was 0.22 A/cm^2. At low humidity, the current density was 0.46 A/cm^2. The highest current density of 0.63 A/cm^2 occurred at the high humidity level. Finally, at very high humidity levels the current level dropped to 0.42 A/cm^2. The drop in current was due to flooding which occurred at the cathode and which limited the number of reaction sites available.

Similar to Dutta et al. [2001], Chu and Jiang [1999] evaluated fuel cell performance at several different humidity conditions. They used an "air-breathing" fuel cell stack consisting of six cells, each with an active area of 32 cm^2. The air was fed to the cell via convection from the surroundings, and the hydrogen was supplied at greater than atmospheric pressure. Temperatures were maintained between 20ºC and 40ºC, and they used a Tenney Environment Chamber to vary the humidity level of the surrounding air. When the air was at a relative humidity of 20%, using humidified hydrogen resulted in a power increase of 17.6%. Likewise, when fully humidified hydrogen was used, an increase in the relative humidity (RH) of the air from 30% to 85% resulted in a power increase of 33%. In conclusion, Chu and Jiang recommended that operation of the stack was acceptable for fully humidified hydrogen gas and air at 36% RH or higher. In addition, they found the optimal operating condition of the stack to be at 35ºC, 85% RH air, and fully humidified hydrogen.

In their measurement of the effective drag transport in a PEFMC, Jansen and Overvelde [2001] were able to draw more general conclusions about the humidification of the inlet gases at higher temperatures. They considered drag to be the sum of the water transport phenomena discussed in section 2.1, and they measured drag by comparing the water content at the inlets and outlets of both gas streams. Jansen and Overvelde used 50 cm^2 membrane electrode assemblies (MEAs) operated between 60ºC and 80ºC with cathode pressures of 1.5 to 3 bar and anode pressures of 1.5 to 4 bar. The gases used were either wet (fully saturated) or dry. At 60ºC, the fuel cell was able to operate with both inlet gases in the dry state. The net rate of water flow was

very high toward the anode and water was drawn away from the cathode. At 80ºC, the membrane became dehydrated when dry oxygen was used, regardless of the saturation level of the hydrogen. The use of dry hydrogen resulted in a very large negative drag that could potentially dry out the cathode, even when saturated oxygen was used. In addition, Jansen and Overvelde noted that for high volume flow rates the membrane would become dehydrated. They concluded by suggesting that dehydration of the membrane could be avoided by increasing the water content at the anode.

Similar to Jansen and Overvelde, Morner and Klein [2001] used only two points for evaluating the effect of inlet gas humidity, either wet or dry. They used a commercial air-breathing fuel cell stack consisting of 22 cells, each with an active area of 25 cm^2. They operated the stack between 30ºC and 70ºC, and used ambient air and compressed hydrogen. As mentioned previously, this configuration caused crossover leaks within the stack, which reduced the stack efficiency. Morner and Klein found that using humidified air improved stack performance, particularly at higher stack temperatures. In addition, they noticed that as the humidity level of the inlet gas increased the stack temperature remained constant. Once the humidity reached 100%, the stack temperature began to rise. When the temperature reached 65ºC, the stack performance degraded rapidly. The higher temperature caused the membrane hydration level to drop, which reduced the current density of the membrane and the cell voltage. They concluded that over time, at this temperature the water evaporation rate would overtake the water production rate and the membrane would dry out. Also, they observed that a balance existed within the cell between oxygen flow and membrane hydration. At low flow rates, the amount of oxygen available to the last cells of the stack and the amount of product water removed from the stack were both reduced. Both of these reductions adversely affected stack performance. At higher flow rates, more oxygen was available, but the water removal rate exceeded the production rate, which could result in dehydration of the membrane. In conclusion, Morner and Klein stated that the optimum flow rate of air was a function of the desired current.

Finally, Sridhar et al. [2001] experimentally evaluated the performance of internal and external humidification on single MEAs. They evaluated MEAs with active areas of 25 cm^2, 100 cm^2, and 300 cm^2 to determine how membrane size and thickness affect water take-up rates. The

water content of both the cell inlet and cell exhaust streams were measured at load and no load conditions. In their study, Sridhar et al. found that the water at the hydrogen outlet decreased as the current density increased. As current density increased, the member of protons traveling through the membrane also increased. So, more water molecules were being transported through the membrane via electro-osmotic drag. Sridhar et al. also observed that as the membrane temperature approached 60ºC, the water transfer rate within the membrane leveled off. They concluded that at high temperatures (in excess of 60ºC), a maximum water transfer rate through the membrane existed, which was based on membrane thickness. Due to this factor, they concluded that external humidification was more effective at higher temperatures than internal membrane humidification, since the transfer rate of water through the membrane is limited by the membrane properties.

2.4 Summary

In the previous section, the work of several researchers was presented and discussed. Table 2-1 organizes this work by the type of research, the focus of the research, and the humidification location. Although the numerical and analytical work of groups such as Yi and Nguyen [1998], Springer et al. [1991], Siegel et al. [2003], and Dutta et al. [2001] do not directly define my scope, these works provide insight into the water transport phenomena found in Proton Exchange Membrane fuel cells. The knowledge of how water is transported within the membrane shows why humidification of the reactant gases is so important. Without reactant gas humidification, the fuel cell membrane will become dehydrated leading to high ohmic losses and potential damage to the membrane.

After establishing the necessity of reactant gas humidification, the discussion then focused on how to achieve reactant gas humidification. The current humidification methods were classified as either internal, where reactant gases enter the flow channel of the fuel cell in the dry state, or external, where reactant gases enter the flow channel after being externally humidified. One notable exception was the “internal membrane” humidifier, which used a portion of the fuel cell membrane for humidification. This method was classified as being external, since the gases enter the active area of the fuel cell membrane in a humidified state.

External humidification methods were used in all of the experimental work discussed in this section.

Although groups such as Chu et al. [1999] and Morner and Klein [2001] directly studied the effect that external humidification of the reactant gases had on fuel cell performance, the research occurred at atmospheric pressure and relatively low temperatures (below 60^{o}C). By operating at higher temperatures (60^{o}C or higher), PEMFCs can achieve higher efficiencies and higher power densities. My research focuses on the higher temperatures (80^{o}C) and higher pressures (2 atm) typcially found in automotive fuel cell systems. Moreover, my research attempts to compare anode and cathode humidification to assess the relative importance of each.

Table 2-1. Summary of research related to humidification of fuel cell reactants.

Authors	**Type of Research**	**Focus of Research**		**Humidification Location**	
Wang et al. [2001]	Numerical		Cathode Flooding		External
Dutta et al. [2001]	Numerical	Anode Drying			External
Spiegel et al. [2003]	Numerical	Anode Drying	Cathode Flooding		External
Bernardi and Verbrugge [1992]	Analytical	Anode Drying		Internal	External
Yi and Nguyen [1998]	Analytical	Anode Drying		Internal	External
Nguyen and White [1993]	Analytical	Anode Drying			External
Springer et al. [1991]	Analytical		Cathode Flooding		External
Johnson et al. [2001]	Experimental				External
Ihonen et al. [2001]	Experimental				External
Chow et al. [1995]	Experimental	Anode Drying			External
Mosdale et al. [1996]	Experimental				External
Chu et al. [1999]	Experimental		Cathode		External
Jansen and Overvelde [2001]	Experimental	Anode Drying			External
Morner and Klein [2001]	Experimental		Cathode		External
Sridhar et al. [2001]	Experimental	Anode		Internal	External
Evans [2002]	Experimental	Anode	Cathode		External

Chapter 3: Test Apparatus

The objective of the research presented here is to develop and/or evaluate various methods for controlling the temperature and humidity of fuel cell reactants and to apply one of these methods to determine the effect of both hydrogen and air humidity on cell performance. This chapter describes the design and construction of a steam injection system for controlling the reactant temperature and humidity for a fuel cell stack. In addition, this chapter describes the characteristics of a commercially available flash humidification system for controlling the reactant humidity for an individual fuel cell. Both humidification systems were incorporated into a fuel cell test apparatus. Experiences with each humidification system are presented in Chapter 4 along with data collected from the flash humidification system that shows how reactant humidification affects fuel cell performance.

Both of the humidification systems that were tested were integrated into Virginia Tech's 5 kW fuel cell test stand. The first generation of this test stand (referred to as Phase I) was conceived and built by Mark Davis over the period of August 1998 to May 2000 [Davis, 2000]. During the course of the present work (refereed to as Phase II), significant modifications were made to the original design. However, several of the components from Phase I were incorporated into Phase II.

3.1 Phase I Test Stand Design

The existing design for the 5kW fuel cell test stand was designed to control the operation of fuel cell stacks. All components in the system were selected based on mass flow rates corresponding to 5kW of power, pressure ratings of at least 400 kPa, and operating temperatures of at least 100^{o}C. The test stand consisted of the following systems; air and hydrogen flow controllers, air and hydrogen heaters, liquid water injection humidifiers for air and hydrogen, coolant water circulating loops, and measurement and control devices. The design and configuration of the Phase I test stand is detailed in Davis' work [Davis, 2000]. Although this system did provide adequate humidification to operate a fuel cell stack, another humidification method was desired to achieve better control.

3.2 Objectives for Phase II Design

The humidification system was the primary focus of many of the design changes between the first and second phases of test apparatus development. Two completely new humidification systems were incorporated into the test stand. One system was a steam injection humidification system with aftercooling which was designed to accommodate fuel cell stacks. The second system was a flash evaporation system designed to accommodate single cells. The objective of these modifications was to improve humidity control and, thus, provide the capability for investigating the influence of reactant humidity on cell performance. In addition to improved humidification, other objectives of the Phase II design were to improve flow control, facilitate operation, and improve safety. Modifications to achieve these objectives included changes to the water piping, flow meter configuration, and overall piping design.

After the humidification subsystem, the next most significant changes in the test stand operation occurred with respect to the water supply. Previously, the water was a separate subsystem, which was capable of supplying a fuel cell stack with coolant water. However, the single Membrane Electrode Assembly fuel cell used in my research did not require coolant water and the coolant water subsystem was removed from the test stand. In addition, the boiler used in the steam injection humidification system required a constant supply of de-ionized water. To accommodate this requirement, the water supply line was reconfigured to include a separate de-ionizing bed for the boiler supply line. The outlet of this de-ionizing bed also includes an additional supply valve to fill vessels with de-ionized water.

The objective of testing individual fuel cells also required the flow meters to be reconfigured. In the previous design, only medium and high flow meters were required to regulate the flow rates for the fuel cell stacks. To accurately test the smaller flow rates found in individual cells, a set of low flow meters had to be added to the test stand. These flow meters are capable of regulating flows between 0 and 1.5 SLPM and 0 and 6 SLPM for hydrogen and oxygen, respectively. Since the flow meters are set with 0-5 V DC signal controlled by LabView, the control scheme was altered to include the additional outputs and inputs. The addition of the two low flow meters required the existing meters to be relocated.

Another factor in the movement of the flow meters was the need to create more space on the main test stand board for the humidification enclosures. Previously, the humidification subsystem was a separate module located on the floor. This module was connected to the fuel and oxidant systems through long lengths of stainless steel piping, which significantly increased the thermal mass of the system and consequently the heat losses from the reactant gases to the atmosphere. To reduce the amount of piping, the humidification subsystem was attached directly to the main board. The humidification enclosure was also expanded to contain both the gas heaters and the measurement probes.

With a final length of almost 2 m and height of almost 1.25 m, the incorporation of the humidification enclosures on the board also required the compaction of the fuel cell outlet piping and the relocation of the nitrogen purge system. Although compacting the reactant piping did reduce the thermal mass of the system, such reductions did not provide significant benefits to fuel cell performance. In contrast, the movement of the nitrogen purge to the backside of the main board allowed the nitrogen lines to be connected before the pressure regulators and flow meters. By doing this, the nitrogen used for purging is routed through the entire fuel and oxidant subsystems on the main board. This not only assures a complete purge of these systems but also provides conditioning and flow control of the purge gas.

Details of the Phase II design that address the issues summarized here are described in the following sections.

3.3 Phase II Design

The Phase II 5kW stack test stand at Virginia Tech is depicted in Figure 3-1 and is organized into six subsystems. The *fuel flow control* (or hydrogen) and *oxidant flow control* (or air) subsystems deliver the reactant gases to the fuel cell at the desired mass flow rate and pressure.

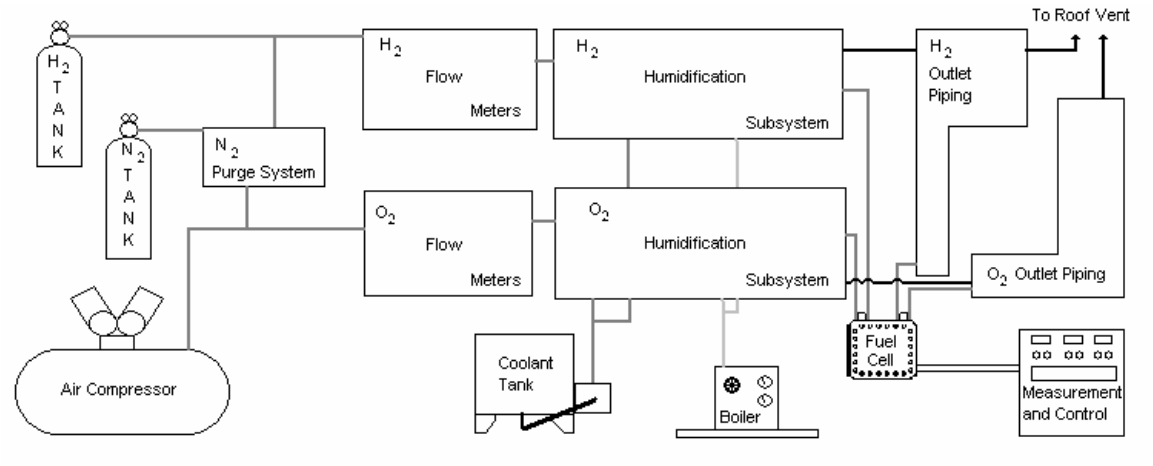

Figure 3-1. Overall systems layout for 5kW fuel cell test stand. Elements of the six subsystems are included and indicated.

The *fuel humidification* subsystem and the *oxidant humidification* subsystem control the temperature and humidity of the reactant gases to the required inlet conditions of the fuel cell. The primary components of the humidification subsystem (discussed in section 3.3.3) are the boiler, the heaters, and the chiller units. Detailed design calculations for the chiller are found in Appendix A.

The *measurement and control* subsystem assures that the reactant gases enter the fuel cell at the proper inlet conditions. This subsystem measures the mass flow rate, pressure, temperature, and relative humidity of the reactant gases and issues control commands to the components of the other subsystems. The main components of this system (discussed in section 3.3.4) are the sensors to measure the four inlet gas criteria, the computer and data acquisition units to record these criteria, and the manual and automatic control systems that issue the control commands.

In contrast to the other subsystems, the *safety* subsystem does not actively control the normal operation of the fuel cell. The purposes of this subsystem are to prevent potentially dangerous conditions from occurring and to isolate the fuel and oxidant sources in the event of an emergency. The safety subsystem (discussed in section 3.3.5) has five main component groupings: the enclosures and insulation to prevent accidental contact with hot surfaces, the exhaust hood which vents any leaking hydrogen, solenoid valves and shut off switches to isolate

the reactant gas sources, and the nitrogen tank and lines to purge the stack test stand of any remaining gases. The following sections review the layout and components for the Phase II test stand.

3.3.1 Fuel Flow Control Subsystem

The fuel flow control subsystem is composed primarily of 316 stainless steel piping and fittings. Fuel cell membranes can be poisoned by metal ions, and most manufacturers recommend the use of parts made of 316 grade or higher stainless steel or Teflon. Since dry gases are unable to carry metal ions, brass may be used in sections of the hydrogen subsystem before the humidification subsystem.

The appropriate piping size for the hydrogen subsystem was a function of the mass flow characteristics. The mass flow of fuel and oxidant are both dependent on the power produced by the cell. During typical operation of the test stand, the hydrogen subsystem will operate in dead-ended mode, meaning that all of the hydrogen will be consumed by the fuel cell. Although the hydrogen subsystem will operate with a stoichiometric ratio of 1, the subsystem was designed to accommodate stoichiometric ratios of 2. In his thesis, Davis (2000) uses the equations in Appendix A to calculate the maximum hydrogen flow rate of 152 SLPM and pipe diameter of ½" required for testing. With this diameter, the calculated pressure drop is less than 20 Pa per meter of piping. The maximum design pressure of the fuel cell test stand is 400 kPa, so a pressure drop of this magnitude will not have a significant effect on fuel cell operation.

The hydrogen supplied to the fuel cell is delivered from a carbon-steel tank. Although this does not meet the 316 SS specification set forth earlier, the hydrogen gas is dry and 99.999% pure, and the possibility of the gas carrying metal ions from the tank into the fuel cell is extremely remote. Since the tank pressure can be as high as 1200 psig, a two stage regulator is used to reduce the pressure. After the regulator, the hydrogen gas passes through a normally closed solenoid valve. The operation of this valve will be discussed in more detail in the safety subsystem section of this chapter.

After the solenoid valve, the hydrogen gas passes through a check valve and a branch flow tee. The branch of the tee is connected to the nitrogen purge line, and when the safety shutdown switch is depressed, nitrogen gas will flood the hydrogen subsystem. The inclusion of the check valve prevents the nitrogen, or any other gas, from flowing back into the hydrogen tank. A second pressure regulator follows the branch tee, and this is used to control the operating pressure of the fuel cell. The hydrogen gas then passes through the Sierra mass flow controllers. The low, medium, and high mass flow controllers can measure and regulate gas flows from 0.03 SLPM to 170 SLPM. The operation of these mass flow controllers is controlled by the computer and will be discussed in more depth in the Measurement and Control section. A ball valve is located before each mass flow controller, and the operator simply opens the valve corresponding to the desired flow range. The test stand was designed such that only one flow meter for a given reactant stream can be operated at any given time. The configuration of these valves and controllers is shown in Figure 3-2.

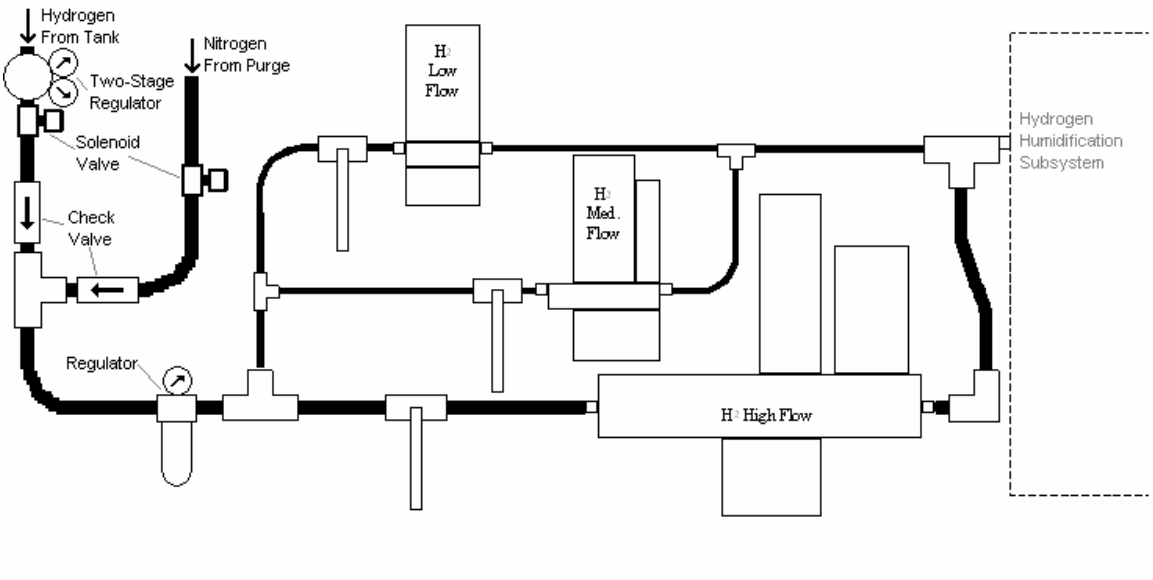

Figure 3-2. Flow controller layout for the fuel flow control subsystem. Flow to each combination mass flow meter/mass flow controller is controlled by a ball valve.

Hydrogen from the flow controllers passes into the fuel humidification subsystem, where the gas is heated and humidified to the desired operating conditions of the fuel cell. The fuel humidification subsystem is enclosed in a stainless steel case and can be completely removed

from the main test stand board if required. The components of this subsystem will be discussed in the fuel humidification section.

After being heated and humidified, a three-way valve located at the end of the fuel humidification subsystem directs the flow of the hydrogen gas. The valve is turned to the lower flow path if the inlet gases are at the proper conditions and to the upper flow path to bypass the fuel cell if they are not. If the fuel cell path is selected, hydrogen flows through a Teflon tube to the fuel cell. Teflon tubing also connects the outlet of the fuel cell to the outlet piping of the test stand, which is shown in Figure 3-3. The outlet piping is connected to the bypass piping, and a check valve prevents the bypass gas from entering the fuel cell outlet.

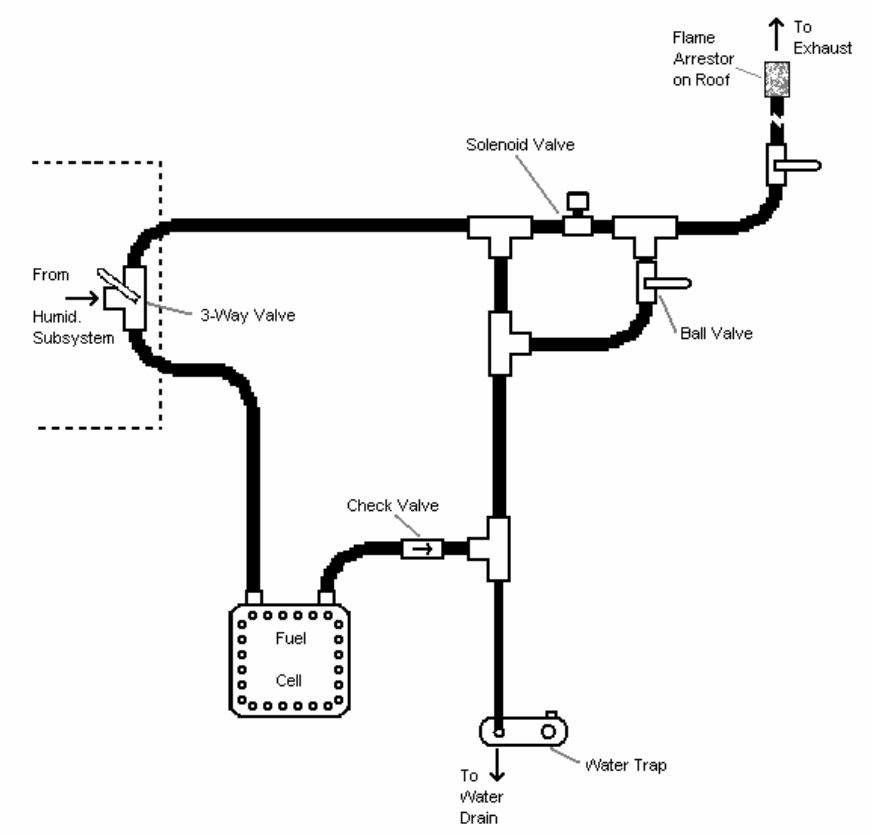

Figure 3-3. Outlet piping for fuel control subsystem.

Liquid water from the outlet pipes is collected and drained by a water trap. Gas from the bypass and outlet pipes can be exhausted through either an automatic valve or a manual valve. The automatic valve is a normally open solenoid valve. During normal operation the solenoid is

energized to close the valve. In the event of either an emergency or a power failure, the valve opens to allow hydrogen gases to be vented to the atmosphere. The manual valve is a ball valve, which can be opened to vent gases, or to operate the fuel cell in open-ended mode. The exhaust from both valves passes through another ball valve before being vented to the atmosphere. A flame arrestor located on the exhaust prevents flames from propagating upstream and injuring operators or damaging equipment.

3.3.2 Oxidant Flow Control Subsystem

Similar to the fuel control subsystem, the oxidant control subsystem must also conform to the material requirements set forth by the fuel cell manufacturer. In contrast to the hydrogen, the air is drawn from the atmosphere and will be at atmospheric humidity levels. As such, all parts which contact the "wet" gas after the compressor must be 316 grade or higher stainless steel or Teflon.

The maximum mass flow rate and pipe sizing requirements for the oxidant subsystem can be calculated using the equations in Appendix B. Using values of for the cell voltage, the number of electrons reacting per mol of O_2 (4), the mol fraction of O_2 in air (21%), and the design stoichiometric ratio of air for the fuel cell (2.5), the maximum mass flow rate of 453 SLPM was determined using Eq. (B.1). Using Eq. (B.2), the minimum pipe diameter to maintain gas velocities below 25 m/s was ¾". Finally, Eq. (B.3) was used to find the pressure drop per unit length of the air piping at maximum flow. The calculated pressure drop of 3.8 kPa is relatively insignificant when compared to the air system design pressure of 400 kPa.

The air is supplied to the oxidant subsystem by a 5 hp Ingersoll Rand oil-free air compressor. Because of the strict limitations placed on the content of the inlet gases, the compressor had to operate without oil, which could become entrained in the supplied air and passed onto the fuel cell. The internal workings of the compressor are aluminum and the storage tank is made of galvanized steel. Although these metals are not approved for fuel cell systems, the assumption was made that the stagnant flow in the tank would prevent any water droplets, containing harmful metallic ions, from entering the fuel cell.

A ¾" 316 stainless steel pipe supplies the compressed air to the main board of the test stand. Similar to the hydrogen subsystem, a solenoid valve operated in normally closed mode isolates the flow of oxidant if the shutdown switch is depressed. The air then passes through a check valve, which prevents back flow into the compressor, and a branch tee, which is connected to the nitrogen purge line. In the event of an emergency, nitrogen will enter the oxidant control subsystem and purge any remaining air. After the branch tee, the air passes through a single stage pressure regulator since the compressor supplies air at relatively low pressure (100-120 psig).

Following the regulator, the air passes through the Sierra mass flow controllers. The low, medium, and high mass flow controllers can measure and regulate gas flows from 0.12 SLPM to 500 SLPM. Labview operates these mass flow controllers by providing a 0-5V DC signal proportional to the desired mass flow rate. The flow meter piping diagram is shown in Figure 3-4. A ball valve is located before each flow controller, and the operator opens the valve corresponding to the desired meter.

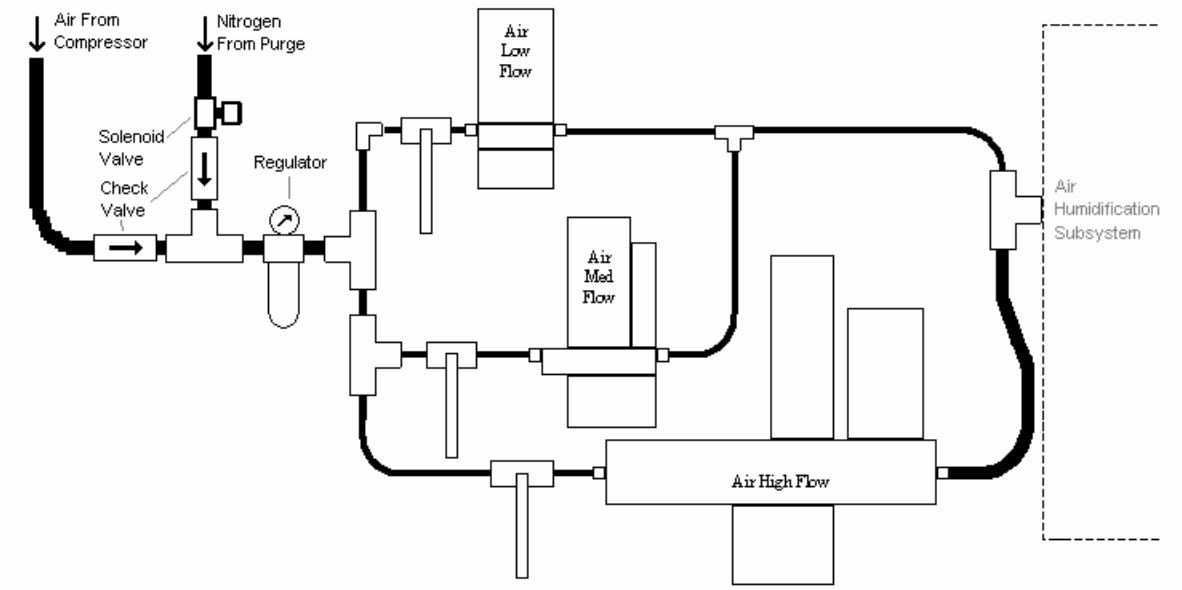

Figure 3-4. Flow controller layout for the air subsystem.

Air from the mass flow controllers passes through the air humidification subsystem, and the gas is heated and humidified to the desired operating conditions of the fuel cell. The air humidification subsystem is enclosed in a stainless steel case and, like the hydrogen

humidification unit, can be completely removed from the main board. The components of this subsystem will be discussed in more detail in the air humidification section.

After being heated and humidified, the operator can select one of two flow paths for the gas. A three-way valve located at the end of the air humidification subsystem allows the operator to either send the gas to the fuel cell or send the gas past the fuel cell and to the outlet. If the gas is at the proper inlet conditions to enter the fuel cell, the valve is turned to the upper flow path (in contrast to the hydrogen subsystem). If the gas is not at the proper conditions, the valve is turned to the lower position and the gases bypass the fuel cell entirely. Similar to the hydrogen subsystem, Teflon tubing is used to make all connections to the fuel cell. The entire subsystem is shown in Figure 3-5.

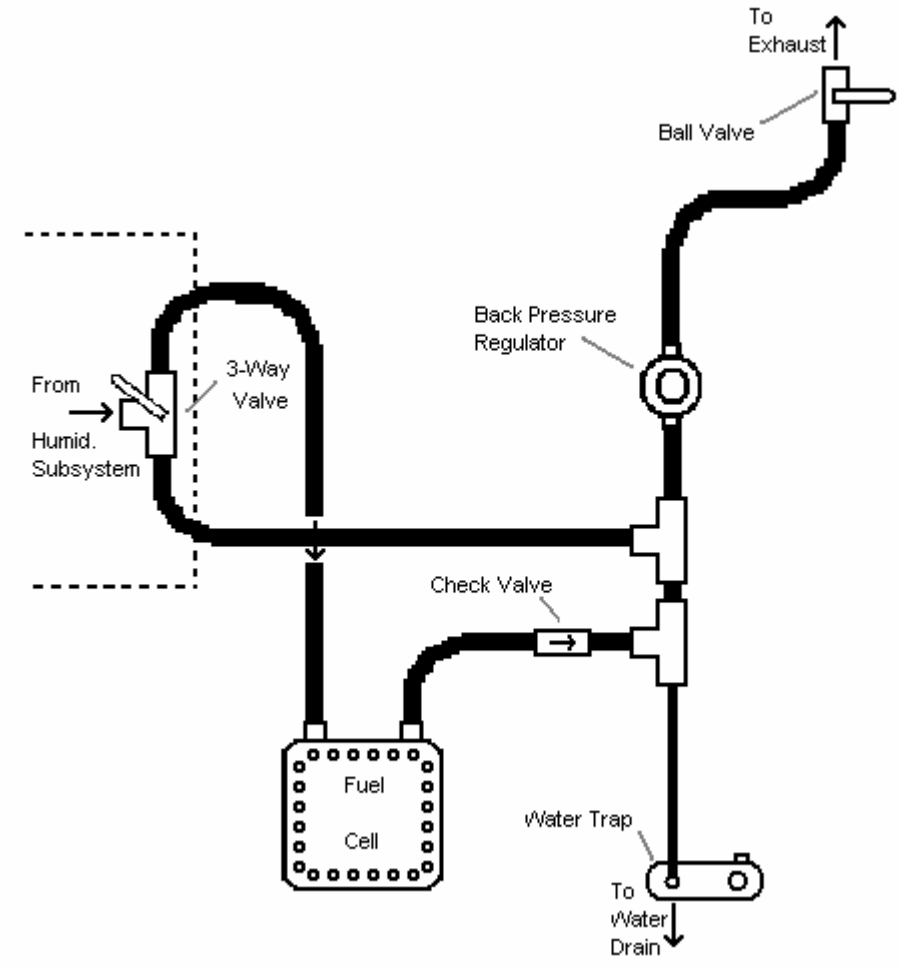

Figure 3-5. Outlet piping of the air subsystem.

Since the air side of the fuel cell is operated in open ended mode, the outlet piping configuration differs from that of the hydrogen. The bypass loop and the outlet piping from the fuel cell combine and pass through a single back pressure regulator. This regulator is made of 316-stainless steel and allows the operator to manually adjust the pressure drop across the fuel cell. Any remaining liquid water drains into a water trap, which is connected to the central drain. After the regulator, the gas passes through a ball valve and is vented to the atmosphere. A flame arrestor is not required for the oxidant piping.

3.3.3 Hydrogen and Air Humidification Subsystem

Maintaining membrane hydration is one of the most difficult aspects of fuel cell operation. Improperly humidifying the inlet gases can either flood the reaction sites of the electrodes (over humidification) or result in the membrane drying out (under humidification). Thus, selection of the appropriate humidification method is paramount to efficient operation of the fuel cell.

The amount of water required to humidify a gas per unit mass of the gas, $\hat{m}_w$, is given by the difference in the humidity ratio at the humidifier inlet, ω_i, and the humidity ratio at the humidifier exit, ω_e:

$$\hat{m}_w = \omega_e - \omega_i \tag{3.1}$$

The humidity ratio is given by:

$$\omega = \frac{R_g \phi P_s(T)}{(P_m - \phi P_s(T))R_w} \tag{3.2}$$

where,

$\omega =$ the humidity ratio of the gas, $\left(\frac{kg_{H_2O}}{kg_{gas}}\right)$,

R_g = gas constant for the gas (air or hydrogen), $\left(\frac{kJ}{kg \cdot K}\right)$,

ϕ = the relative humidity of the gas,

$P_s(T)$ = the saturation pressure of water at temperature, T, (kPa),

$P_m(T)$ = the mixture pressure, (kPa),

R_w = gas constant for water vapor, $\left(\frac{kJ}{kg \cdot K}\right)$,

The saturation pressure of water increases with temperature. As shown by Eq. (3.2), increasing saturation pressure leads to both a larger numerator and a smaller denominator. The result is a dramatic increase in the humidity ratio as the temperature increases. Since the reactant gases start with relatively low moisture content, a humidifier must supply a large amount of water to condition the gases to a high relative humidity at high temperatures. Figure 3-6 shows the mass flow rate of water per kg of gas necessary to fully saturate the gas as a function of temperature. Hydrogen is the gas represented in this figure, and the inlet moisture content of the gas is assumed to be zero.

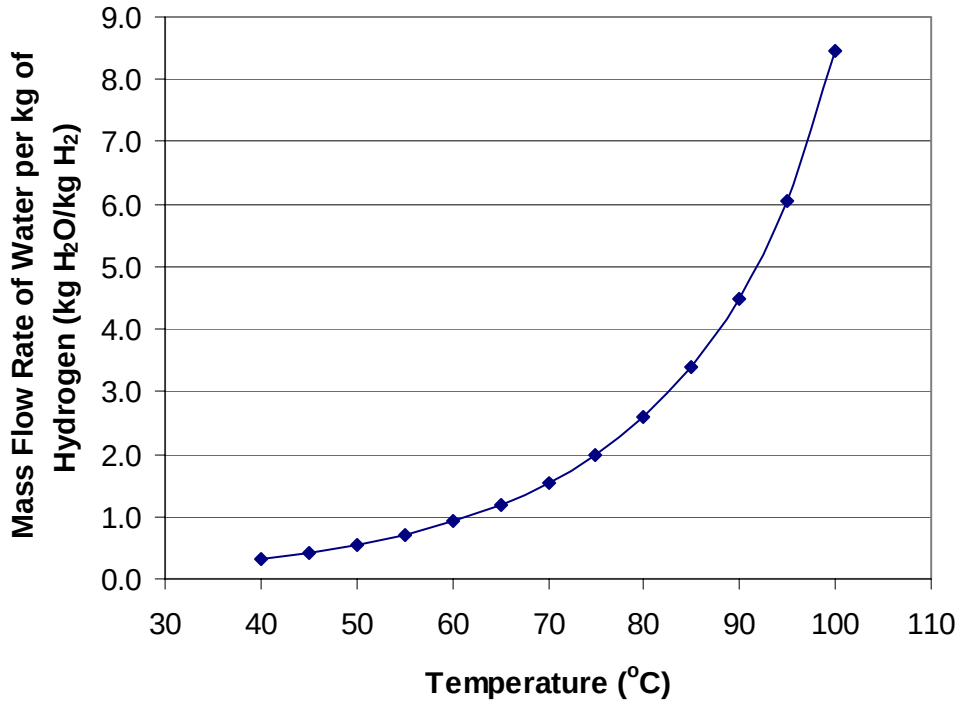

Figure 3-6. Plot of the mass flow rate of water required to fully saturate hydrogen as a function of temperature**.** The graph shows that the required water flow rate increases exponentially as a function of temperature.

As mentioned in Chapter 2, there are four methods commonly used to humidify fuel cells: internal self-humidification, internal membrane humidification, external humidification by

evaporation, and external humidification by vapor injection. Internal self-humidification is possible when working with single MEAs, since the gases can absorb moisture from the porous electrodes. However, this method can be problematic for larger MEAs [Sridhar et al., 2001], particularly at low current densities and temperatures exceeding 60^{o}C. Internal membrane humidification occurs within the fuel cell stack when a portion of the active area of the fuel cell is used solely for heating and humidifying the inlet gases, and is not electrochemically active. By definition, the gases are conditioned in the inactive portion of the fuel cell and introduced to the active area of the cell in the humidified state. Neither of the internal techniques can achieve the high rates of moisture addition required by operation at high temperatures. Thus, external methods including contact humidification, liquid injection, steam injection and flash evaporation were evaluated for this project.

3.3.3.1 Bubbling and Packed Tower Humidification

Initially, Davis [2000] selected a variant of external humidification by evaporation. The humidifier consisted of a vertical cylinder packed with glass beads and flooded with water. The gas was introduced to the bottom of the cylinder and allowed to bubble up through the beads and water. Since the beads created a large surface area for evaporation, the exit gas would approach saturation. This method did achieve high humidity at low rates, but temperature and humidity were difficult to control. In addition, carryover of liquid water at the outlet became a problem at higher flow rates.

3.3.3.2 Liquid Injection

To eliminate this problem, Davis [2000] switched to a humidifier using liquid injection, which consisted of an injection chamber, a length of piping for evaporation, and an expansion chamber to remove excess moisture. In the first stage, water was injected into the gas stream through the use of a fogging nozzle. The fogging nozzle used high pressure gas to atomize water droplets and inject them into the core gas stream. These atomized liquid droplets could then be evaporated into the gas stream over a sufficiently long section of pipe, 24” in the first design phase. After the water had evaporated, the gas passed into an expansion chamber, which was the same cylinder of packed beads used in the previous design. However, in this design the cylinder was not flooded. As the gas-water mixture moved through the packed bed, the large surface area

of the beads collected excess water. Due to the large thermal mass of the system, strip heaters were added at a later date to help evaporate the liquid water.

Although the external humidifier was capable of delivering hot humidified gases to the fuel cell, the control of the system was difficult. Davis [2000] reported problems with water carryover and slow response times. Thus, while the liquid injection system was sufficient to conduct the preliminary evaluations for Phase I, a more precise humidification method and control scheme had to be developed to accurately test the effect of inlet gas humidity on the performance of the fuel cell.

3.3.3.3 Vapor Injection

The problems associated with both bubbling and liquid injection can be overcome by using water in the vapor state for humidification. When water is injected in the liquid phase, energy from the gas is required for evaporation. This lowers the temperature of the gas/vapor mixture. The coupling between the liquid injection rate and the air temperature makes control of the humidity and temperature difficult. Furthermore, evaporation of the liquid may not be complete, leaving an undesirable mist of liquid water in the air. By injecting steam, the water is delivered to the gas stream in the vapor phase at a temperature higher than the gas temperature. This assures that there is no decrease in the gas temperature due to evaporation. In fact, the post injection temperature exceeds the inlet temperature. Gas coolers are then used to reduce the gas temperature to the desired value. By cooling the gas, excess moisture will condense leaving a 100% saturated mixture at the desired inlet temperature to the fuel cell. Figure 3-7 shows the hydrogen/air humidification subsystem used on the stack test stand.

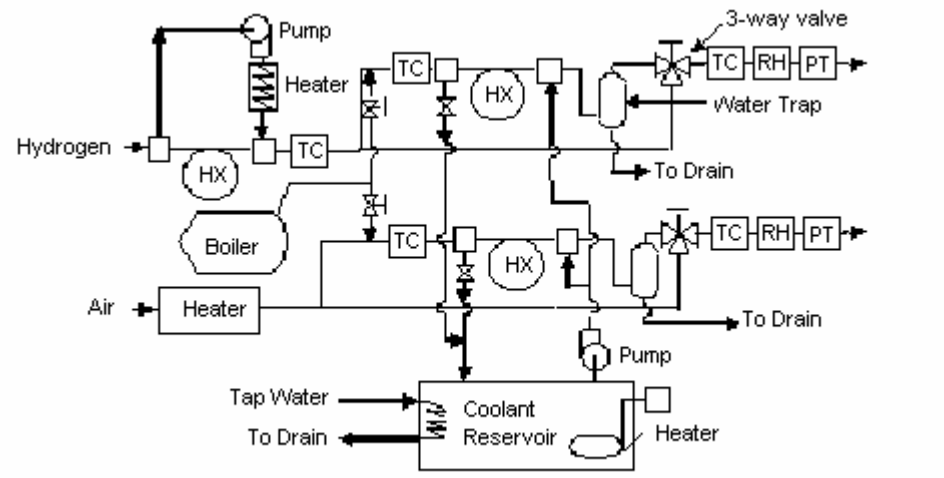

Figure 3-7. Diagram showing the arrangement of components within the hydrogen/air humidification subsystem.

As shown in Figure 3-7, when the gases first enter the hydrogen/air humidification subsystem they each enter a gas heater. For the air, an Omega inline 100 W electrical resistance heater is used to bring the gas to the desired operating temperature. However, special note should be taken of the hydrogen heater. Hydrogen is flammable at 570^{o}C (~1060 ^{o}F) and inline heaters can produce outlet temperatures as high as 470^{o}C (~880 ^{o}F) during normal operation. In the event of a malfunction or abnormal conditions, the high temperature in the hydrogen heater could potentially ignite the hydrogen. To improve safety, the hydrogen is heated indirectly through the use of a tube-in-tube heat exchanger. The heat transfer fluid, propylene glycol, is kept in a closed loop, and a GrundFos 1 HP circulating pump constantly circulates fluid through the heat exchanger. The fluid is heated through the same type of inline heater used in the air system. The hydrogen gas temperature is adjusted by controlling the operation of the heater through a Eurotherm control unit.

After being heated, the gas flow streams are then divided into two separate branches, denoted as “dry” and “wet.” The dry branch completely bypasses the steam injection-chiller units and recombines with the wet branch at the outlet of the water trap. Each dry and wet branch contains a globe valve that regulates the flow through that section. The wet branch then passes into the steam injection body, where steam is supplied at 80 psig from a 1kW boiler. The boiler is located directly below the outlets of the humidification enclosures. Within each enclosure, a globe valve regulates the flow of steam into the fuel and oxidant control subsystems and

consequently the desired post-injection temperature of the mixture. The combined gas and mixture temperatures are then measured with thermocouples.

The wet gas streams then pass into the two chiller units, which are tube-in-tube heater exchangers that use a 90% propylene glycol – 10% water mixture as the heat transfer fluid. The humidified gases are cooled to the desired temperature, and the excess vapor condenses into water droplets. Cooling water for the chillers is supplied by a large coolant bath and a ¼ HP circulating pump. Both a resistance heater and a cooling coil, which is connected to the city water supply, control the coolant bath temperature. This coolant bath should typically operate at a temperature slightly below the desired reactant gas temperature, and the globe valves on the outlets of the gas coolers are used to adjust the coolant flow rate and the outlet temperature of the humidified gas. In addition, the coolant loop supplies heat trace tubing wrapped around the water trap and measurement devices.

After exiting the chiller units, the wet streams are saturated with water. Each stream flows to a water separator, where liquid water is removed. As the gas enters the water separator, the velocity decreases and droplets simply fall out of the flow. In addition, two baffles require the flow to make two 180^{o} turns, thus, removing any remaining droplets. The liquid water drains out through tubing connected to drain traps located on the bottom of the board. The drain traps are controlled by a solenoid valve and level switch. When the water level reaches the switch, the solenoid valve opens and allows water to drain from the trap. The switch is operated by a delay and automatically closes the solenoid in a matter of seconds.

After exiting the water separator, the wet stream is recombined with the dry stream, which bypassed the steam injection system. The combined flow then passes through the measurement devices which include, a thermocouple, pressure transducers, and relative humidity transmitters. If the flow meets the operating conditions, the three-way valve on the outlet of each humidification subsystem is opened to allow flow into the fuel cell. If the flow is not at the proper temperature, pressure, or humidity, then the manual valve can be used to bypass the fuel cell and vent gas to the atmosphere. This prevents damage to the fuel cell.

The hydrogen/air humidification subsystem can be divided into four separate elements: the hydrogen humidification enclosure, the air humidification enclosure, the boiler, and the coolant subsystem.

Hydrogen Humidification Enclosure. The first component of the humidification subsystem is the hydrogen humidification enclosure. Dry hydrogen gas enters this unit and is heated and humidified to the desired inlet conditions for the fuel cell. The enclosure is shown in Figure 3-8.

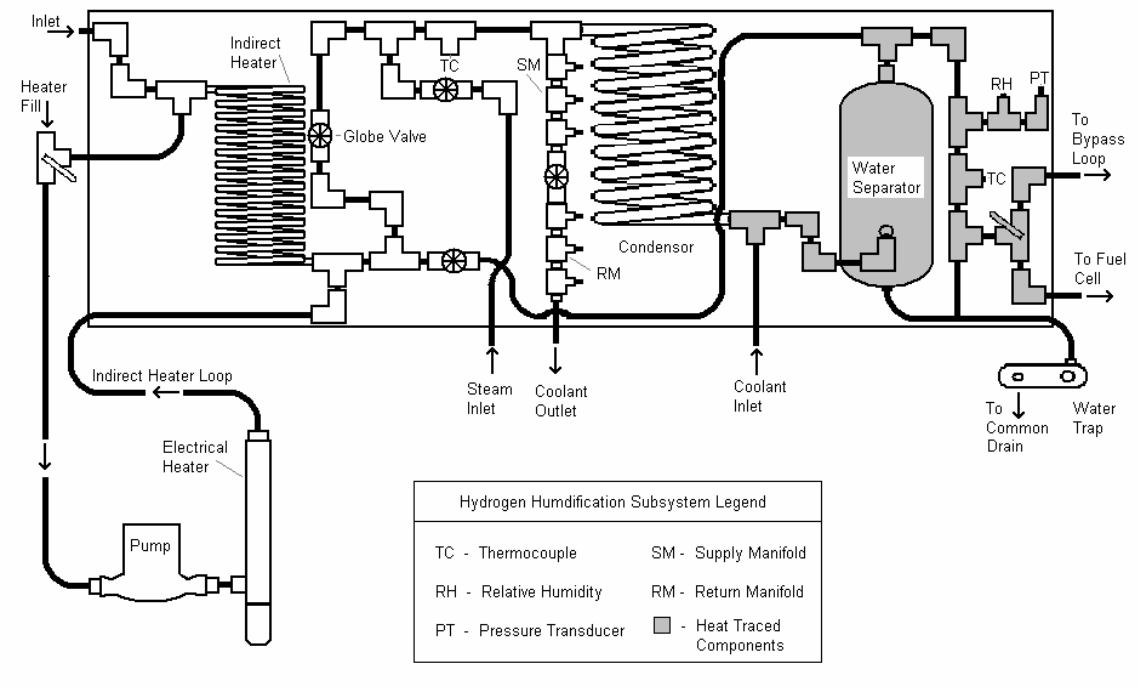

Figure 3-8. Diagram of hydrogen humidification enclosure piping. The gray shading indicates components which have been heat traced with silicon tubing.

Hydrogen is supplied to the hydrogen humidification enclosure by the stainless steel outlet tube from the flow controllers (see Figure 3-2). After entering the enclosure, the gas flows through the indirect heater, which is a tube-in-tube heat exchanger. The parameters of the three tube-in-tube heat exchangers used in the hydrogen humidification subsystem are summarized in Appendix C. To avoid potential ignition of hydrogen, the indirect method of humidification was selected over direct resistance heating. Dry hydrogen gas passes through the inner coil of the heat exchanger and a 90% propylene glycol / 10% water mixture passes through the outer coil in a counter flow configuration. A 1/25 hp pump re-circulates the fluid through a closed loop and the

fluid is heated by a 100 W resistance heater similar to the one used in the air humidification subsystem.

After passing through the indirect heater, the hydrogen gas is divided into two flow paths. The first path is the “dry” branch, which bypasses the steam injection and cooler units and reconnects to the subsystem above the outlet of the water separator. The second path is the “wet” branch and flow is controlled through this path with a globe valve. After passing through the globe valve, steam is injected into the hydrogen gas through the branch of a tee. The steam is supplied to the enclosure by the boiler, and flow is controlled by a globe valve.

After the injection point, the hydrogen and water vapor are given a length of 7” in which to fully mix. A length of at least 5” (ten pipe diameters) was recommended, which is more than satisfied by the 7” section. A thermocouple inserted into the flow path measures the temperature at the end of the mixing length. If the gas temperature is too low or too high, the operator may need to adjust either the heat transfer fluid flow rate through the heater or the amount of steam being injected. The hydrogen – water vapor mixture then passes through the inner coil of the hydrogen gas cooler. The coolant mixture passes through the outer loop of the gas cooler in a counter flow configuration and into a brass supply manifold for the heat trace tubing. To reduce the heat loss to the environment, all elements of the hydrogen humidification enclosure following the gas cooler were heat traced with silicon tubing. After absorbing the heat from the hydrogen – water vapor mixture, a portion of the coolant circulates through this tubing and helps maintain the temperature of the piping within the enclosure. The fluid returns to the coolant system through a return manifold, which is then connected to the coolant bath.

As the hydrogen-water vapor mixture is cooled, excess water may condense as droplets, which either collect on the inner coil walls or become entrained in the flow. Water collecting on the inner walls drains down into the water separator via gravity. Entrained water droplets are removed from the hydrogen – water vapor mixture by the water separator itself. Because the diameter of the vessel is significantly larger than the hydrogen system piping, the hydrogen – water vapor mixture expands within the vessel and decelerates. As the flow velocity drops, water

droplets simply fall out due to the higher density of water. Water collected in the moisture separator then drains to an automatic trap.

After passing through the water separator, the hydrogen – water vapor mixture recombines with the dry branch in a tee above the outlet. The combined flow then passes through two measurement tees, one containing a relative humidity sensor and a pressure transducer and the other containing a thermocouple. After measurement, a three-way valve allows the operator to select either the lower flow path to the fuel cell or the upper flow path to bypass the fuel cell.

Air Humidification Enclosure. Most of the components for the air humidification enclosure are similar to those used in the hydrogen humidification enclosure. However, the air can be directly heated by a 100 W resistance heater. The air humidification enclosure is shown in Figure 3-9.

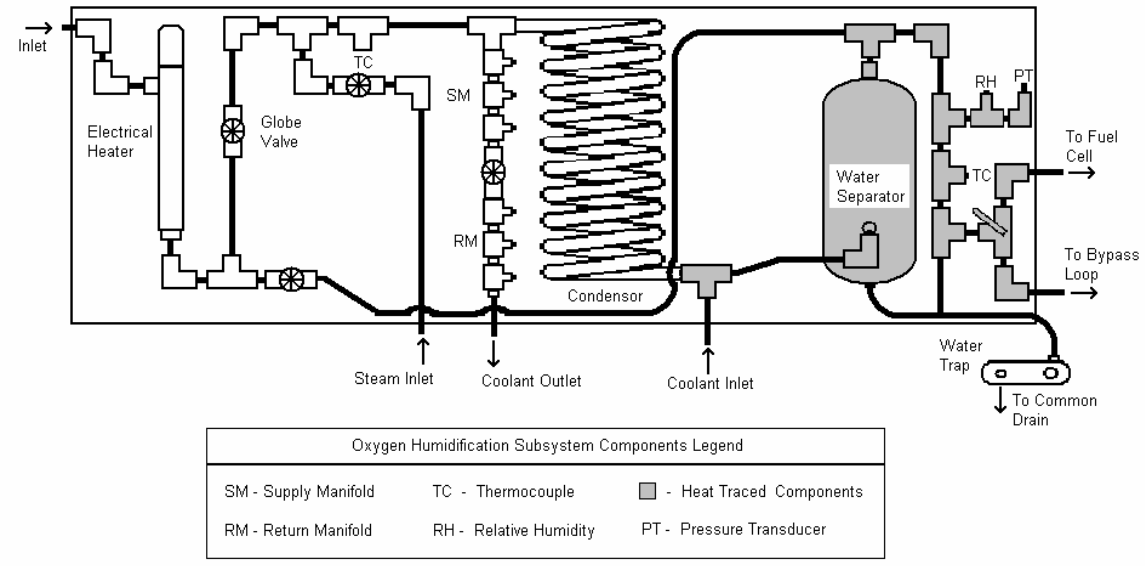

Figure 3-9. Humidification enclosure for the air humidification subsystem. Heat traced components are indicated with gray shading.

Air enters the air humidification enclosure through tubing from the flow controllers (see Figure 3-4). This directly connects the inlet of the 100 W electrical resistance heater. A thermocouple measures the temperature at the outlet of the air heater, and the heater operation is controlled through a PID temperature controller manufactured by Eurotherm. After the outlet of the heater, the pipe is divided into two flow paths. The first path is the dry branch, which

bypasses the steam injection and coolers and reconnects at the outlet of the water separator. The second path also passes through a globe valve, which controls the flow rate, and into the steam injection tee. The steam is supplied to this tee in the exact same manner as the hydrogen. However, a 10" mixing length follows the tee in the air humidification enclosure although only a length of 7.5" inches is required. At the end of the mixing length, the temperature of the air – water vapor mixture is measured by a thermocouple inserted into the flow path. If the temperature is either too low or too high, the operator can either adjust the output temperature of the resistance heater with the Eurotherm or adjust the flow rate of steam.

Once the temperature of the mixture has been measured, the mixture passes into the inner coil of the air side cooler. The heat transfer fluid passes through the outer loop of the condenser in a counter flow configuration and is supplied by silicon tubing from the coolant bath. At the outlet of the outer loop of the cooler, the coolant passes through a brass supply manifold for the heat trace tubing. Similar to the hydrogen system, all elements of the air humidification enclosure following the cooler were heat traced with silicon tubing. A globe valve, located after the supply manifold, regulates the flow rate through the cooler and through the heat trace tubing. The tubing returns to the coolant system through a return manifold.

As the air-water vapor mixture chills in the cooler, excess water may condense out as droplets, which will either collect on the inner coil walls or become entrained in the flow. Water from the cooler will drain down through this tubing into the water separator via gravity. The water separator configuration and operation is exactly the same as the one used in the hydrogen humidification enclosure, and the trap operates in the same manner. After passing through the water separator, the air – water vapor mixture recombines with the dry branch in a tee located on the outlet. The combined flow then passes through two measurement tees, one containing a relative humidity sensor and a pressure transducer and the other containing a thermocouple. The flow then passes through a tee and the branch goes to a three-way valve. This valve allows the operator to select either the upper flow path to the fuel cell or the lower flow path to bypass the fuel cell.

Boiler. The steam is supplied to the humidification enclosures by a small boiler located under the outlet piping of the main board. The boiler is made of 316 SS and can supply a maximum pressure of 125 psig and flow rate of 21 lbm/hr. The assembly includes a stainless steel centrifugal pump, level control switches, and safety controls. Water is supplied to the boiler feed pump from a mixed bed de-ionizer located adjacent to the main test station. A diagram of the steam system piping is in shown in Figure 3-10.

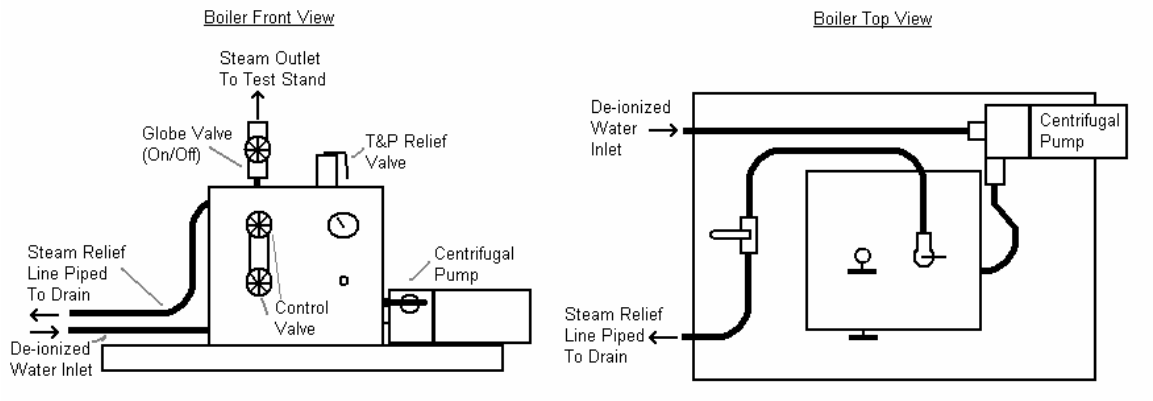

Figure 3-10. Front view and top view of boiler system and piping. Two valves control the steam level within the boiler, and an automatic shutdown switch activates when the boiler is full.

Coolant Subsystem**.** The coolant subsystem consists primarily of the water supply module, the coolant bath, and the coolant water supply board. The water supply module provides both de-ionized water to the boiler and normal water to the coolant water supply board. City water is introduced to the system and flows through a back flow preventer, which prevents contamination of the main water supply for the building. Copper tubing is used for all of the city water piping in the module. The main supply then splits into two branches, one going to the coolant water supply board and the other going to a de-ionizing bed. The de-ionizing bed supplies water to both the boiler and a tap for de-ionized water supply. Figure 3-11 shows the piping scheme for the water supply module. The subsystem piping diagram for the coolant bath and coolant water supply board is shown in Figure 3-12.

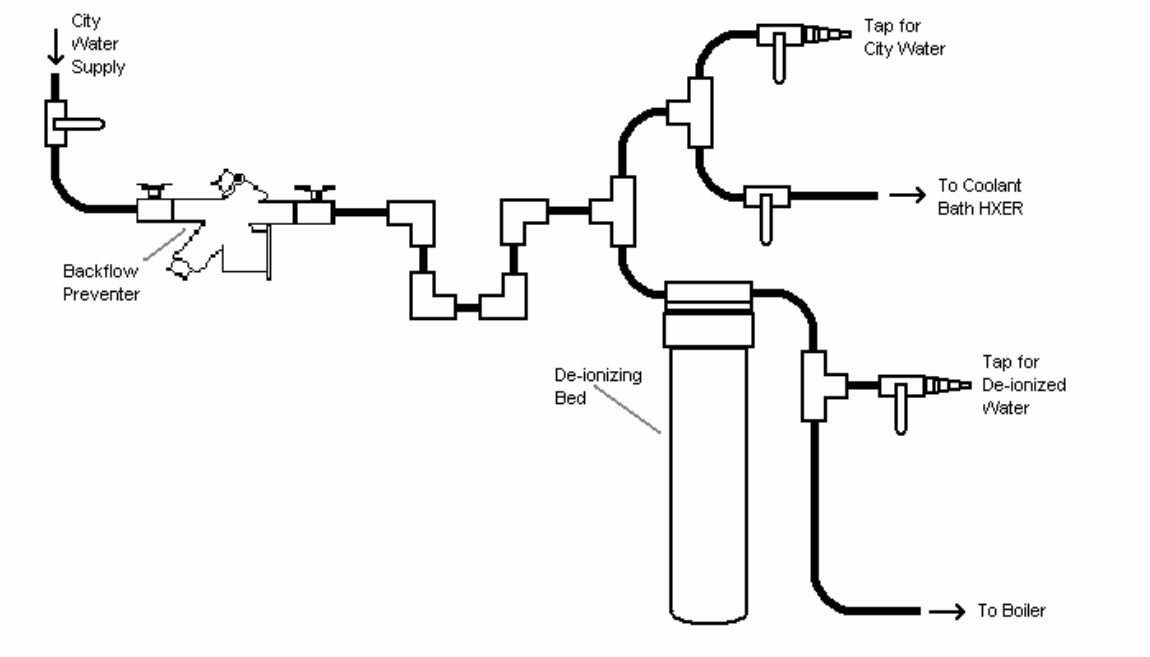

Figure 3-11. Piping scheme for the water supply module. The inlet is supplied with water from the main supply for the building. Four outlets supply water in the normal or de-ionized state: one tap for access to the main water supply, one line running to the coolant bath HXER, one tap for access to de-ionized water, and one line of de-ionized water running to the boiler.

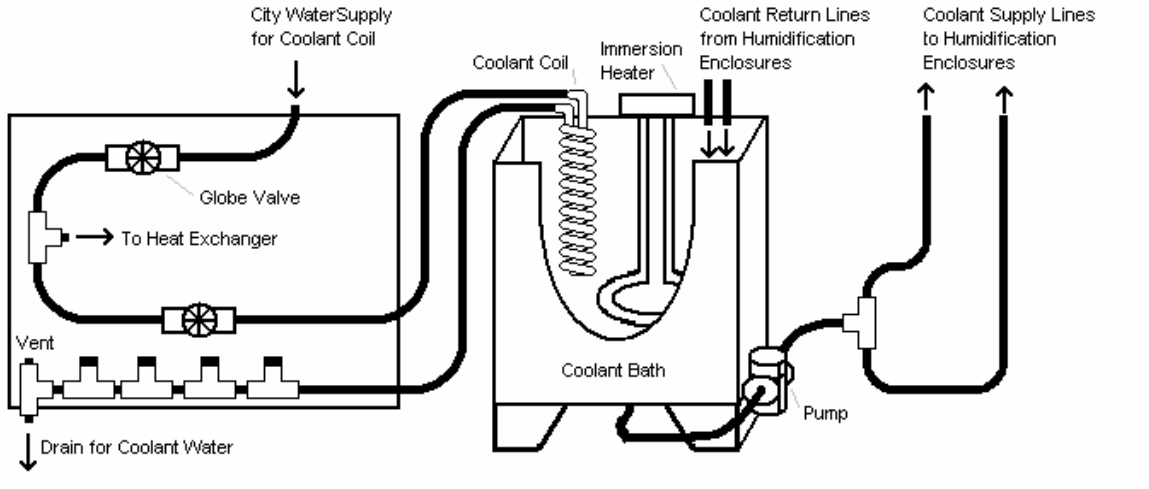

Figure 3-12. Diagram for the coolant system piping. The coolant bath wall is cutaway to show the location of the heat rejection coil and immersion heater.

The coolant bath is made of galvanized steel and is insulated via double walled construction. The coolant mixture is drawn from the bottom of the bath by a 1/25 hp centrifugal

pump. The outlet of the pump divides into two branches, a tube going to the air humidification enclosure and a tube going to the hydrogen humidification enclosure.

The coolant bath contains two components that maintain its temperature. The first component is a 600 W immersion heater. The bath temperature is measured by a Type T thermocouple and is controlled by the Eurotherm temperature controller. The second component is a heat rejection coil made of copper tubing. City water at 18°C enters the coil, and the flow rate can be varied according to the desired amount of heat rejection needed from the bath. As calculated in Appendix C, the maximum heat rejection rate through the coil was 1660 W.

The city water is supplied from the coolant water supply board, which is located on the lower left side of the main board. Water is supplied to the board from the water module through a ½" neoprene hose. Copper tubing of ½" diameter is used for the supply line piping on the board. Two globe valves control the flow rate on the board. The first valve is the main shutoff for the board and the second valve controls the flow rate to the coolant bath heat rejection coil. A central drain exists on the bottom of the board, into which the return line from the heat rejection coil is connected. This line is vented and connects to the common drain.

3.3.3.4 Flash Evaporation System

The Lynntech flash evaporation system used to humidify the reactant gases was essentially a self-contained unit. All that was needed to operate was a source of de-ionized water fed through ¼" Teflon tubing to the humidifier and the connections for the inlet and outlet gases. These gases were supplied with ¼" Teflon tubing as well. Once connected to a power source, operation of the humidifier was controlled by the computer. Two methods of control were provided: constant dewpoint method where the Lynntech would achieve a target dewpoint by adjusting the injection rate and constant injection method where the Lynntech would simply inject water into the flash evaporation chamber at specified rate continuously. The performance of both control methods will be discussed in detail in Chapter 4.

3.3.4 Measurement and Control Subsystem

The operation of the 5kW test stand is highly dependent on the accurate measurement and control of the operating variables of the fuel cell. These variables include pressure, mass flow rate, temperature, and relative humidity. This section will review the devices used to measure these variables, as well as the manual and automatic control schemes to achieve their desired levels.

3.3.4.1 Data Acquisition and Control

The data acquisition system is composed primarily of a computer and HP 3852A DAQ, which collect and record the data from the test stand. The data acquisition system is diagramed in Figure 3-13. Measurement signals from the mass flow controllers, thermocouples, pressure transducers, and relative humidity transmitters all enter into the junction box located in the data acquisition cabinet. This junction box also supplies ± 15 VDC power to the flow controllers.

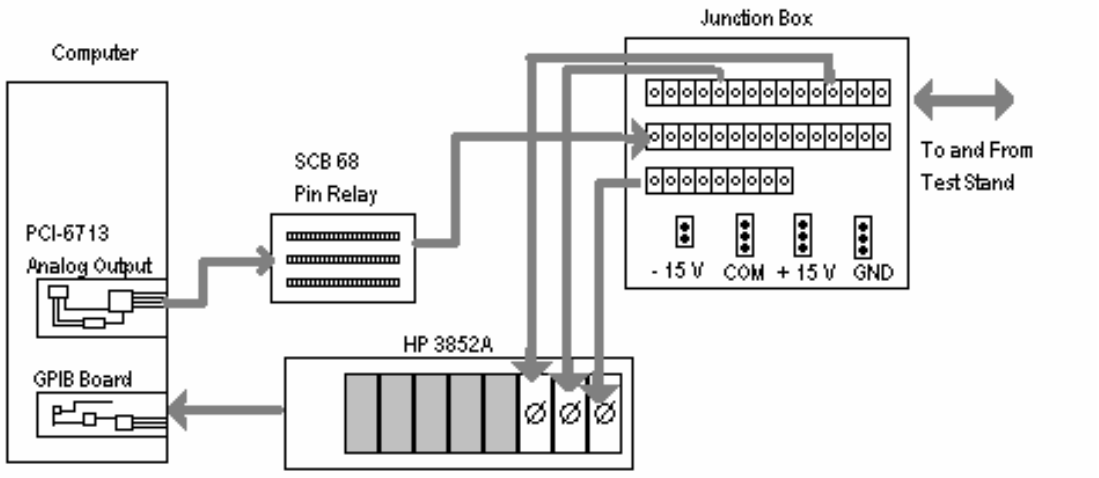

Figure 3-13. Diagram of data acquisition system. This system consists of the computer, the GPIB card, the HP 3852A DAQ, the PCI 6713 analog output, the SCB 68 pin relay board, and the Junction box.

After entering the junction box, the wires are connected to individual junctions. These wires from these junctions are then grouped into types and passed to the HP 3852A data

acquisition system. This system is capable of taking readings every 0.5 seconds. These readings are then sent to the GPIB board in the computer. This board then relays the information to the LabView software, which displays the readings in the graphical interface on the screen.

Based on the desired mass flow rate specified by the user, LabView communicates with the PCI-6713 analog output board to provide a 0-5 VDC input signal to the mass flow controllers. The PCI-6713 board has the capability of simultaneously outputting eight control signals with a range of 5-20 mA and 0-5 V. The output of this board is connected to an SCB 68 pin relay board, which separates out the individual control signals sent from the card. These signals are then wired back into the junction box, and then to the mass flow controllers.

3.3.4.2 Measurement Devices

Measurement devices measure gas flow, pressure, temperature, and relative humidity. The mass flow controllers provide both measurement and control functions. The specifications of the measurement devices (and the combined measurement and control devices) are provided in this section.

Mass Flow Controllers. The mass flow rates of the reactant gases are both measured and controlled by Sierra Side-Trak model 840 mass flow controllers. Each of these devices requires both a + 15 VDC and – 15 VDC power input. The desired output of the controller is controlled by a 0-5 VDC signal supplied by an analog output board in the computer. The measured flow rate is output as a 0-5 VDC signal, which is read by the HP 3852A data acquisition system. Labview then converts this voltage signal to the corresponding flow rate.

Three flow meters are currently used with each reactant gas subsystem. The error rate given by Sierra is ± 1% of full scale. The measured flow rate and maximum actual error for each flow meter are given in Table 3-1.

Table 3-1. Flow rate and error values for Sierra Side-Trak model 840 flow meters.

Subsystem	Flow Type	Flow Range (SLPM) Minimum	Maximum	Maximum Error (SLPM)	Tube Connections (in)
Fuel	Low	0.03	1.5	± 0.015	0.250
Fuel	Medium	0.8	40	± 0.400	0.250
Fuel	High	3.4	170	± 1.700	0.500
Oxidant	Low	0.12	6	± 0.060	0.250
Oxidant	Medium	2	100	± 1.000	0.375
Oxidant	High	10	500	± 5.000	0.500

Pressure Transducers. Before the fuel cell inlets, two Kobold pressure transducers measure the pressure of the reactant gases. These transducers output a 0-20 mA signal and are capable of measuring between 0 and 100 psig. The error of these pressure transducers is given as ± 0.12% of full scale, so the value is 0.12 psig for the models being used. Since these transducers are measuring "wet" gases, all materials in contact with the flow gases are 316-stainless steel.

Thermocouples. All thermocouples used on the test stand are type T, which use a copper-constantan junction. The sheath is made of 321-stainless steel with a diameter of 1/8", and the junction is grounded to the sheath. Grounded junction thermocouples both protect the junction within the sealed sheath and provide response times comparable to those with exposed junctions. All thermocouples are incorporated in the system using 1/8" stainless steel compression fittings to prevent leaks and all electrical connections are made with 24-gauge type T thermocouple wire. The thermocouples are read using the Eurotherm temperature control modules and the HP 3852A data acquisition system. The Eurotherm unit reads and controls the temperatures for hydrogen heater, the air heater, and the coolant tank. The HP 3852A reads the temperatures for the humidification system, the fuel cell inlet gases, and the operating temperature for the fuel cell, but does not control any of these readings.

Relative Humidity Sensors. The relative humidity of the fuel and oxidant streams is measured with VAISALA HMP 230 transmitters and HMP 234 sensors. The transmitter requires a 120 VAC signal to operate and outputs a 0-5 V DC signal proportional to 0–100% relative humidity. The sensors are accurate to 1% for a relative humidity of 90% or lower. The accuracy decreases to within 2% for a relative humidity level above 90%. The HMP 230 humidity

transmitter is an enclosed unit and is mounted on the outside of each humidification enclosure. The HMP 234 sensor body is made of 316-stainless steel, and a 316-stainless steel sintered metal cap prevents contamination of the sensor head by particles or water droplets.

3.3.4.3 Control Devices

This section reviews devices used to control the operation of the test stand.

Manual Pressure Regulation Valves. Several devices control the pressures of the reactant gases. For the fuel flow control subsystem, the pressure is primarily controlled by a two stage pressure regulator located on the tank and a single stage regulator located after the solenoid valve. The operator can manually adjust both of these regulators to alter the hydrogen pressure at the inlet to the mass flow controller. If the fuel cell is being operated in open-ended mode on the fuel side, the mass flow controllers regulate the pressure of the gases entering the fuel cell. The mass flow controllers operate by regulating the pressure drop across a variable position valve. As a result, the pressure at the inlet to fuel cell is a function of the mass flow rate. The pressure at the outlet of the fuel cell can be controlled with a back pressure regulator and will be at or above 1 atm when operating in open-ended mode.

Similar to the fuel flow control subsystem, the oxidant flow control subsystem also uses two regulators as the primary control of the inlet gas pressure. A regulator controls the tank pressure of the compressor, which cannot be adjusted by the operator. However, the single stage regulator located immediately after the solenoid valve may be manually adjusted. Likewise, the backpressure regulator located after the outlet of the oxidant side of the fuel cell also can be manually adjusted to achieve a desired outlet pressure for the fuel cell, typically between 1 atm and 3 atm.

Manual Flow Control Valves. The reactant gas flow paths in the fuel and oxidant flow control subsystems are controlled by three stages of valves. Initially, the operator selects which mass flow controller to use by opening the corresponding ball valve. After selecting the flow controller, the operator must then decide the desired ratio of dry and wet gases to use. This is accomplished by adjusting the globe valves located on the wet and dry branches of each

humidification enclosure. The operator must select whether to send the gas to the fuel cell or through the bypass loop to be vented to the atmosphere.

Relative humidity is also controlled by three groups of valves: the steam valve, the wet and dry gas branch valves, and the coolant flow rate valves. Increasing or decreasing the amount of steam injected into the reactant gas stream can adjust the saturation temperature of the gas and vapor mixture. This mixture then passes through the gas coolers where it is cooled to the desired final temperature. Finally, the gas from the humidifier is mixed with dry gas that has bypassed the humidifier to achieve the desired humidity.

Temperature Controllers. Eurotherm model 810 temperature controllers are used to regulate the hydrogen heaters, air heaters, and humidification coolant bath heaters. These controllers use a type T thermocouple to measure the temperature and a continuous PID control routine to adjust the duty cycle of a 120 VAC heater accordingly. The set point is input by the operator using a series of buttons located on the front of the controller.

Mass Flow Controllers. The mass flow controllers provide both a measurement function (described previously in the data acquisition section) and a control function. The control function varies the flow of gas linearly in response to a 0-5 VDC signal from the PCI-6713 analog output card located in the PC. In the control panel window, the operator sets the desired mass flow rate and selects the appropriate mass flow controller. The LabView software then directs the analog output card to send an output signal to the mass flow controller that corresponds to the desired flow rate.

Programmable Load. The programmable load varies the electrical characteristics of the fuel cell load and provides safety features to prevent damage to the load and the fuel cell. When connected to the fuel cell, the Dynaload RBL-100-600-4000 simulates an electric load. The load operates to control the voltage, current, or power within the ranges given in Table 3-2.

Table 3-2. Range of operation for Dynaload RBL-100-600-4000.

Parameter	Range
Voltage	0-100 Volts
Current	0-600 Amps
Power	0-4,000 Watts

Switches on the front panel of the load select the control variable and range. The setpoint is remotely programmed via a 0-10 VDC signal supplied by the analog output card in response to the LabView control program. In the control panel window, the operator selects the control variable and range corresponding to the settings on the front panel of the load. The operator then enters the desired setpoint value, which is then passed to the load.

The load also provides several safety features to protect both the load and the fuel cell. The voltage of the load is limited to 105% of the selected range, the current is also limited to 105% of the selected range, and the power is limited to 4,250 Watts. If any one of these limits is exceeded, then the load is automatically disconnected. In addition, the load can be automatically disconnected in response to a signal from the control software.

3.3.5 Safety Subsystem

The safe operation of PEM fuel cell systems requires the awareness of potentially dangerous conditions and the inclusion of procedures to avoid these conditions. Since hydrogen is the fuel used for our fuel cell evaluation, particular care must be taken to assure its safe handling. The lower flammability limit of hydrogen in air is 4.1% by volume and almost any concentration of leaking hydrogen in air could ignite. This chapter will review the procedures and devices in place on the test stand to alleviate the risk associated with hydrogen, as well as other safety concerns associated with high temperatures.

3.3.5.1 Hydrogen Leak Detection

The first line of defense against ignition of hydrogen-air is the rapid detection of hydrogen leaks. This detection is accomplished through the use of two Figaro detection units

designed to measure the volumetric concentration of hydrogen in air. Both visual and audible alarms will be activated when the units detect concentrations of hydrogen in excess of 0.41% (10% of the Lower Flammability Limit). Typically, these units are mounted at the highest point in a facility. Hydrogen's lower density, with respect to air, results in the hydrogen rising to the highest point and collecting there. However, a significant cross flow of air exists in the ceiling of the Ware Lab facility. It was decided that the hydrogen sensors would be more effective if placed closer to the source of a potential leak.

Three such sources of hydrogen leaks exist: the hydrogen tank, the piping of the fuel cell test stand, and the water trap outlet piping which exits into a common drain. A hydrogen sensor was mounted directly above the hydrogen tank, and a second sensor was mounted above the common drain to which the trap outlets are piped. Because of the high flow rates generated by the exhaust hood, a sensor was not required above the piping system.

3.3.5.2 Exhaust Hood

As mentioned in the previous section, the inclusion of an exhaust hood eliminated the need for leak detection units to be located in close proximity to the piping of the test stand. The hood is located directly above the main board of the test stand. A blower draws 3150 cfm of air from the area of the test apparatus and discharges this air above the roof. For a maximum hydrogen flow rate of 170 SLPM, the concentration of leaking hydrogen is only 0.19% of the air moving through the hood. The hood will be in continuous operation any time the test stand is operating.

3.3.5.3 Emergency Shutdown Switch

In the event of a hydrogen leak or other unsafe condition, an emergency shutdown switch is located on the right side of the main board. By depressing the shutdown switch, the power is disconnected from five solenoid valves. The first solenoid is located immediately after the hydrogen tank, and is operated in a normally closed mode. When power is disconnected, this valve will close and isolate the hydrogen source. Likewise, the second solenoid valve is located after the compressor and also operates in a normally closed mode. Loss of power to the valve will isolate the oxidant source. The third and fourth solenoid valves are part of the nitrogen purge

system and operate in a normally open mode. When power is disconnected, the third and fourth valves open and allow nitrogen to flow into the fuel and oxidant systems, respectively. The fifth solenoid valve is located in the outlet piping of the hydrogen subsystem. This valve operates in normally open mode, which will allow all hydrogen to be purged from the fuel cell and vented to the atmosphere in the event that the power is disconnected.

3.3.5.4 Nitrogen Purge

The use of a nitrogen purge helps to prevent ignition of hydrogen and air mixtures by displacing both gases with inert nitrogen. When the emergency shutdown switch is depressed, the solenoid valves will open and allow nitrogen to flow through the fuel and oxidant systems. The nitrogen is supplied from a carbon steel tank, but should not pick up any metal ions since the gas will be in a dry state. After passing through a two-stage regulator, the nitrogen splits into two flow paths. The first flow path is composed of ¼" Teflon tubing and allows for nitrogen to be used for evaluation of individual components not connected to the main fuel and oxidant flow control subsystems. The second flow path is used to purge the fuel and oxidant flow control subsystems.

After flowing into the second flow path, the nitrogen immediately flows through a simple sight gauge flow meter. Following the flow meter, the stream is then divided into two paths, with each path passing through a solenoid valve and check valve before entering the fuel and oxidant flow control subsystems. The check valves prevent the reactant gases from flowing upstream toward the nitrogen tank. By introducing the gases at the inlet of the main board, the nitrogen passes through the fuel and oxidant subsystems and will be at the proper pressure, mass flow rate, temperature, and humidity required by the fuel cell.

3.3.5.5 Flame Arrestor

As an added precaution, two flame arrestors are provided in the hydrogen flow control subsystem. Passages within these elements cause the main hydrogen flow to be broken up into smaller streams. The main principle behind these flame arrestors is that flames are limited by their propagation speed. If the flow velocity exceeds the propagation speed, flames cannot propagate upstream. The first flame arrestor is a simple inline model and is located between the

two-stage regulator on the hydrogen tank and the solenoid valve. This location prevents any flame found in the hydrogen piping from traveling into the tank and igniting the hydrogen there. The second flame arrestor is located on the exhaust of the hydrogen vent pipe to the atmosphere. The Superflash flame arrestor can handle outlet pressures of up to 50 psig and flow rates over 100 scfh.

3.3.5.6 High Temperature Safety Precautions

There are two potential high temperature sources that could cause serious injury to an operator - the boiler and the inline air heater. The boiler is used to supply steam at a pressure of 5.4 atm and a temperature 162^{o}C (324^{o}F) to the hydrogen/air humidification system. The majority of this piping is located within the humidification enclosures and should not present any danger to operators during normal operation. However, special care must be taken around these pipes when working inside the humidification enclosures. The boiler automatically shuts off when either the desired pressure is reached or no water is available, which prevents damage to the heating element. Likewise, the boiler is fitted with an ASME temperature and pressure relief valve hard piped to the common drain. This valve will prevent over pressure and rupture of the boiler.

The second source of potentially dangerous temperatures is the inline air heater. The Omega inline heater is capable of producing outlet gas temperatures of 430^{o}C (800^{o}F). Even when supplying 80^{o}C air, heater surfaces can reach up to. Between the first and second design phases, the air heater was moved into the humidification enclosure. In addition, the heater is heavily insulated to increase heat transfer into the reactant gas. Both of these actions have reduced the risk to the operator during normal operation of the test stand, although caution must be taken when working inside the enclosure.

3.4 Validation of Test Apparatus

To assure proper operation of the test stand, all components were thoroughly evaluated over a two month period before the operation of a fuel cell. The following section reviews the evaluation process for each of the subsystems, with particular focus on the Humidification and Measurement and Control Subsystems.

3.4.1 Fuel Flow Control Subsystem

For safety concerns, the fuel flow control subsystem was evaluated with nitrogen instead of hydrogen. The subsystem was tested both for leaks and for proper evaluation of all control valves and components. Leak testing occurred both during the assembly of the fuel flow control subsystem and after its completion, and the evaluation of the other components occurred after the subsystem was fully assembled. The subsystem was pressurized to 90 psig and the pressure drop per minute was then recorded. During evaluation, the pressure drop due to leakage from the hydrogen system was found to be 0.14 psig/min, which was adequate for testing, particularly given the location of the apparatus under the exhaust hood.

The evaluation of other components involved verifying the proper operation during normal use of the test stand. The solenoid valves, ball valves, and globe valves were found to be working properly and capable of performing the desired design functions.

3.4.2 Oxidant Flow Control Subsystem

The evaluations for the oxidant flow control subsystem were similar to those used for the hydrogen flow control subsystem. The leak testing procedure was the same, and the subsystem pressure loss was found to be 0.13 psig/min. The solenoid valves, ball valves, and globe valves used in the system were found to be operating within the design parameters of the system.

3.4.3 Hydrogen/Air Humidification Subsystem

Evaluation of this subsystem took place after completion of the test stand assembly. Two tests were performed to verify that the subsystem was operating properly: relative humidity

control and water droplet removal. The methods and results of each of these tests are reviewed in this section.

3.4.3.4 Relative Humidity Control

The procedure for achieving relative humidity control involved allowing the system to reach the desired testing temperature and then proceeding with steam injection. When the system achieved a steady state humidity value, the wet and dry branches of the hydrogen/air humidification system were adjusted to reach a desired humidity level. During the initial test period, the discovery was made that the level switches in the drain traps were not functioning properly. Because of the malfunctioning switches, the solenoid valves on both hydrogen/air humidification system water traps were not opening and the subsystems were becoming filled with liquid water. To allow the solenoid valves to operate properly, the level switches were replaced with toggle switches that allow the operator to open and close the solenoid valves manually at desired intervals.

After replacing the level switches, the evaluation of the relative humidity control resumed. After reaching steady state, the relative humidity level had to remain within ± 3 % of the target humidity level at the desired temperature for a period of 10 minutes. Because of the dependence of relative humidity on temperature, a change of $1^{o}C$ could result in relative humidity level inaccuracies of 3% RH below 90% RH and 6% above 90% RH. So, the ability to maintain a stable temperature was critical. For flow rates of 100 SLPM of air and 50 SLPM of hydrogen, the humidification subsystem was capable of providing sustainable humidity levels of 50% RH, 75% RH, and 90% RH at a temperature of $60\pm1^{o}C$. At the higher temperature of $80^{o}C$, the coolant system was not able to remove enough heat from the mixture above humidity levels of 75% RH. At 75% RH, the system temperature began to rise to as high as $100^{o}C$, which could potentially damage the fuel cell membrane.

3.4.3.4 Water Droplet Removal

Once the ability to control relative humidity had been verified, the subsystem was tested to assure that all water droplets were being removed from the inlet gas streams in the water separator. The procedure for this test was to allow the subsystem to reach a steady state humidity

level, and then to connect the fuel cell branch of the outlet of the humidification modules to cylindrical pleated air filters. The filters were 10 in long with a 1 in ID and a 3 in OD, with the outlets plugged. This filter design was chosen because only gas and vapor could pass through the pleats and any liquid water would be retained. Before testing, the filters were allowed to equilibrate in the lab for 24 hours. After the equilibration period, the filters were weighed on an electronic scale and their weights were recorded.

Before steam injection began, the filters were connected to the fuel cell branch of the outlets of the humidification modules and hot dry gases were flowed through the filters to bring them up to the system temperature. The surface temperatures of the filters were measured with an infrared thermometer, and when the surface temperature had reached within $10^{o}C$ of the system temperature the filters were placed in insulated jackets and the flow was switched to the bypass branch of the humidification modules. Steam injection then commenced, and the humidity level was allowed to reach a steady state value. When steady state was achieved, the humidified gases were switched to the fuel cell branch and allowed to flow through the filters for a period of 10 minutes. At the end of that period, the filters were disconnected and immediately weighed to determine the amount of liquid water retained.

The evaluation of each humidification subsystem took place individually and at different temperatures. The air was evaluated at the higher temperature of $86^{o}C$ since removal of water droplets from the air is more critical to successful operation of the fuel cell. At a relative humidity level of 75% RH and a flowrate of 100 SLPM, a mass of 439.2 g of water vapor passed through the air filter during the test period. During the test, the filter collected 5.4 g of liquid water. This represents only 1.2% of the total water present in the gas stream and is a small enough fraction that it will not cause problems with the operation of the fuel cell. For a temperature of $73^{o}C$, a relative humidity level of 63%, a flowrate of 50 SLPM, a mass of 184.5 g of water vapor passed through the hydrogen filter during the test period. During the test, the filter collected 6.8 g of liquid water. This represents 3.7% of the total water present in the gas stream and, although higher than the air system value, is still not large enough to adversely affect the operation of the fuel cell.

3.4.4 Measurement and Control Subsystems

The most important portion of the validation process was the evaluation of the measurement and control subsystems. The pressure transducers, relative humidity sensors, mass flow controllers, and thermocouples were all tested against known values and calibrated as needed. The following section reviews the testing and calibration of these devices.

3.4.4.4 Pressure Transducer

The accuracy of the pressure transducers was verified through the use of a dead weight tester. Most dead weight testing devices employee a piston and small weights to produce desired pressures. A hydraulic fluid is pumped into the piston until the weights float freely. A calibration mark on the piston shaft assures that the piston and weights are raised to the same float level during the calibration process.

The outlet of the tester was connected to a tee, along with an analog pressure gauge and the transducer being calibrated. The initial pressure required to float the piston without any additional weight was 5 psig. Calibration occurred in 5 psig increments from 5 to 100 psig. The best fits for each transducer calibration are shown below in Eqs. (3.3) and (3.4):

$$\text{Actual } H_2 \text{ Pressure} = 0.977 \cdot H_2 \text{ Transducer Reading} - 0.445 \tag{3.3}$$

$$\text{Actual Air Pressure} = 0.980 \cdot \text{Air Transducer Reading} - 0.804 \tag{3.4}$$

where the pressures are expressed in psig and the transducer reading is in mA.

3.4.4.2 Relative Humidity Transmitter

According to the specifications set forth by the manufacturer, the humidity sensors were tested against supersaturated salt solutions of Sodium Chloride and Potassium Sulfate. Each salt solution produced a known humidity level at a given temperature. In addition, the sensors were tested against a desiccant to verify the 0% RH level. For humidity values below 90% RH, the humidity sensors should have errors of ±1% RH or less. For readings above 90% RH, the errors should be ±2% RH or less. The evaluations took place at an atmospheric temperature of 22^{o}C. Both humidity sensors were found to be operating within the acceptable error ranges set forth by the manufacturer.

3.4.4.3 Mass Flow Controllers

The mass flow controllers were factory calibrated but were checked for functionality by connecting a rotometer flow gauge to each flow controller's outlet. The high mass flow controllers were found to be operating within the specified error of ±1% full scale, as was the medium flow controller for the fuel system. Unfortunately, the medium flow controller for the oxidant system was found to be malfunctioning, but this component is not integral to the fuel cell testing performed for this research work.

The validation of the low mass flow controllers was performed in the same manner, but the initial results exceeded the allowable error of ±1% full scale. Both controllers were offset from the desired values specified by the operator in the computer. As such, the manufacturer recommended a two part calibration procedure. The first part involved testing the zero reading of the controller and adjusting the set screw to re-zero the instrument if necessary. Re-zeroing was required for both the fuel and oxidant low flow controllers. After completion of the first part, the flow controllers were re-evaluated to determine if further calibration was required. The fuel low flow controller was found to be operating within the combined error of the flow controller and the rotometer. During testing, this flow meter failed and was replaced by a rotometer ±3% full scale according the manufacturer.

After re-zeroing the oxidant low flow controller, the offset had not been completely removed and the second part of the calibration was required. The second portion of the calibration involved adjusting the 25%, 50%, 75%, and 100% scale settings within the flow controller to verify that the desired output is being achieved. After the second calibration procedure, the oxidant low flow controller was found to be operating within the combined error of the controller and the rotometer. However, since the flow meter was calibrated against the rotameter, the accuracy of the flow meter was reduced to that of the rotameter which is ±3% full scale according the manufacturer.

3.4.4.4 Thermocouples

The nine thermocouples in the test stand were validated against mercury thermometers in ice water baths and boiling water. First, each thermocouple was read with the same channel in

the computer. This evaluation yielded an average error of ±0.09°C and maximum error of +0.17°C for the thermocouples when calibrated in boiling water. For the ice water bath, the thermocouples had an average error of ±0.26°C and maximum error of +0.40°C. All of these values were below the error of 0.75°C specified by the manufacturer over the temperature range used.

The second evaluation of the thermocouples involved determining the error of the two measurement devices, the Eurotherm and HP DAQ. Each thermocouple was plugged into the corresponding device channel and validated against mercury thermometers in an ice water bath and boiling water. In the ice bath, the maximum error for the Eurotherm was ±0.60°C and the average error was ±0.19°C. In the boiling water, the maximum error for the Eurotherm was ±0.57°C and the average error was ±0.16°C. All values were below the error of 0.75°C specified by the manufacturer over the temperature range used.

3.4.5 Safety Subsystem

The safety subsystem was evaluated during the pre-test operation of the fuel cell. During this period, the emergency shutdown switch was activated at the end of each test to verify its operation. When the button was pressed, both reactants were shutdown and nitrogen purged the system. In addition, the hydrogen leak detectors were tested against small releases of hydrogen in a controlled laboratory environment. Both detectors were found to be working properly.

3.4.6 Summary

During the validation of the test apparatus all systems performed as they were expected to. The fuel and oxidant flow control subsystems delivered the desired amounts of reactants to the test apparatus. Once they were delivered, the reactants were successfully humidified with the steam injection humidification. During evaluation, all parameters were recorded with the measurement and controls subsystems. Most importantly, all safety systems operated effectively to maintain a safe testing environment. The results of these evaluations will be discussed in the following chapter.

Chapter 4: Results of Humidification System Evaluations

The results from this project provide a qualitative evaluation of three methods of humidification as implemented in a fuel cell stack test stand - liquid water evaporation, steam injection, and flash evaporation. The final method was also suitable for use in testing 50 cm^2 fuel cells. The results from the individual fuel cell tests show the influence of reactant gas humidification on fuel cell performance.

4.1 Evaluation of Humidification System Performance

Experiences with the Phase I and Phase II fuel cell test stands allow qualitative evaluation of three fuel cell humidification systems: water evaporation, steam injection, and flash evaporation. The following sections summarize the results of these evaluations.

4.1.1 Water Evaporation

Two methods of water evaporation humidification were evaluated during the first design phase: packed bed bubbling and liquid injection. Initially, Davis [2000] selected packed bed bubbling for humidification of the inlet gases. This method could achieve high humidity at medium flow rates: Davis documented 96% RH at 120 SCFH (~56.7 SLPM). However, Davis reported difficulty controlling temperature and humidity over long durations. In addition, at higher flow rates liquid water carryover at the outlet caused flooding of the fuel cell inlet lines.

Liquid injection humidification was the second method employed by Davis [2000]. This consisted of an injection chamber, a length of piping for evaporation, and a moisture separator to remove excess water droplets. Due to the large thermal mass of the system, strip heaters were added at a later date to help evaporate the liquid water. Davis [2000] found the system to be capable of delivering hot humidified gases to the fuel cell, but controlling the system proved to be difficult. In particular, problems were observed with water carryover and slow response times. A review of the experiences with water injection reveals several problems with this approach. When water is injected in the liquid phase, energy from the gas is required for evaporation. This latent heat of evaporation required for water phase transition lowers the temperature of the

gas/vapor mixture. The coupling between the liquid injection rate and the gas temperature makes control of the humidity and temperature difficult. Furthermore, transition from the liquid to vapor phase may not be complete, leaving an undesirable mist of liquid water in the air. While a water injection system was sufficient for Phase I, Phase II required a more exact humidification method to evaluate fuel cell performance.

4.1.2 Steam Injection

To avoid the control problems associated with liquid water evaporation, the Phase II relied on steam injection. With steam injection, the water is delivered to the gas stream in the vapor phase at a temperature higher than that of the gas. This assures that there will be no decrease in the gas temperature due to evaporation. In fact, the post injection temperature exceeds the inlet temperature to the fuel cell. A heat exchanger can then be used to reduce the gas temperature to the desired value. By cooling the gas, excess moisture is condensed, leaving a 100% saturated mixture at the desired inlet temperature to the fuel cell. Theoretically, the combination of direct vapor injection, cooling, and mixing with dry gas should be capable of delivering precise levels of temperature and humidity.

This hypothesis was evaluated over a four month period during the Spring of 2002. The procedure for achieving relative humidity control involved allowing the system to reach the desired testing temperature and then proceeding with steam injection. When the system achieved a steady state temperature at the exit of the cooler, the wet and dry branches of the humidification system were adjusted to reach a desired humidity level. During testing, several areas of concern were identified: the operation of the level switches on the water drains, the strong dependence of humidity on temperature, the sensitivity of the humidity sensor to liquid water, the dependence of humidity on steam pressure, and the sizing of the steam injection valves.

During the initial test period, the level switches in the drain traps were not functioning properly. Because of the malfunctioning switches, the solenoid valves on both humidification system water traps were not opening and the two humidification subsystems were becoming filled with liquid water. The gas bubbled up through the liquid water, which created a second

stage evaporative humidifier that cooled the gas/vapor mixture and allowed liquid water droplets to become entrained in the gas flow. To allow the solenoid valves to operate properly, the level switches were replaced with toggle switches that allow the operator to open and close the solenoid valves manually at desired intervals.

Upon reaching steady state, the relative humidity level had to remain within ± 3 % of the target humidity level at the desired temperature for a sufficient time to gather test data (typically 10-15 minutes) at a pressure of 2 atm. Because of the dependence of relative humidity on temperature, a change of $1^{o}C$ could result in relative humidity level inaccuracies of 3% RH below 90% RH and 6% above 90% RH. So, the ability to maintain a stable temperature was critical. At a temperature of $60\pm1^{o}C$, the humidification subsystem was capable of generating sustainable humidity levels of 50% RH, 75% RH, and 90% RH for flow rates of 100 SLPM of air and 50 SLPM of hydrogen. At a temperature of $80^{o}C$, the system did not adequately cool the mixture when the humidity exceed 75% RH at flow rates of 100 SLPM and 50 SLPM. In addition, numerous problems were experienced with the humidity sensors because contact with water droplets or the occurrence of a transient saturation condition could saturate the sensor with liquid water and render the sensor useless until it could be removed and dried out.

Temperature and humidity control at the lower mass flow rates required to test the fuel cell proved to be even more problematic. At flow rates on the order of 3 SLPM for the air and 1 SLPM for the hydrogen, three principal control issues were observed: cycling of relative humidity as the boiler pressure cycled, improper sizing of the steam injection valves, and over saturation of the relative humidity sensors. These difficulties were reduced by obtaining precision metering valves for the steam injection system. However, even with the addition of the precision metering valves, relative humidity control was not possible at low flow rates. Ultimately, it was apparent that the steam injection system which was sized and built for stacks on the order of 1 kW or greater could not accurately test the effects of inlet gas humidification for an individual fuel cell. Thus a third approach to humidification, flash evaporation, was considered.

4.1.3 Flash Evaporation

An adequate method of humidifying reactant gas streams for single cell membranes was found in Lynntech's reactant gas humidifier. Unlike most dewpoint humidifiers, which rely on bubbling gas through liquid water, Lynntech's system uses flash evaporation to instantaneously vaporize water into the gas stream. So, the system allows a user defined amount of water vapor to be entrained into the gas stream [Lynntech, 2002].

The system is capable of operating in two modes, *constant dewpoint temperature* or *constant water injection*. When operating in constant dewpoint temperature, the humidifier varies the liquid water flow rate to achieve a desired temperature at the outlet. With this approach, the user specifies the dewpoint temperature and the system control algorithm attempts to determine the proper evaporation rate to achieve the desired dewpoint. During testing, the constant dewpoint method could not achieve control at air flow rates below 5 SLPM and hydrogen flow rates below 3 SLPM. At low flow rates, the system injected too much water which caused the temperature to overshoot the setpoint. In response to the overshoot, the system would prevent further water injection until the temperature dropped significantly below the setpoint. Lynntech did not provide a maximum limiting water injection rate in the control scheme. Also, it was not possible to tune the injection pump controller to resolve this problem of overshoot and the system cycled between excess or inadequate humidification.

In contrast, the constant water injection method proved to be adequate for controlling inlet gas humidity level. With this approach, the user pre-calculates the water flow rate required for the desired flow rate and outlet humidity. The humidifier injects water into the flash evaporation chamber at the user specified rate via a metering pump. The user can make corrections to the water injection rate to more closely approach the desired dewpoint. During evaluation with pre-calculated water injection rates, dewpoint temperature control within +/-1 ^{o}C could be achieved for 15 minute test periods, which was sufficient for taking polarization curves at multiple humidity levels. The results of these evaluations are presented in the following section. To prevent formation of liquid droplets caused by post humidifier cooling of the inlet gases, strip heaters were used on the outlet lines to achieve temperatures between 4 to 5 ^{o}C higher than the operating temperature of the fuel cell.

4.2 Effects of Humidity on Fuel Cell Performance

Using the Lynntech dewpoint humidifier operating in a constant water injection mode, an Electrochem 50 cm^2 fuel cell (membrane of Dupont Nafion 115 with platinum catalyst loading of 1 mg/cm^2) was evaluated at an operating temperature of 75^oC, a pressure of 2 atm, and at multiple humidity levels of both the inlet gases. This section will present a discussion of these results.

To test the effect of humidity on fuel cell performance a 3 X 3 test matrix was evaluated. The target humidity levels for the air were 60%, 75%, and 90% and for the hydrogen were 60%, 75%, and 90%. Table 4-1 shows the actual level of humidity control achieved during the evaluation of the fuel cell. The range observed is consistent with the error associated with temperature variation, 3% RH for each degree change below 90% and 6% RH for each degree change above 90%. Control of the system was more precise for the air due primarily to the higher flow rates. The higher gas flows allowed for quicker uptake of water vapor from the flash evaporation chamber and prevented control lag, which could occur at lower flow rates.

Table 4-1. Actual humidity levels achieved during testing of the fuel cell membrane.

Humidity Level	Hydrogen %RH Target	Hydrogen %RH Range	Air %RH Target	Air %RH Range
Low	60%	63.5% - 65.7%	60%	59.8% - 62.1%
Medium	75%	71.4% - 77.7%	75%	74.3% - 77.2%
High	90%	86.1% - 92.5%	90%	87.7% - 90.7%

For presentation purposes, the polarization curves obtained from the nine evaluation points will be grouped according to relative humidity levels of the air. Figure 4-1 shows the polarization curves obtained at low, medium, and high relative humidity levels of hydrogen with a low relative humidity for the air. The best case observed for low air humidity levels, particularly at current densities greater than 0.3 A/cm^2, was the high hydrogen humidity level. This observation is consistent with the results of Nguyen and White [1993] who found that at high current density the transport from the anode by electro-osmotic drag exceeds transport to

the anode by back diffusion from the cathode thus leading to membrane dehydration and performance degradation. Low humidity air can exacerbate this effect by reducing the rate of back diffusion from the cathode. Humidification of the anode gases helps to counteract this effect leading to higher performance at high levels of anode humidification. All polarization curves were fit empirically to the data with the following equation:

$$V = E - ri - A\ln i + A\ln i_0 + B\ln\frac{1-i}{i_L} \tag{4.1}$$

where V is the cell voltage, E is the open circuit voltage, i is the actual current density, i_o is the exchange current density, i_l is the limiting current density, and r, A, and B are coefficients solved with a regression analysis. For this analysis, E was assumed to be the maximum observed test voltage for each case and i_l was assumed to be the maximum observed current density.

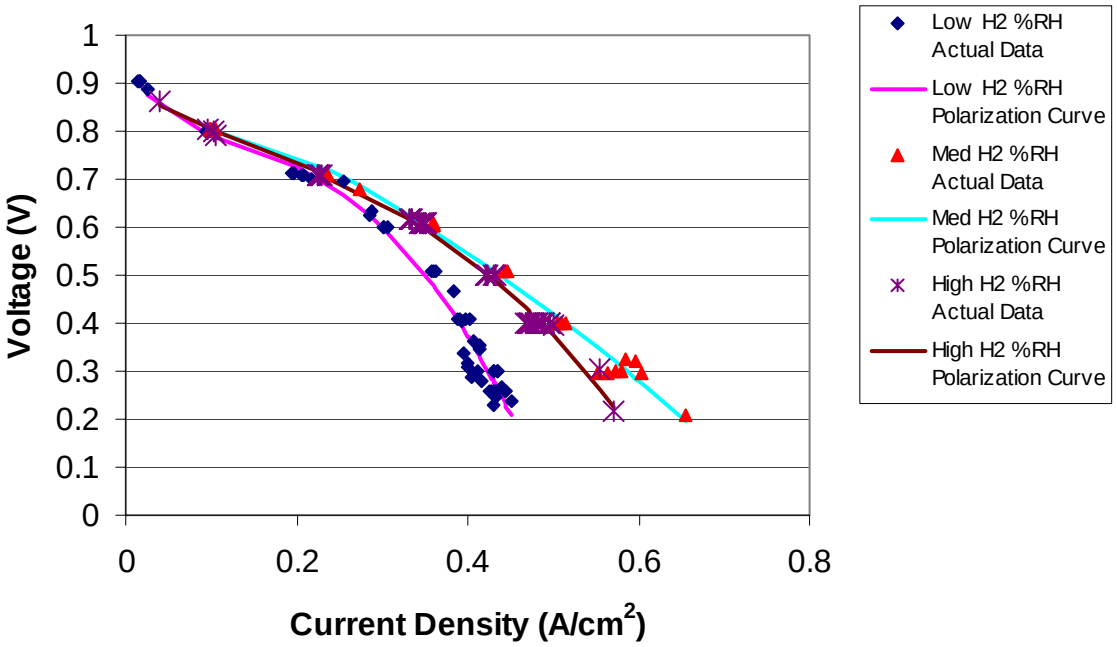

Figure 4-1. Polarization curves for low relative humidity of air. High relative humidity of hydrogen provided the best polarization curve for these cases.

Figure 4-2 shows the polarization curves for the test points with medium relative humidity levels of air. The trend toward improved performance with higher humidity levels of hydrogen was not observed. Similarly, for high relative humidity levels of air, the performance was only marginally improved with increased hydrogen humidification. Figure 4-3 shows these results. These results suggest that with the medium and high levels of air humidification, there

was sufficient back diffusion to keep the membrane hydrated and that further humidification of the anode did not significantly improve the performance. Overall, the best performance occurred at low air relative humidity and high hydrogen humidity.

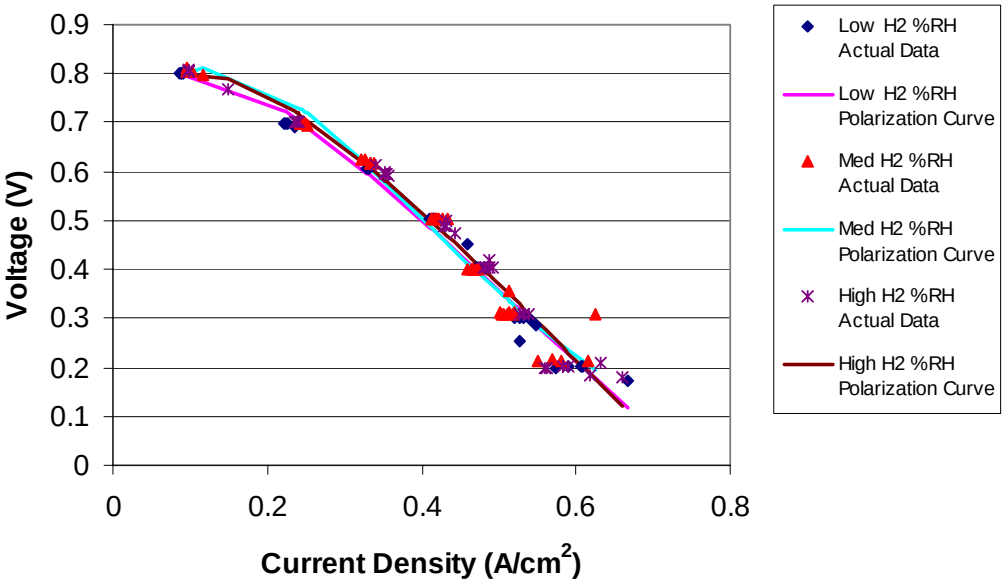

Figure 4-2. Polarization curves for medium relative humidity levels of air.

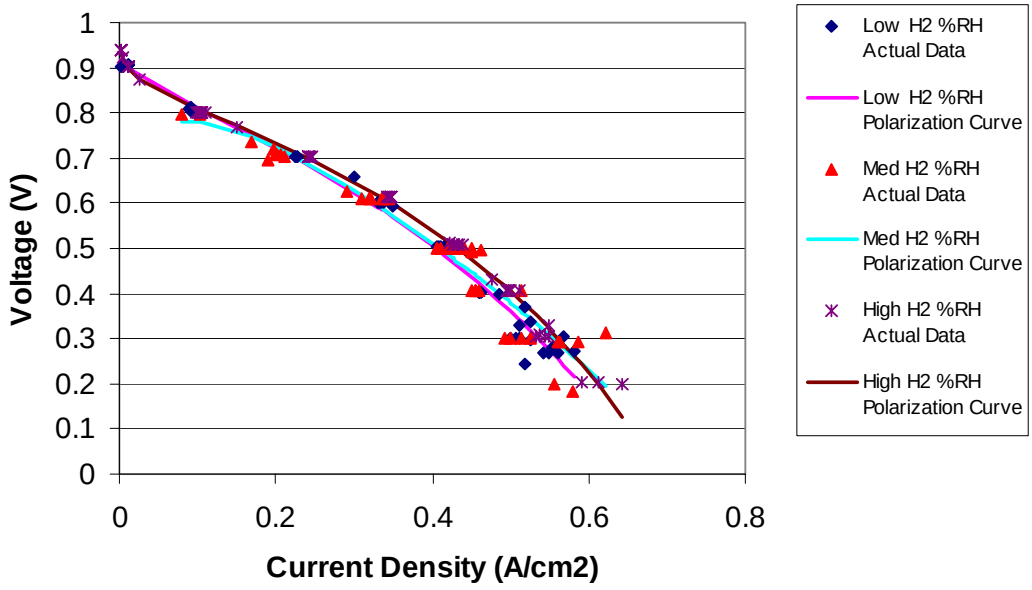

Figure 4-3. Polarization curves for high relative humidity levels of air. For current densities higher than 0.3 A/cm^2, a high relative humidity level of the hydrogen inlet gas was best.

The maximum power output is an important single point measurement of fuel cell performance. For each curve, the maximum power point was obtained from a curve fit to the data. The resulting maximum power points are listed in Table 4-2 and compared graphically in Figure 4-4. Overall, the benefits achieved by humidifying hydrogen are greater than those achieved by humidifying air. On average, power output input increased by 8.5% when hydrogen relative humidity increased from 60% to 75%. A comparable increase in air relative humidity only yielded a 2.7% increase. However, the results obtained from increasing relative humidity levels from 75% to 90% were comparable for hydrogen and air, 1.6% and 1.5% respectively. In total, increasing relative humidity from 60% to 90% on the hydrogen inlet gas resulted in 10.2% increase in power output from the fuel cell. A similar increase in air relative humidity resulted in a 4.2% increase in power output. So, as long as a minimum humidity level of 60% RH is maintained in both the inlet gases, further humidification of the hydrogen stream will provide twice the performance improvement of a similar increase in the relative humidity level of air.

Table 4.2. Maximum power points obtained from each cell of the test matrix. The maximum power achieved for all test conditions, identified in bold, occurred at the low relative humidity level of air and high relative humidity level of hydrogen.

		Relative Humidity of Air		
		Low	**Medium**	**High**
Relative Humidity of Hydrogen	**Low**	9.2 W	10.5 W	10.5 W
	Medium	10.8 W	10.9 W	11.1 W
	High	**11.4 W**	10.8 W	11.1 W

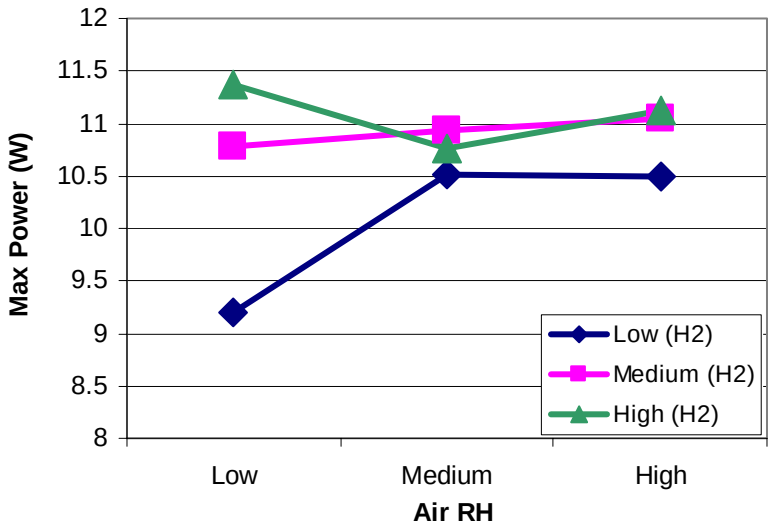

Figure 4-4. Maximum power showing that the maximum power was achieved at low relative humidity of air and high relative humidity of hydrogen.

4.3 Analysis of Uncertainty

Uncertainty in the results is attributable to uncertainty in the controlled parameters, measured parameters, and in the fuel cell itself. This section will review the numeric values associated with these uncertainties, as well as the potential impact these uncertainties have on the results obtained during evaluation.

4.3.1 Uncertainty of Controlled Parameters

The three critical parameters controlled during the operation of the fuel cell were dew point temperature of the inlet gases, temperature of the fuel cell, and mass flow rate of the inlet gases. The controlled parameter of the Lynntech humidifier the was actual injection rate of the water into the flash evaporation chamber. By assuming that all water is fully evaporated into the reactant gas, the accuracy of the injection rate of the water into the water becomes secondary to the accuracy of the actual temperature of the gases exiting the humidifier. The Lynntech humidifier uses T-type thermocouples, which were specified by the manufacturer to have an error of $\pm$ 0.75 ^{o}C.

In contrast, the error associated with the control of the fuel cell temperature was slightly smaller. The Eurotherm temperature controller was found during earlier evaluations to have a maximum error of ± 0.58 ^{o}C. When calculating relative humidity of the reactant gases, the dew point temperature of gas is the humidifier exit temperature. The dry bulb gas temperature is assumed to be the operating temperature of the fuel cell. Thus, these two temperature yield humidity uncertainties of ±2.25% RH for the wet bulb and ±1.75% RH for the dry bulb. When these two uncertainties are combined, this results in a relative humidity uncertainty of ±2.84% RH. Using this calculated uncertainty level, the values of relative humidity between targeted relative humidity levels of 60% RH, 75% RH, and 90% RH were evaluated to determine if they were statistically different. The evaluation was carried out by taking maximum value at the lower humidity level and adding the uncertainty. Then, the minimum value at the upper humidity level had the relative humidity uncertainty subtracted from it. For instance, this method for the 60% RH and 75% RH target cases of hydrogen relative humidity yielded a 68.5% RH at the lower humidity level and 68.6% RH at the upper humidity level. While close, these values are still statistically significant enough to conclude that the humidity levels tested were different from each other.

The final source of uncertainty in the controlled parameters was the mass flow rate of the inlet gases to the fuel cell. At the actual flow rate of 5 SLPM used during test, the full scale error represents an error of 1.2%. In contrast, the error associated with the rotometer used for the measuring the hydrogen flow was 0.1 SLPM, which at the testing flow rate of 3.0 SLPM results in an error of 3.33%. For both reactant gases, the high stoichiometries used during testing (8.0 for air and 26.6 for hydrogen) makes uncertainties in the reactant flow rate negligible.

4.3.2 Uncertainty of Measured Parameters

Four measured parameters could contribute error to the final results; pressure, relative humidity, temperature, and power (function of voltage and current). This section will review the uncertainties associated with each of these parameters and the impact that this uncertainty could have on results.

To obtain the pressures of the gases entering the fuel cell, Kobold pressure transducers were placed in line immediately following the humidifier. The accuracy of each pressure transducer was verified through the use of a dead weight tester. During calibration, the maximum observed difference between the actual and measured pressure values was 1.5 psig, which corresponds to an error of 4.8% at the test pressures.

The thermocouples used in the test stand were validated against known temperature values to determine the error. The thermocouples were evaluated against mercury thermometers in ice water baths and boiling water. First, each thermocouple was read with the same channel in the HP DAQ. This evaluation yielded an average error of ±0.09^{o}C and maximum error of +0.17^{o}C for the thermocouples when calibrated in boiling water. For the ice water bath, the nine thermocouples had an average error of ±0.26^{o}C and maximum error of +0.40^{o}C. All of these values were below the error of 0.75^{o}C specified by the manufacturer over the temperature range used.

The second evaluation of the thermocouples involved determining the error of the Eurotherm. Each thermocouple was plugged into the corresponding device channel and validated against mercury thermometers in an ice water bath and boiling water. In the ice bath, the maximum error for the Eurotherm was ±0.60^{o}C and the average error was ±0.19^{o}C. In the boiling water, the maximum error for the Eurotherm was ±0.57^{o}C and the average error was ±0.16^{o}C. All values were below the error of 0.75^{o}C specified by the manufacturer over the temperature range used.

The calculated power of the fuel cell is the final measured parameter that could contribute uncertainty to the results. This uncertainty in the measured power of the fuel cell is determined by the uncertainty in the measured voltage and current. According to the manufacturer of the load, the error in the voltage is 0.05V and the error in the current is 0.10 A. When expressed as a function of current density, the current measurement error of 0.10 A becomes 0.002 A/cm2. Differences larger than this were observed during testing. With regards to voltage error, at constant current densities the voltage error of 0.05V makes it statistically impossible to distinguish between the results observed for the three hydrogen humidity levels in Figures 4.2

and 4.3. However, it is possible to conclude that the differences observed in Figure 4.1 are significant. The combined errors of the voltage and current yield a power error of 0.11 W, which equals a maximum error of 1.12%. The power error makes it difficult to conclude that there are statistically significant differences between the maximum power observed at medium and high relative humidity levels of air and hydrogen. Finally, it can be concluded that the difference between maximum power at low, medium, and high relative humidity levels of hydrogen at the low relative humidity level of air are statistically significant.

4.3.3 Uncertainty from Additional Sources

The final source of uncertainty during the evaluations was the fuel cell itself. Over time, the membrane may respond differently to inlet gas conditions, depending on the number of hours of operation. During the evaluation of inlet gas humidity on fuel cell performance, the testing took place over a period of 36 hours. The membrane was pre-conditioned for a total period of 12 hours before testing began. However, the pre-conditioning time was assumed to be adequate so the design of experiment was not constructed to evaluate the effect of membrane conditioning. This conditioning effect could have been evaluated by randomizing the test order.

4.3.4 Summary of Uncertainties

As discussed in the previous sections, there were three sources of uncertainty present during the evaluation of the fuel cell. First, the control parameters were subject to measurement errors that could have contributed to uncertainties in the temperature, pressure, and relative humidity levels observed during testing. The most important parameter was relative humidity level, and it was possible to conclude that different relative humidity levels were used during testing. Second, the measured parameters of temperature, voltage, and current were subject to similar measurement errors. The voltage and current errors did make it difficult to conclude that differences existed between the low, medium, and high relative humidity levels of hydrogen at low, medium, and high relative humidity levels of air. However, it was possible to conclude that the differences observed at the low relative humidity level of air were statistically significant. Finally, additional factors, such as the properties of the membrane and its state of conditioning could have affected the results obtained. For the purposes of this evaluation, the membrane was assumed to be fully hydrated and conditioned.

Chapter 5: Conclusion

One of the most complex issues associated with fuel cell operation is adequate humidification of the inlet gases. Lack of water vapor in the inlet gases will initially cause dehydration of the fuel cell membrane and will ultimately result in a degradation of fuel cell power output and damage to the membrane. On the other hand, liquid water droplets present in the inlet gases or excessive air relative humidity can result in flooding of the reaction sites and also cause a drop in the power output. The previous chapters have detailed approaches for humidifying both stacks and single MEAs, and presented the test results for humidification studies on a single MEA. This chapter summarizes conclusions regarding approaches for humidification based on experiences with the test stand. Conclusions from the single cell testing are also reviewed.

A variety of approaches are possible for humidifying reactant gases each of which has limitations, particularly when the goal is careful control of both temperature and humidity across a wide range of gas flow rates. Evaporation from extended surfaces (e.g. gas flowing over wetted glass beads) was found to be difficult to control due to thermal inertia and water carryover. Water spray injection is relatively simple but simultaneous control of both temperature and relative humidity is difficult and water carryover is a problem (Davis, 2000). The approach described here which involves steam injection followed by gas cooling is feasible at high flow rates but does not work well at low flow rates. If the gas flow is limited to relatively low flow rates, other options such as bubbling of gas through a water column (not considered here) or flash evaporation are possible. For the low flow rates associated with single cell testing, humidification by flash evaporation seemed to work better than the other methods which were evaluated.

Regardless of the method of humidification, experiences with this project suggest a number of recommendations for the design of a fuel cell test apparatus including:

Automate as many test stand functions as possible. Coordination of the numerous sub-systems is difficult to accomplish accurately for an operator. Further, the system typically requires extended periods of operation for the apparatus and fuel cell to reach equilibrium. Unless all systems are designed for unattended operation, this becomes a very time consuming activity for the operator.

Heat trace all humidified lines on the inlet side of the fuel cell. Heat losses to the surroundings as well as heat transfer to the lines during the warm-up period lead to condensation in the lines and unreliable humidity control. Further, the specific heat rate of the gases is relatively small and the warm-up period is extremely long without heat tracing.

Avoid the use of humidity controllers for high relative humidity gases. At high relative humidity, humidity sensors become less accurate and very susceptible to saturation. The system will be more reliable if designed to control humidity indirectly by controlling dewpoint. This can be accomplished by saturating the gas at a controlled temperature (e.g., by steam injection followed by condensation at the dewpoint temperature or by flash evaporation to reach saturation).

Size the system to meet the desired service. The development of an apparatus to operate across a wide range of fuel cell power and flow rates is problematic. An undersized system clearly cannot meet the requirements for high flow. But, an oversized system also presents difficulties including inaccuracies in the flow controls and electronic load, limited turndown ratios for control valves, and excessive warm-up times. For testing across a wide range, two separate systems should be considered.

For the individual fuel cell tests, the flash evaporation system inteconnnected with the flow control, measurement and control, and safety sub-systems proved to be adequate for gathering data to investigate the effect of humidification on fuel cell performance. This system achieved control of ±1°C and ±3%RH for the duration of the test intervals. These tests were taken with the flash evaporation system operating in the constant injection flow rate mode. Instabilities in the algorithm for the constant dewpoint control method resulted in oscillation in

the dewpoint. This oscillation could likely be avoided if the injection metering pump were more closely matched to the required flow rate or if the manufacturer were to provide an adjustable maximum flow rate control limit.

Based on the data gathered for a fuel cell incorporating Dupont Nafion 115 with platinum catalyst loading of 1 mg/cm^2, the best performance was achieved with low relative humidity of air and high relative humidity of hydrogen. When the air was humidified to medium levels, no clear benefit was obtained by humidifying hydrogen beyond 60%RH. Likewise, for high humidity levels of air, humidification of hydrogen in excess of 60%RH provided only marginal improvement. For fuel cell and reactant gas temperatures of 75^{o}C and air humidified to the medium value (75%RH), changing the hydrogen humidity from from 60%RH to 90%RH resulted in an 2.9% increase in maximum fuel cell power. In contrast, for reactant gas temperatures of 75^{o}C, pressures of 2 atm, and hydrogen humidified to the medium value (75%RH), changing the air humidity from from 60%RH to 90%RH resulted in an 2.8% increase in maximum fuel cell power. Thus, for the temperatures considered here, if both reactants are humidified to 60% or greater, then further humidification of the hydrogen provides 2.5 times the benefit to maximum power that humidifying air does.

References

Arbin Instruments, Multi-Channel Fuel Cell Testing System Product Literature, http://www.arbin.com, revised on 28 March 2001.

Bernardi, D. M., M. W. Verbrugge, "A Mathematical Model of the Solid-Polymer-Electrolyte Fuel Cell" (1992), *J. Electrochem. Soc.*, Vol. 139, No. 9, pp. 2477-2490.

Buchi, F., S. Srinivasan, "Operating Proton Exchange Membrane Fuel Cells Without External Humidification of the Reactant Gases" (1997), *J. Electrochem. Soc.*, Vol. 144, pp. 2767-2772.

Burns, L. D., General Motors Vice President of Research, Development, and Planning (Traverse City, MI: 10 Aug 2000), address to shareholders meeting.

Casten, S., R. Zogg, "Preliminary Assessment of Battery Energy Storage and Fuel Cell Systems in Building Applications," Final Report to National Energy Technology Laboratory: US Department of Energy, (Cambridge, MA: Arthur D. Little, 2000).

Chow, C. Y., B. M. Wogniczka, U.S. Patent No. 5,382,478, 17 January 1995.

Chu, D., R. Jiang, "Performance of Polymer Electrolyte Membrane Fuel Cell (PEMFC) Stacks Part I. Evaluation and Simulation of an Air-Breathing PEMFC Stack" (1999), *J. of Power Sources*, Vol. 83, No. 1, pp. 128-133.

Davis, M. W., *Development and Evaluation of a Test Apparatus for Fuel Cells* (2000), Electronic Thesis, Mechanical Engineering Department, Virginia Tech.

Dicks, A., Laramie, J., *Fuel Cell Systems Explained*, Chichester, Sussex, England: John Wiley & Sons, 2000.

Dutta, S., S. Shimpalee, J. W. Van Zee, "Numerical Prediction of Mass-Exchange Between Cathode and Anode Channels in a PEM Fuel Cell" (2001), *Int. J. of Heat and Mass Transfer*. Vol. 44, No. 11, pp. 2029-2042.

Ellis, M., D. Nelson, M. von Spakovsky, *ME5984 Fuel Cell Systems* (Spring 2000), Class Notes, Mechanical Engineering Department, Virginia Tech.

Energy Partners, Inc., How Does it Work Website, http://www.energypartners.org/fuel_cells_101/how_does_it.htm [visited 12 Oct 2001].

FuelCells.org, Fuel Cell Information Website, http://www.fuelcells.org/fcfaqs.htm [visited 12 Oct 2001].

General Motors, Advanced Technology Vehicles – Fuel Cell Timeline, http://www.gm.com/company/gmability/environment/road_to_future/adv_tech_vehicles/future_fuel_cells/milestones.html [visited 8 Sep 2003]

Ihonen, J., F. Jaouen, F. Lindbergh, F. Sundhom, "A Novel Polymer Electrolyte Fuel Cell For Laboratory Investigations and In-Situ Contact Resistance Measurements" (2001), *Electrochemica Acta*, Vol. 46, No. 19, pp. 2899-2911.

Jansen, G. J. M., M. L. J. Overvelde, "Water Transport in the Proton-Exchange-Membrane Fuel Cell: Measurements on the Effective Drag Coefficient" (2001), *J. of Power Sources*, Vol. 101, No. 1, pp. 117-125.

Johnson, R., C. Morgan, D. Witmer, T. Johnson, "Performance of a Proton Exchange Membrane Fuel Cell Stack" (2001), *Int. J. of Hydrogen Energy*, Vol. 26, No. 8, pp. 879-887.

Morner, S. O., S. A. Klein, "Experimental Evaluation of the Dynamic Behavior of an Air-Breathing Fuel Cell Stack" (2001), *J. of Solar Energy Eng.*, Vol. 123, pp. 225-231.

Mosdale, R., G. Gebel, M. Pineri, "Water Profile Determination in a Running Proton Exchange Membrane Fuel Cell Using Small-Angle Neutron Scattering" (1996), *J. of Membrane Science*, Vol. 118, pp. 269-277.

Nguyen, T. V., R. E. White, "A Water and Heat Management Model for Proton-Exchange-Membrane Fuel Cells" (1993), *J. Electrochem. Soc.*, Vol. 140, No. 8, pp. 2178-2186.

ONSI Corporation, International Fuel Cells Website, http://www.onsicorp.com/index_fl.htm [visited 12 Oct 2001].

Siegel, N.P., Ellis, M.W., Nelson, D.J., von Spakovsky, M.R., "A Two-Dimensional Computational Model of a PEMFC with Liquid Water Transport" (2003), Submitted to *J. of Power Sources* for publication in Spring 2004

Springer, T. E., T. A. Zawodzinski, S. Gottesfeld, "Polymer Electrolyte Fuel Cell Model" (1991), *J. Electrochem. Soc.*, Vol. 138, No. 8, pp. 2334-2341.

Sridhar, P., R. Perumal, N. Rajalakshmi, M. Raja, K.S. Dhathathreyan, "Humidification Studies on Polymer Electrolyte Membrane Fuel Cell" (2001*), J. Power Sources*, Vol. 101, No. 1, pp. 72-78.

Tenney Environmental, Benchmaster Test Chambers Website, http://www.lunaire.com/products/tbenchmc.htm [visited 24 Oct 2001].

Wang, Z. H., C. Y. Wang, K. S. Chen, "Two-Phase Flow and Transport in the Air Cathode of Proton Exchange Membrane Fuel Cells" (2001), *J. of Power Sources*, Vol. 94, No. 1, pp. 40-50.

Yi, J. S., T. V. Nguyen, "An Along-the-Channel Model for Proton Exchange Membrane Fuel Cells" (1998), *J. Electrochem. Soc.*, Vol. 145, No. 4, pp. 1149-1159.

Appendix A: Humidification Subsystem Calculations

To assure that all four design criteria have been met, the proposed design for the humidification subsystem was analyzed using the principles of thermodynamics and heat transfer. The first step in this process was to perform an energy balance, shown in Figure A-1. The inputs are dry gas, steam (at 80 psig), and coolant and the outputs are a gas and vapor mixture and coolant.

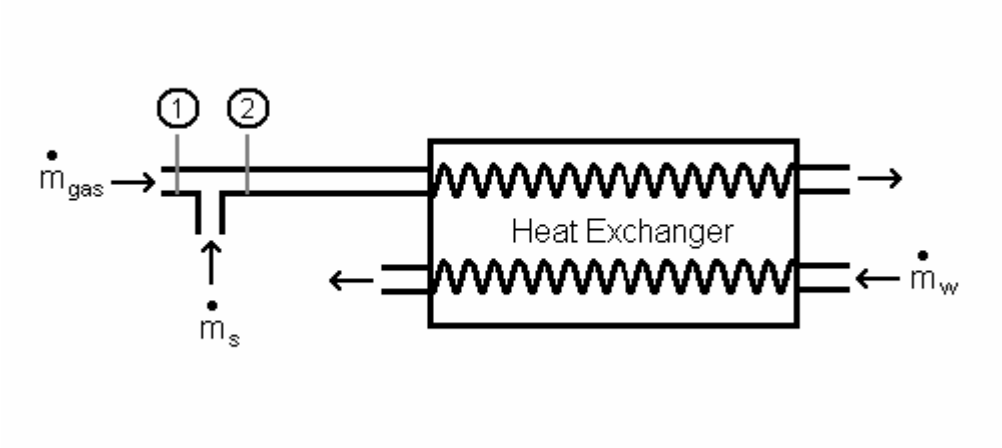

Figure A-1. Block diagram of energy balance on the current system. At state 1, dry gas enters the system and is mixed with steam at 80pisg. At state 2, the gas – vapor mixture enters the heat exchanger. Coolant passes through the heat exchanger in a counter-flow configuration.

A.1 Steam Injection Humidifier Calculations

The calculations presented in this section will use the properties of the hydrogen humidification subsystem. Equations A.1, A.2, and A.3 are used to find the desired humidity ratio of a gas at the inlet temperature of the fuel cell (80^{o}C). The values used in the calculations for the air humidification subsystem are found in Table A-1. The desired humidity ratio of the fuel cell inlet gas can be determined from the specified relative humidity and temperature of the inlet gas. The humidity ratio is defined by:

$$\omega = \frac{m_v}{m_g} \tag{A.1}$$

where m_υ is the mass of the vapor and m_g is the mass of the dry gas, either hydrogen or air. Assuming both the gas and vapor behave as ideal gases:

$$\omega = \frac{\left(\frac{p_\upsilon V}{R_\upsilon T}\right)}{\left(\frac{p_g V}{R_g T}\right)} = \frac{R_g p_\upsilon}{R_\upsilon p_g} = K \frac{p_\upsilon}{p_m - p_\upsilon} \tag{A.2}$$

where p_υ is the pressure of the vapor, p_g is the pressure of the dry gas, and p_m is the pressure of the mixture. R_υ is the gas constant for the vapor and R_g is the gas constant for the dry gas. K is the ratio of gas constants, and has a value of 8.94 for hydrogen and 0.622 for air. The pressure of the vapor can be determined from the definition of relative humidity:

$$\Phi = \frac{p_\upsilon}{p_{SAT}(T)} \tag{A.3}$$

where $p_{sat}(T)$ is the saturation pressure at the mixture temperature, which can be found in steam tables. For a given temperature, relative humidity, and mixture pressure, Equations A.2 and A.3 can be used to determine the desired humidity ratio. Figure A-2 shows humidity ratio as a function of temperature for various RH levels. Similar results for air are shown in Figure A-3.

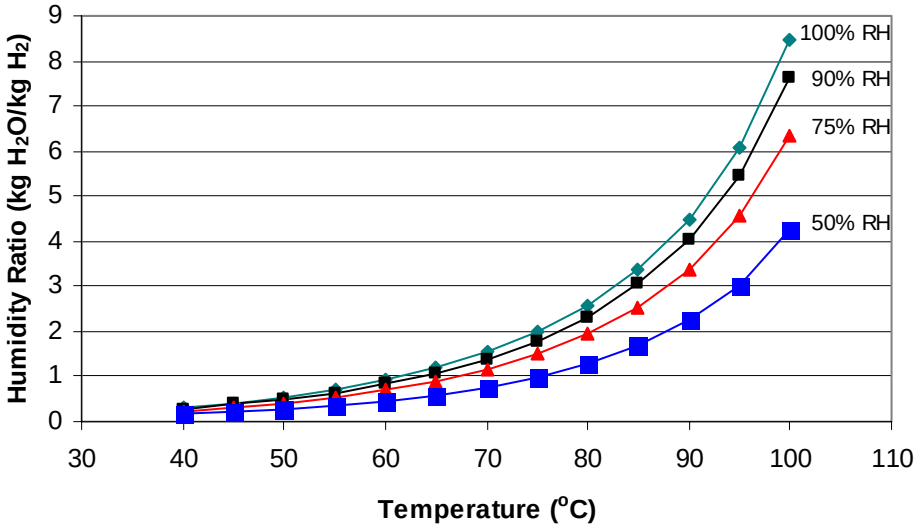

Figure A-2. Humidity ratio as a function of desired temperature for relative humidity levels of 50%, 75%, 90%, and 100% and a total pressure of 2 atm.

Since air has a higher molar mass than hydrogen, the mass fraction of water in air is lower than the mass fraction of water in hydrogen for the same relative humidity. Figure A-3 shows the humidity ratio as a function of the temperature for relative humidity levels of 50%, 75%, 90%, and 100%.

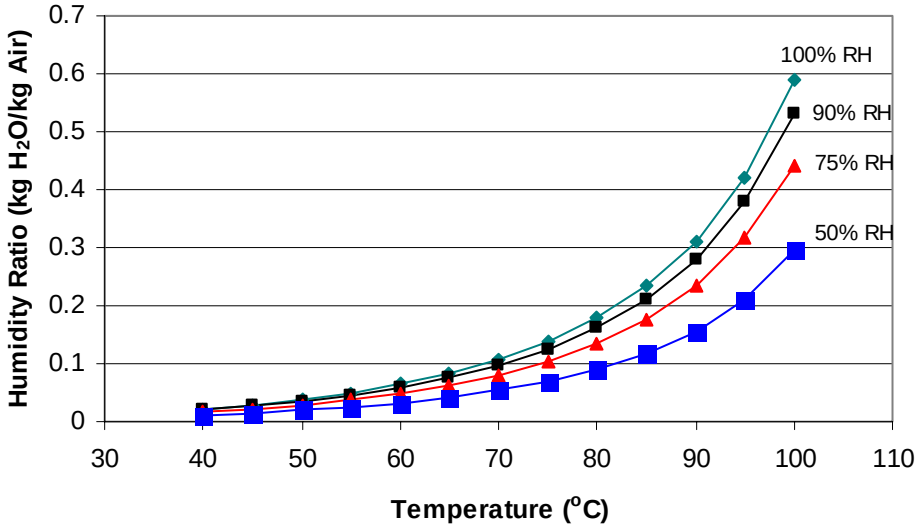

Figure A-3. Humidity ratio of the air as a function of desired temperature for relative humidity levels of 50%, 75%, 90%, and 100% at a pressure of 2 atm.

After calculating the desired humidity ratio, mass and energy balances can be performed on the injection point to determine the required flow rate of steam and the exit gas temperature. Assuming steady flow, the mass balance for the water is given by:

$$\omega_1 \dot{m}_{gas} + \dot{m}_S = \omega_2 \dot{m}_{gas}\,, \tag{A.4}$$

where the subscripts refer to Figure A-1. Equation (A.4) can be solved for the mass flow of steam required to achieve the desired humidity ratio ω_2:

$$\dot{m}_S = (\omega_2 - \omega_1)\dot{m}_{gas}\,. \tag{A.4 a)}$$

If the steady flow assumption is maintained, the energy balance for the injection process is given by:

$$\dot{m}_{gas} h_{gas1} + \omega_1 \dot{m}_{gas} h_{V1} + \dot{m}_s h_s = \dot{m}_{gas} h_{gas2} + \omega_2 \dot{m}_{gas} h_{V2} \tag{A.5}$$

where h_{gas1} and h_{gas2} are the gas enthalpies at states 1 and 2 respectively, h_{v1} and h_{v2} are the enthalpies of the vapor at states 1 and 2 respectively, and h_s is the enthalpy of the steam. Substituting for the steam mass flow from Equation A.4a and rearranging yields:

$$\omega_1 h_{V1} + (\omega_2 - \omega_1) h_S + h_{gas1} = h_{gas2} + \omega_2 h_{V2} \tag{A.6}$$

The values for the humidity ratios at states 1 and 2 and the enthalpies on the left side of Equation A.6 are known. The values for the enthalpies on the right side of the equation are dependent on the outlet temperature. Thus, Equation A.6 is an implicit equation that can be solved for the outlet temperature using tabulated values for the gas and steam enthalpies. For hydrogen, the gas is in the dry state and the value of ω_1 is zero. The value of ω_1 for air is 0.002817 kg water/kg dry air.

Post injection humidified hydrogen temperature as a function of the humidity ratio is shown in Figure A.4 for a total mixture pressure of 202.6 kPa (2 atm), an inlet steam enthalpy corresponding to saturated vapor at 80 psig, and an inlet hydrogen temperature of 80°C. At the desired humidity ratio of 2.58 kg water / kg dry hydrogen, the outlet temperature is 97°C.

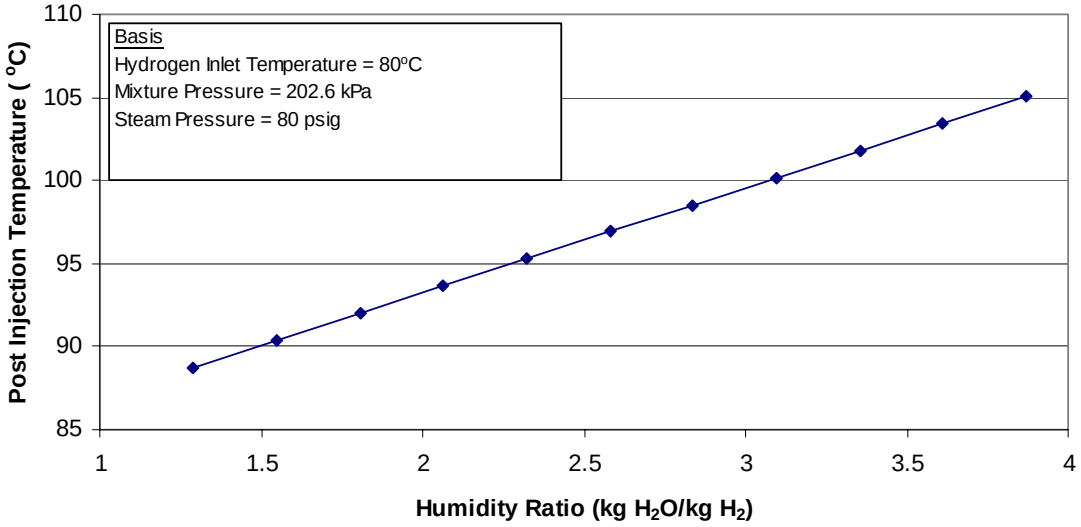

Figure A-4. Temperature of the hydrogen vapor mixture following steam injection as a function of the humidity ratio. The trend is linear and increasing with respect to the humidity ratio. The mass basis for the calculation is shown on the chart.

Figure A-5 shows the exit gas temperature as a function of the humidity ratio for air. The non-linearity is caused by the presence of water vapor at state 1. At the desired humidity ratio of 0.1924 kg water / kg air, the outlet temperature is 97°C.

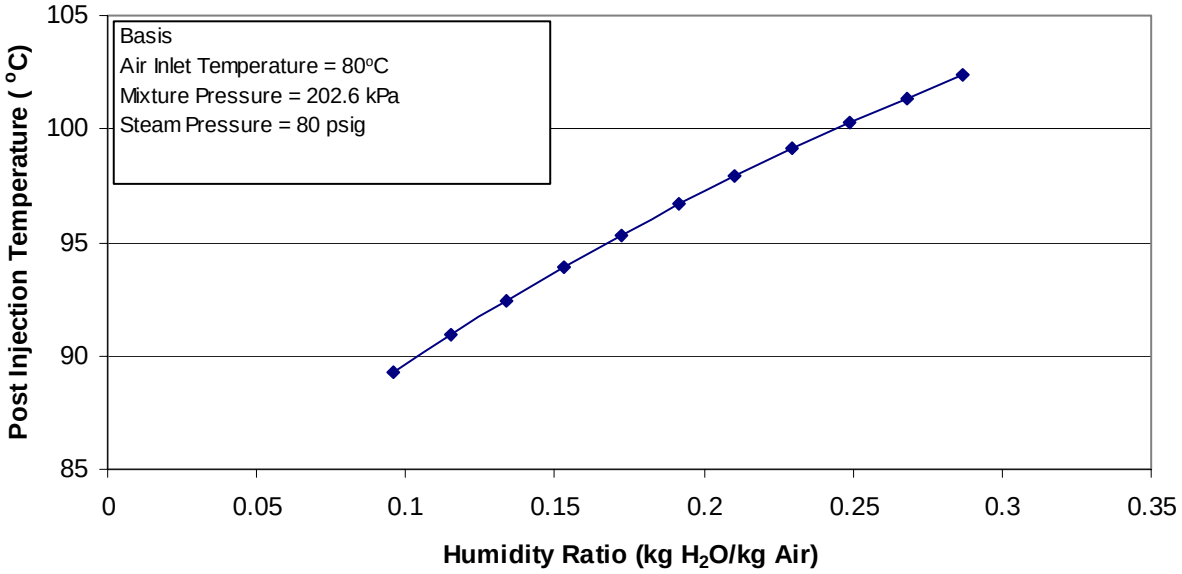

Figure A-5. Temperature of the air vapor mixture following steam injection as a function of the humidity ratio. The trend is non-linear and increasing with respect to the humidity ratio. The mass basis for the calculation is shown on the chart.

A.2 Hydrogen Cooler Calculations

The results from the calculations for the hydrogen coolers are shown in Table A-1. The following section will review the methodology used for sizing the heat exchanger for the hydrogen cooler.

Since the temperature of the mixture after the steam injection is higher than the desired inlet temperature of the fuel cell, coolers have been included to reduce the mixture temperature. To size the coolers, the heat transfer required to cool the hydrogen gas was calculated using Equation A.7:

$$q_{req} = \left(\dot{m}_{gas} + \dot{m}_{V2}\right) C_{P,H_2} \left(T_{hi} - T_{ho}\right) \qquad (A.7)$$

where q_{req} is the required amount of heat transfer, Cp_{H_2} is the specific heat of the gas - vapor mixture T_{hi} is the inlet temperature of the gas, and T_{ho} is the outlet temperature of the gas.

Table A-1. Values resulting from the hydrogen cooler calculations using equations A.1 to A.16. The description for each symbol used in the calculations is shown in the second column.

Symbol	Description	Value
T_{hi}	Inlet temperature for gas side	370 K
T_{ho}	Outlet temperature for gas side	353 K
$\dot{m}_{mix}$	Mass flow rate of the gas – vapor mixture	7.42*10-4 kg/s
q_{req}	Heat transfer required from the gas – vapor mixture	69.2 W
Re_{mix}	Reynold's number for the gas – vapor mixture	8,678
Pr_{mix}	Prandtl number for the gas – vapor mixture	0.899
Nu_{mix}	Nusselt number for the gas – vapor mixture	31.5
h_{mix}	Heat transfer coefficient for the gas –vapor mixture	255 W/m^2*K
Re_w	Reynold's number for the water – coolant mixture	1,460
Nu_w	Nusselt number for the water – coolant mixture	5.56
$\dot{m}_w$	Mass flow rate fore the water – coolant mixture	0.042 kg/s
h_w	Heat transfer coefficient for the water – coolant mix	134 W/m^2*K
U	Overall heat transfer coefficient	79 W/m^2*K
T_{co}	Outlet temperature for the water – coolant mixture	351.5 K
T_{ci}	Inlet temperature for the water – coolant mixture	351 K
A_{req}	The required heat transfer area	0.118 m^2
A_{act}	The actual heat transfer area	0.215 m^2
% Over	Percent the actual area exceeds the required area	82%
Δp_{mix}	Pressure drop on the gas – vapor side	3,300 Pa
Δp_w	Pressure drop on the water – coolant side	849 Pa

The cooler was tentatively chosen to be a tube-in-tube heat exchanger, manufactured by Parker. The heat exchanger has an inner diameter of 3/8" and an outer diameter of 5/8". There are a total of 9 coils, which spiral around a radius of 10 in. A propylene glycol-water mixture was used as the heat transfer fluid on the coolant side. To determine if the preliminary selection of the heat exchanger was adequate, the required heat transfer area was determined based on the design conditions outlined in Table A-2.

Table A-2. Design conditions used for heat exchanger.

Description	Temperature
Inlet hydrogen – vapor mixture temperature	97°C
Outlet hydrogen – vapor mixture temperature	80°C
Inlet Coolant Temperature	78°C
Outlet Coolant Temperature	78.5°C

Since the heat exchanger is in a counterflow configuration, the Inlet Coolant Temperature of 78°C was selected to be close to the desired Outlet Temperature of the mixture, 80°C. The Outlet Coolant Temperature was found by using Equation A.8:

$$T_{co} = T_{ci} + \frac{q_{req}}{\dot{m}_w C_{Pw}}, \tag{A.8}$$

where the mass flow rate of the coolant (0.042 $\frac{kg}{s}$) corresponds to a volumetric flow rate of 3.785 liters per minute (1 gallon per minute).

The required area was then compared to the actual area of the preliminary selection for the heat exchanger. To evaluate the required area, the overall heat transfer coefficient U was calculated. The first step was to calculate the Reynold's number for the gas side:

$$Re_{mix} = \frac{\dot{m}_{mix} D_{inner}}{\pi \frac{D_{inner}^{2}}{4} \mu_{mix}} \tag{A.9}$$

Since the Reynold's number of 8,678 was in the transition region, the flow was assumed to be turbulent. The following formula was used to calculate the Nusselt number:

$$Nu_{mix} = 0.023 Re_{mix}^{0.8} Pr_{mix}^{0.3} \tag{A.10}$$

which yields a value of 31.5. The heat transfer coefficient for the gas side was then calculated from:

$$h_{mix} = Nu_{mix} \frac{k_{mix}}{D_{inner}} \tag{A.11}$$

which yields a value for the heat transfer coefficient of the gas, h_{H2}, of 192 $\frac{W}{m^2 K}$.

The next step was to calculate the Reynold's number for the propylene glycol-water mixture in the annular region:

$$Re_w = \frac{4\dot{m}_w}{\pi(D_{outer} + D_{inner})\mu_w} \tag{A.12}$$

The Reynold's number of 1,460 is in the laminar region for the outer tube of a concentric tube annulus. Using a correlation from Incropera and Dewitt the Nusselt number was found to be 5.60. Using this value for the Nusselt number, the heat transfer coefficient was found from:

$$h_w = Nu_w \frac{k_w}{D_h} \tag{A.13}$$

where D_h is the hydraulic diameter for the annular region. Solving Eq. (A.13) yields a value for the heat transfer coefficient, h_w, of where $h_w = 131 \frac{W}{m^2 K}$).

With the inner and outer heat transfer coefficients determined, the overall heat transfer coefficient was calculated with Equation A.14:

$$U = \frac{1}{\frac{1}{h_{mix}} + \frac{1}{h_w}} \tag{A.14}$$

and found to be $U = 77.9 \frac{W}{m^2 K}$.

The required heat transfer area can then be calculated from:

$$\text{Area} = \frac{q_{req}}{U \Delta T_{LM}} \tag{A.15}$$

with the log mean temperature difference calculated as follows:

$$\Delta T_{LM} = \frac{(T_{hi} - T_{co}) - (T_{ho} - T_{ci})}{\ln\left[\frac{(T_{hi} - T_{co})}{(T_{ho} - T_{ci})}\right]}. \tag{A.16}$$

Substituting the log mean temperature difference of 7.41 K, the overall heat transfer coefficient, and the required heat transfer into Equation A.15 yields a required heat transfer area of 0.120 m^2. The actual heat transfer area provided by the preliminary heat exchanger selection is given by Equation A.17:

$$A = \pi D_{inner}\left(D_{coil} N_{coil} \pi\right) \tag{A.17}$$

where A = 0.215 m^2. The actual area exceeds the required area by 80%, so the preliminary selection is adequate.

The pressure drop across the hydrogen – vapor side of the heat exchanger can be found by first determining the gas velocity:

$$V_{mix} = \frac{\dot{m}_{mix}}{\rho_{mix} \frac{\pi}{4} D_{inner}^{\ 2}} \tag{A.18}$$

The gas velocity of 25.7 m/s can then be substituted into Equation A.19 to solve for the pressure drop:

$$\Delta p_{mix} = fr_{mix} \rho_{mix} \frac{V_{mix}^{\ 2}}{D_{inner}^{\ 2}} D_{coil} N_{coil} \pi \tag{A.19}$$

where Δp_{mix} = 3,300 Pa. The friction factor value of 0.0327 was found using Figure 8.3 on page 425 of Incropera and Dewitt's Fundaments of Heat and Mass Transfer [1996]. The pressure drop across the coolant side of the heat exchanger was determined in a similar manner and found to be 849 Pa. These same calculations were used for the hydrogen heater, which at maximum flow has an actual heat transfer rate of 163 W, a hydrogen pressure drop of 3,903 Pa, and a propylene glycol-water mixture pressure drop of 3,771 Pa.

A.3 Air Cooler Calculations

The air cooler was tentatively chosen to be a tube-in-tube heat exchanger in counter-flow configuration. The preliminary selection was evaluated with an approach similar to that for the cooler, and Table A-3 summarizes the results.

Table A-3. Values resulting from the air side calculations with equations A.1 to A.16.

Symbol	Description	Value
T_{hi}	Inlet temperature for gas – vapor side	370 K
T_{ho}	Outlet temperature for gas – vapor side	353 K
$\dot{m}_{mix}$	Mass flow rate of the gas – vapor mixture	0.0121 kg/s
q_{req}	Heat transfer required from the gas – vapor mixture	241 W
Re_{mix}	Reynold's number for the gas – vapor mixture	61,300
Pr_{mix}	Prandtl number for the gas – vapor mixture	0.744
Nu_{mix}	Nusselt number for the gas – vapor mixture	142
h_{mix}	Heat transfer coefficient for the gas – vapor mixture	336 W/m^2*K
Re_w	Reynold's number for the water – coolant mixture	1506
Nu_w	Nusselt number for the water – coolant mixture	5.61
$\dot{m}_w$	Mass flow rate fore the water – coolant mixture	0.065 kg/s
h_w	Heat transfer coefficient for the water – coolant mixture	87 W/m^2*K
U	Overall heat transfer coefficient	69 W/m^2*K
T_{co}	Outlet temperature for the water – coolant side	352.1 K
T_{ci}	Inlet temperature for the water – coolant side	351 K
A_{req}	The required heat transfer area	0.479 m^2
A_{act}	The actual heat transfer area	0.318 m^2
% Over	Percent the actual area exceeds the required area	-33.5%
Δp_{mix}	Pressure drop on the gas – vapor side	65,500 Pa
Δp_w	Pressure drop on the water – coolant side	1,140 Pa

A.4 Energy Balance for the Coolant System

After calculating both values of the amount of heat transferred from each humidification subsystem, an energy balance was performed to assure that the coolant bath could reject enough heat through the coil. This balance is shown in Equation A.20.

$$\begin{aligned} q_{out} &\geq q_{in} \\ q_{out} &\geq q_{ACTH_2} + q_{ACTair} \end{aligned} \tag{A.20}$$

where q_{out} = the required heat rejection from the coil (311 W).

To calculate the heat transfer rate from the bath, the temperature coefficient of volume expansion (β), Rayleigh number, and Nusselt number from the bath to the coil were calculated using Equations A.21, A.22, and A.23.

$$\beta_b = \frac{-1}{\rho_{b2}} * \frac{\rho_b - \rho_{b2}}{T_b - T_{b2}} \tag{A.21}$$

$$Ra_b = \frac{g * \beta_b * D_{pipe} * \left|T_b - T_{ci}\right|}{\nu_b * \alpha_b} \tag{A.22}$$

$$Nu_b = \left[0.6 + \frac{0.387 + Ra_b^{1/6}}{\left[1 + \left(\frac{0.559}{\mathrm{Pr}_b} \right)^{9/16} \right]^{8/27}} \right]^2 \tag{A.23}$$

where,

β_b = the temperature coefficient of volume expansion (8.829×10^{-4} $\frac{1}{K}$),

ρ_b = the density of the bath at the lower temperature (1,039 $\frac{kg}{m^3}$),

ρ_{b2} = the density of the bath at the higher temperature (1,030 $\frac{kg}{m^3}$),

T_b = the lower bath temperature (343 K),

T_{b2} = the higher bath temperature (353 K),

Ra_b = the Rayleigh number for the bath ($4.72*10^5$),

g = specific gravity (9.8 $\frac{m}{s^2}$),

D_{pipe} = the pipe diameter for the heat rejection coil ($6.35*10^{-3}\,m$),

T_{ci} = the inlet temperature of the coil (291 K),

ν_b = the kinematic viscosity of the fluid in the bath ($3.097*10^{-6}$ $\frac{m^2}{s}$),

α_b = the absorptance of the fluid in the bath ($7.881*10^{-8}$ $\frac{m^2}{s}$),

Nu_b = the Nusselt number for the bath (15.425), and

Pr_b = the Prandtl number for the bath (39.29).

The heat transfer coefficient from the bath was then calculated using Equation A.24.

$$h_b = Nu_b \frac{k_b}{D_{pipe}} \tag{A.24}$$

where, k_b = the thermal conductivity of the bath (0.2596 $\frac{W}{m*K}$). Solving Eq. (A.24) yields a value for the heat transfer coefficient for the bath, h_b , of 630.6 $\frac{W}{m^2*K}$.

All calculations for the city water side used water properties at 291 K and a flow velocity of 1 m/s. The Reynold's number was found to be in the turbulent region (58,700) and a Nusselt number of 276 was calculated with Equation A.10. By inserting the values for the water flow rate into Equation A.8, the equation was then solved to find an outlet temperature of 292.6 K. Next, Equations A.25 and A.26 were used to find the heat transfer coefficient for the city water side of the coil and the overall heat transfer coefficient, respectively.

$$h_w = Nu_w \frac{k_w}{D_{pipe}} \tag{A.25}$$

$$U = \frac{1}{\frac{1}{h_b} + \frac{1}{h_w}} \tag{A.26}$$

where,

h_w = the heat transfer coefficient to the water coil ($8.832*10^3$ $\frac{W}{m^2 K}$),

k_w = the conductivity rate for the water (0.5996 $\frac{W}{mK}$), and

U = the overall heat transfer coefficient (588.58 $\frac{W}{mK}$).

The copper coil has a pipe diameter of 6.35×10^{-3} m (¼"), a coil diameter of 0.038 m (1.5 in), and consists of 23 turns. These values can be used in Equation A.17 to solve for the heat transfer area, which was found to be 0.055 m^2. The log-mean-temperature formula from Equation A.16 was used to find the temperature difference of 51.9 K. The temperature difference, overall heat transfer coefficient, and heat transfer area were then used in Equation A.15 to solve for the required amount of heat transfer area, 0.00972 m^2. This actual area exceeded the required area by 465%, which is more than sufficient to satisfy the requirements of the system. The operator controls the flow rate of city water through the coil, so the actual amount of heat transfer can be reduced.

Appendix B: Calculations for Design of Fuel Subsystem

The appropriate piping size for each of the reactant gas subsystems was a function of the mass flow characteristics. The mass flow of fuel and oxidant are both dependent on the power produced by the cell. As discussed in Chapter 1, the hydrogen entering the fuel cell reacts to yield a hydrogen proton, which travels through the membrane, and an electron, which travels from the anode to the cathode. Since current is a measure of the flow of electrons, the hydrogen mass flow is proportional to the fuel cell current. The hydrogen subsystem is designed to operate with a stoichiometric ratio of 1 to 2. Equation B.1 yields the hydrogen flow rate expressed in SLPM based on the design values for the test stand.

$$\text{SLPM} = \frac{\text{Pwr} \times \text{SR}_{\text{Gas}} \times \text{R}_{\text{u}} \times \text{T}_0}{\text{n} \times \text{F} \times \text{V}_{\text{c}} \times \text{P}_0} \times 60 \frac{\text{s}}{\text{min}} \times \frac{1{,}000 \text{ liters}}{\text{m}^3} \tag{B.1}$$

where,

Pwr = the design fuel cell power, 5,000 W,

SR_{Gas} = the design stoichiometric ratio for the gas, 2 for hydrogen,

R_u = universal gas constant, 8.314 Pa·m3/mol·K

T_0 = standard temperature, 298 K,

P_0 = standard pressure, 101,000 Pa,

n = the number of electrons, 2 for H_2 and 4 for O_2,

F = Faraday's constant 96,484 $\frac{C}{mol}$, and

V_c = the cell voltage, 0.5V.

From Equation B.1, the mass flow rate for the hydrogen subsystem was determined to be 152 SLPM. The second design criterion for the hydrogen subsystem was the flow velocity. Davis (2000) selected a maximum velocity of 25 m/s, to both minimize the noise created by the flow of gas through the piping and the pressure drop. Equation B.2 is used to calculate the flow velocity and the pressure drop is calculated in Equation B.3.

$$V_{Gas} = \frac{\dot{m}_{Gas}}{\frac{P_{Gas}}{R_{Gas}T_{Gas}} \bullet \frac{\pi D^2}{4}} \tag{B.2}$$

$$\frac{\Delta p}{L} = 0.158 \frac{\rho_{Gas}^{0.75} \mu_{Gas}^{0.25} V_{Gas}^{1.75}}{D^{1.25}} \tag{B.3}$$

where,

$\dot{m}_{Gas}$ = the mass flow rate for the gas $\left(\frac{kg}{s}\right)$,

P_{Gas} = the lowest pressure for each gas (kPa),

T_{Gas} = the highest temperature for each gas (K),

R_{Gas} = the gas constant $\left(\frac{kJ}{kgK}\right)$,

D = the inner diameter of the tubing (m),

ρ_{Gas} = the density of the gas $\left(\frac{kg}{m^3}\right)$,

μ_{Gas} = the viscosity of the gas (Pas), and

V_{Gas} = the flow velocity of the gas $\left(\frac{m}{s}\right)$.

From Equation B.2, the velocity criterion is achieved for a pipe diameter of ½". In addition, the calculated pressure drop was less than 20 Pa per meter of piping. The maximum design pressure of the fuel cell test stand is 400 kPa, so a pressure drop of this magnitude will not have a significant effect on fuel cell operation.

Appendix C: Properties of Tube-in-Tube Heat Exchanger

Table C-1. Properties of tube-in-tube heat exchangers used in the humidification subsystem.

Property	Dimension	Hydrogen Heater	Hydrogen Cooler	Air Cooler
Inner Tube Diameter	in.	¼	3/8	½
Inner Tube Material		316 SS	316 SS	316 SS
Outer Tube Diameter	in.	½	¾	1
Outer Tube Material		Copper	Copper	Copper
Number of Coils		15	9	10
Outer Coil Max Pressure	Psia	1200	1100	1000
Outer Coil Max Flow Rate	GPM	1.8	4.5	10
Inner Coil Max Flow Rate	lbm/hr	80	188	200

VITA

The author, John Evans, enrolled in the Bachelor's degree program in mechanical engineering at Virginia Tech in fall 1995. As an undergraduate, John worked as a co-op for Allied Signal Corporation at the industrial nylon manufacturing facility in Hopewell, VA, and as a research assistant to Dr. Wng Ng. In his final year, he participated in the combined MS/BS program and completed his undergraduate degree in spring 2000. Following graduation, he continued his coursework in the Master's program with the Mechanical Engineering department and began working with the Center for Automotive Fuel Cell Systems as a graduate research assistant. Mr. Evans finished his coursework in fall 2001 and in spring 2002 became employed as a Process Engineer at the Celanese Acetate plant in Narrows, Va. Since then John has been promoted and is currently responsible for six sigma projects totaling $1.5M in corporate savings for 2003. He completed his Master's degree requirements in fall 2003. John plans to reside in Christiansburg, VA, with his wife and they are expecting their first child in spring 2004.